

## 5. Results

The down-core records of sediment texture, calcite-oxygen and -nitrogen isotopes, sedimentary organic components and their isotopes, and sedimentary inorganic components exhibit in general smooth variations suggesting at the outset a) the variations are natural and b) the sediment cores are free from post depositional perturbations such as bioturbation or turbidite or slumping. These characters of the present sedimentary records would help in reconstructing the past oceanic responses to the climate change with reasonable confidence. In the following sub-sections, I describe the salient features of the results separately for each sediment core.

### 5.1. Age-model and chronology

#### SK 117/GC08 (Figure 2):

The  $\delta^{18}\text{O}_{G.sacculifer}$  in the core-top section is  $-1.37\text{‰}$ . The lowest value of the entire down-core record is at a depth of 15 cm ( $-1.65\text{‰}$ ). The down-core fluctuations of the  $\delta^{18}\text{O}_{G.sacculifer}$  are marginal up to 19 cm depth. From 19 cm the  $\delta^{18}\text{O}_{G.sacculifer}$  rapidly increases to  $\sim 0.4\text{‰}$  and further down up to 90 cm varies within a narrow range of  $\sim 0.2\text{‰}$ . The heaviest ( $0.47\text{‰}$ )  $\delta^{18}\text{O}_{G.sacculifer}$  is recorded at 75 cm depth. From 90 cm to 123 cm these values significantly decrease from  $0.47$  up to  $-0.33\text{‰}$  and remain more or less constant  $\sim 0.2\text{‰}$  up to 280 cm depth. The second and third lowest  $\delta^{18}\text{O}_{G.sacculifer}$  events are located at 329 cm ( $-1.10\text{‰}$ ) and at 397 cm ( $-1.19\text{‰}$ ).

The down-core  $\delta^{18}\text{O}_{G.sacculifer}$  profile shows well-defined Marine Oxygen Isotope Stages (MIS). The age model is constructed by tuning the down-core  $\delta^{18}\text{O}_{G.sacculifer}$  profile to the low latitude SPECMAP stack (Bassinot et al. 1994), which is a modified version of the original SPECMAP of Imbrie et al., (1984). This enabled to demarcate the Holocene/LGP boundary (11 Ka) at 25 cm; LGP/MIS3 (24 Ka) at 105 cm; MIS 3/4 (57 Ka) at 227 cm; and MIS 4/5 (71 Ka) at 290 cm. The marine

isotopic stage boundaries are drawn at the mean of the highest and lowest oxygen isotopic values between the two adjacent warm and cold oxygen isotope events defined in the SPECMAP. Four tie-points are used to evolve fairly accurate age model, viz., 1) The Last Glacial Maximum (LGM) occurring at 18 Ka identified at 75 cm exhibiting the latest heaviest oxygen isotope event (0.47 ‰), 2) occurrence of the well-dated Youngest Toba Tuff (YTT) at ~ 72 Ka (Ninkovitch et al., 1978) identified by the presence of abundant YTT-characteristic glass-shards (Pattan et al., 2000) at 297 cm, and 3) the interstadials of MIS5, viz., MIS5.1 occurring at 330 cm and MIS5.3 at 397 cm dated to be 79 Ka and 97 Ka respectively (Bassinot et al., 1994).

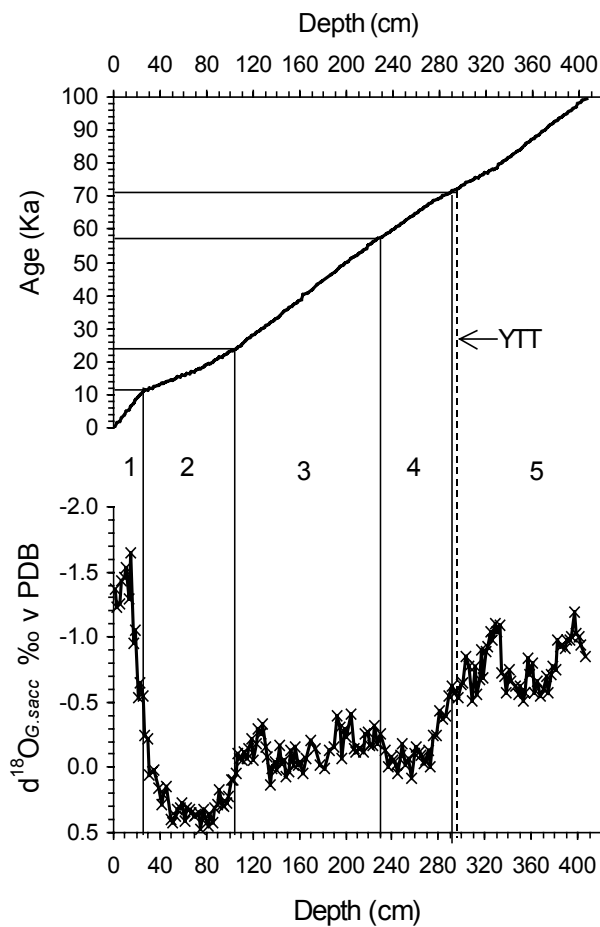


Figure 2: Marine oxygen isotope stage (MIS) boundaries recognized in the SK117-GC08 core. The age model (upper panel) is derived from tuning the *G.sacculifer* oxygen isotope depth curve to the tropical-stack SPECMAP. The horizontal and vertical lines indicate depth-age relationship. The numbers are the marine oxygen isotope stages. The core covers last 100 Ky time-span. YTT=Youngest Toba Tuff that occurs at 297 cm depth in core. Two lighter oxygen-isotope peaks in MIS5 are the two warm interstadials 5.1 and 5.3 separated by colder stadial 5.2.

**SK-129/CR-04 (Figure 3):**

The  $\delta^{18}\text{O}_{G.sacculifer}$  in the core-top section is  $-1.82\text{‰}$  and remains more or less uniform up to 32 cm where it begins to increase rapidly down-core reaching  $\sim 0.00\text{‰}$  at 70 cm forming the peak of the heaviest  $\delta^{18}\text{O}_{G.sacculifer}$ . The lightest  $\delta^{18}\text{O}_{G.sacculifer}$  in the entire down-core profile occurs at 358 cm ( $-2.14\text{‰}$ ). The lighter  $\delta^{18}\text{O}_{G.sacculifer}$  peak is located at 15 cm depth ( $-2.04\text{‰}$ ). The isotopic values remain more or less constant at around  $-0.6\text{‰}$  from 90 cm to 230 cm but with a marginally heavy  $\delta^{18}\text{O}_{G.sacculifer}$   $\sim 200$  cm. A decrease from  $-1.55\text{‰}$  to  $-2.2\text{‰}$  is evident between 230 cm and 380 cm. This increase contains three distinct increasingly lighter  $\delta^{18}\text{O}_{G.sacculifer}$  peaks down-core (i.e., at  $\sim 258$  cm, at  $\sim 308$  cm, and at  $\sim 356$  cm). Further down-core the profile exhibits heavy  $\delta^{18}\text{O}_{G.sacculifer}$  similar to that found  $\sim 70$  cm depth. Thus a distinct transition from the heavy  $\delta^{18}\text{O}_{G.sacculifer}$  to light  $\delta^{18}\text{O}_{G.sacculifer}$  is evident between 400 cm and 360 cm depths in core. The structure of this transition is quite similar to that found between the 70 cm and 30 cm depths in the core.

The above-described depth versus  $\delta^{18}\text{O}_{G.sacculifer}$  profile of SK129-CR4 core is tuned to the low latitude SPECMAP stack (Bassinot et al., 1994). Thus identified marine oxygen isotope boundaries are, Holocene/LGP boundary (11 Ka) at 40 cm, LGP/MIS3 (24 Ka) at 94 cm, 3/4 (57 Ka) at 181 cm, 4/5 (71 Ka) at 220 cm and 5/6 (122 Ka) at 358 cm. Several tie points are also used to evaluate the precision of the age model. They are, 1) the LGM (18 Ka) at 70 cm depth, 2) Youngest Toba Tuff ( $\sim 72$  Ka) at 224 cm, 3) Last Appearance Datum (LAD) of *G. ruber* (pink variety) (120 Ka) at 354 cm and, 4) the interstadials of MIS5, viz MIS5.1 (79 Ka), MIS5.3 (97 Ka) and MIS5.5 (122 Ka) at 258 cm, 308 cm, and 358 cm depths respectively. The derived age model for SK129-CR4 indicates that the core covers the last 148 Ka.

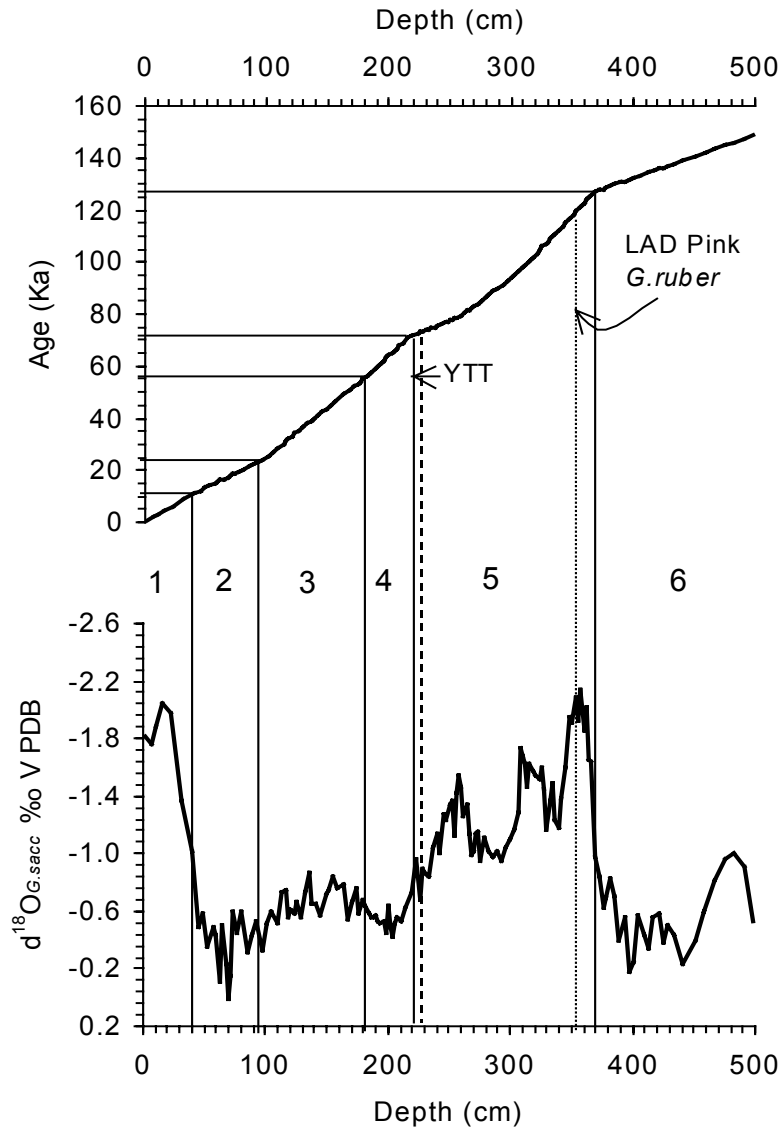


Figure 3: The age model for SK129-CR04 core. The vertical and horizontal lines are the marine oxygen isotope stage boundaries recognized in the core with corresponding ages as defined in the SPECMAP. The vertical lines with labels are the independent tie-points in the form of YTT (~72 Ka) located at 228 cm depth and the last appearance datum of *G. ruber* (pink variety) at 352 cm dated to be 120 Ka (Thompson and Duplessy, 1982). Clearly defined LGM and interstadials of MIS5 (5.1, 5.3, and 5.5) provided additional control points for the age model. The numbers are the marine oxygen isotope stages.

**SK-117/GC-02 (Figure 4):**

The core top  $\delta^{18}\text{O}_{G.sacculifer}$  is  $-1.83$  ‰, which is nearly uniform with marginal fluctuations down-core up to  $\sim 20$  cm. Further down the  $\delta^{18}\text{O}_{G.sacculifer}$  increases rapidly to  $-0.6$  ‰ at  $\sim 85$  cm. From 85 cm down to  $\sim 350$  cm the increase is rather gentle (from  $-0.6$  ‰ to  $0.2$  ‰). The lightest  $\delta^{18}\text{O}_{G.sacculifer}$  of the entire core ( $-2.04$  ‰) is recorded at 11 cm depth and the heaviest  $\delta^{18}\text{O}_{G.sacculifer}$  ( $0.18$  ‰) is at 293 cm. Further down-core the  $\delta^{18}\text{O}_{G.sacculifer}$  decrease to  $-0.45$  ‰ at 386 cm (bottom of the core) from  $0.17$  ‰ at 347 cm depth.

The comparison of the  $\delta^{18}\text{O}_{G.sacculifer}$  depth-profile with the SPECMAP suggests that the core appears to cover a maximum of 24 Ka, i.e., the Holocene and LGP. The Holocene and the LGP boundary and the isotopic variation within this time-span can be appreciated by referring to the compressed inset and the exploded versions of the isotope-depth profiles together in Figure 4. The Holocene/LGP boundary (11 Ka) is located at 44 cm depth and LGP/MIS3 boundary (24 Ka) appears to be at 386 cm depth. There were no independent tie-points available to verify the accuracy of this age model, but based on the structure of the isotope-depth profile, the derived age model appears to be fairly accurate. The latest heaviest  $\delta^{18}\text{O}_{G.sacculifer}$  ( $0.18$  ‰) at 293 cm depth is considered as the LGM. However, the AMS  $^{14}\text{C}$  dating would help to overcome any ambiguity if at all evident in the present age model.

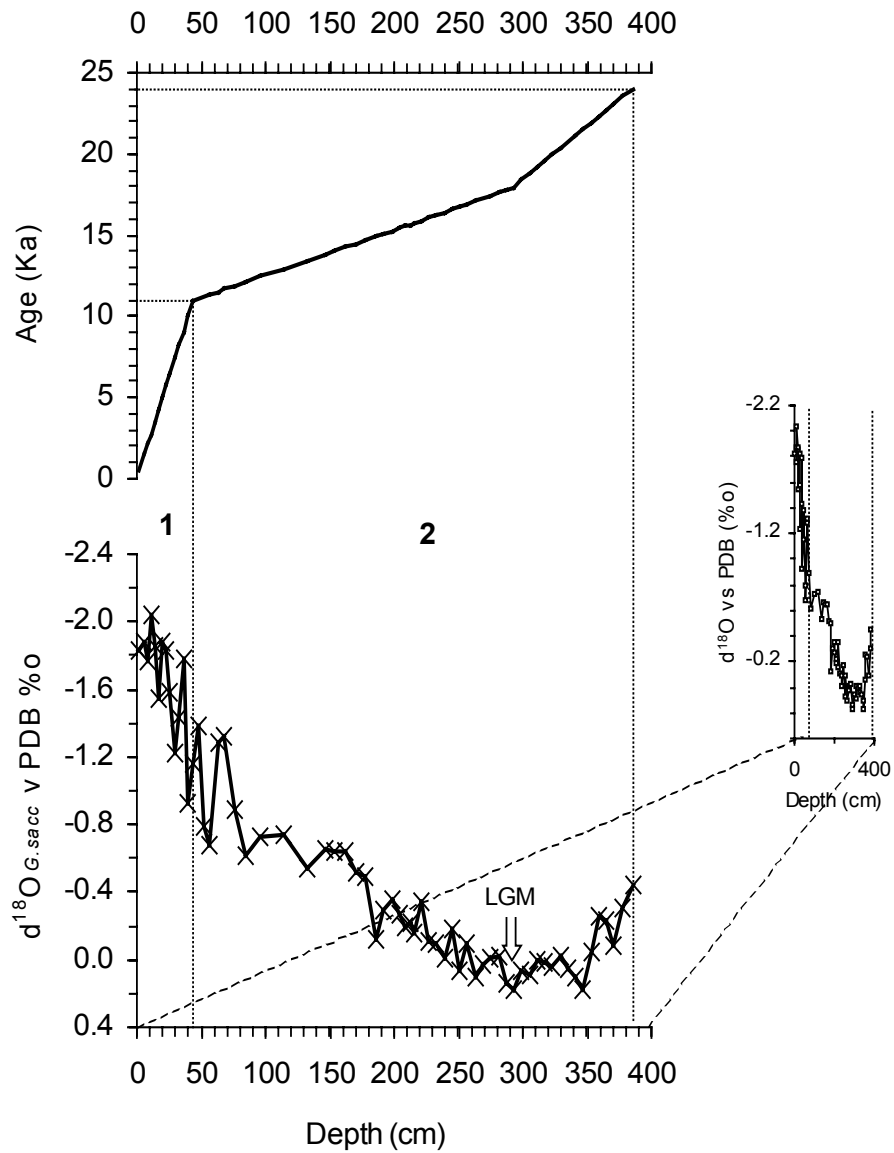


Figure 4: Depth versus oxygen isotope profile used for the Age-Model of SK117/GC-02 core. The compressed inset on the right-hand-side is presented for ready comparison with the SPECMAP. The upper exploded panel is the depth-age curve used to define the age-model. Vertical and horizontal broken lines indicate the marine oxygen isotope stage boundaries and corresponding ages. LGM=Last Glacial Maximum (~18 Ka) identified as the latest heaviest oxygen-isotope event in the depth profile.

## 5.2. Sedimentation rates:

The changes in marine sedimentation rates in the proximity of continents provide preliminary clues about the past variation in aeolian dust, fluvial erosion input, and the marine productivity (Prins et al., 2000; Sirocko et al., 1993). The sedimentation rates are essential to estimate the mass accumulation rates of the components at the seafloor, which eliminates the bias (due to dilution effect) associated with interpreting direct weight concentrations in sediments with varying physical properties. In the present case, the sedimentation rates in GC2 and GC8 from the shelf and slope off Goa are expected to provide a cumulative scenario of fluvial erosion input from the Mandovi-Zuari river draining the hinterland of Goa (part of Deccan Mountain belt), continental dust input mainly from the adjoining Indian peninsula by the winter monsoon winds and the water column productivity. On the other hand, sedimentation rates in the third core (CR4) would dominantly indicate changes in productivity, because this core is far removed from the land and the winter monsoon wind influence is less dominant. The calculated sedimentation rates using the depths at which various isotope stage boundaries are defined, isotope stage boundary timings, and the total thickness of the sediment represented by the each isotope stage are presented in Table 4.

**Table 4: Linear sedimentation rates**

Core	Sedimentation rate (cm/ky)					
	Holocene	LGP	MIS-3	MIS-4	MIS-5	MIS-6
SK117/GC02	4.0	25.6				
SK117/GC08	2.3	6.1	3.8	4.0	4.6	
SK129/CR04	3.6	4.4	2.6	2.2	3.1	4.1

From Table 4 it is clear that the sedimentation rates in all the three cores are highest during the LGP. The Holocene sections exhibit moderately varying sedimentation rates, i.e., 2-4 cm/ky in all the cores. The GC-02 core (continental shelf) shows extremely high sedimentation rate (by ~6 times) during the LGP than during the Holocene. The deep-water core (GC-08) from the same longitude exhibits three times higher rate of sedimentation during the LGP than during the Holocene. The southern EAS deep-water core (CR-04), on the other hand shows marginal increase during the LGP. This core records nearly similar sedimentation rate during the penultimate glacial period (MIS6) as that during the LGP. In the GC08 the sedimentation rates during the MIS5 through MIS3 time-slice are same (~4 cm/ky) and are nearly two times higher than the Holocene.

### 5.3. Sediment texture

#### SK117/GC08 (Figure 5):

In general the +63  $\mu\text{m}$  (sand) fraction exhibits decreasing trend down-core. The variation is of an order of magnitude (between ~25 % and ~2 %). The Holocene section contains high percentage (Av. ~22%) than the sections corresponding to

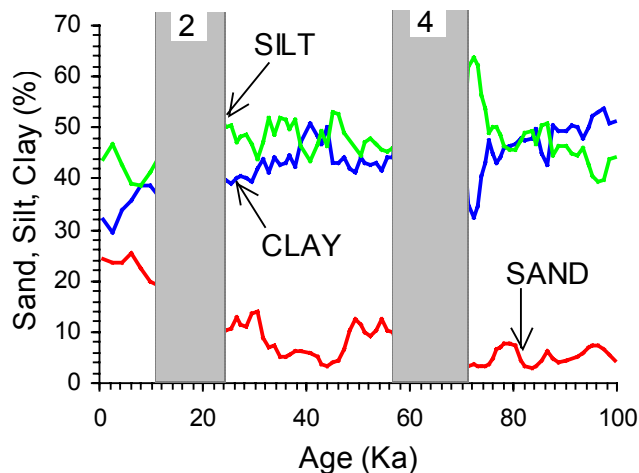


Figure 5: Temporal distribution of the three sediment fractions in continental slope core off Goa (SK117/GC-08). Note the mirror image variation in silt and clay fractions independent of the sand fraction. The minimum clay and maximum silt characterize the LGP. Where as, the maximum sand characterizes the Holocene. The vertical shaded bars are the glacial stages defined by the age model.

other time periods. The LGP contains on an average ~10 % sand but with a peak of ~20 % at ~16 Ka. The MIS3 period exhibits two minor peaks of sand at ~30 Ka (14 %) and ~50 Ka (12 %) separated by broad trough of nearly 20 ky time-span. The



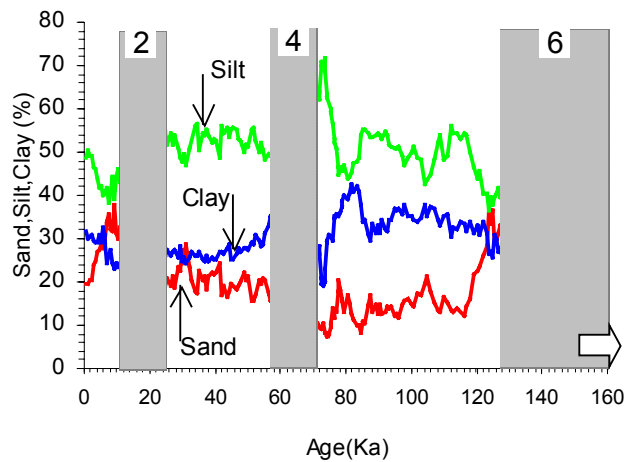
sand content in the MIS4 and MIS5 sections is the lowest (~3%) of the entire record without any significant variation.

The silt- and clay-fractions exhibit an interesting mirror-image temporal-trend independent of sand. The clay content varies between 20% and 50 %. The dominant fraction of the sediment is the silt, which varies between 40 % and 65 %. The LGP interval exhibits highest silt content (~65%) and lowest clay content (~20%). The Holocene period records ~42% silt and ~35% clay. Nearly equal content (~45%) of both these fractions dominate the rest of the time period prior to the beginning of the LGP. The only significant feature of the pre-LGP silt-clay variation is the second highest silt-lowest clay pairing (62% vs 32%) at around the closure of MIS5.

**SK129/CR04 (Figure 6):**

Down the core, the sand fraction increases from 20 % (core-top) to 38 % at ~9 Ka, reduces to ~18 % (~16 Ka), and remains more or less constant ~20% through the MIS3 period. A further reduction by ~10 % through the MIS4 section results in the lowest (~7 %) sand content at ~72 Ka. The second peak of ~40 % sand is located at MIS5.5 (~122 Ka) and further down-core reduces to ~10 % through the MIS6. Interestingly, the sand fraction monotonously increases through all the three glacial events leading to peaked concentration at the commencement of succeeding warm events. The structure of the temporal sand profile for the Holocene and the MIS5.5 appear to be very similar. The silt and sand exhibit more or less opposite trend. The prominent low-silt events in the core are identified at ~9 Ka (40 %), ~82 Ka (45 %) and ~ 123 Ka (36 %), where as, the high-silt events are located at 17 Ka (59 %) and 73 Ka (~72 %). The rest of the silt distribution varies marginally around 50 % throughout. Even though the clay is second abundant sediment fraction, it follows partly the sand and partly the silt. There are three low clay events located at ~15 Ka (22 %), ~ 72 Ka (28 %) and ~ 125 Ka (31 %). Overall marginally high clay content is restricted to the warm stages like Holocene and the MIS5.

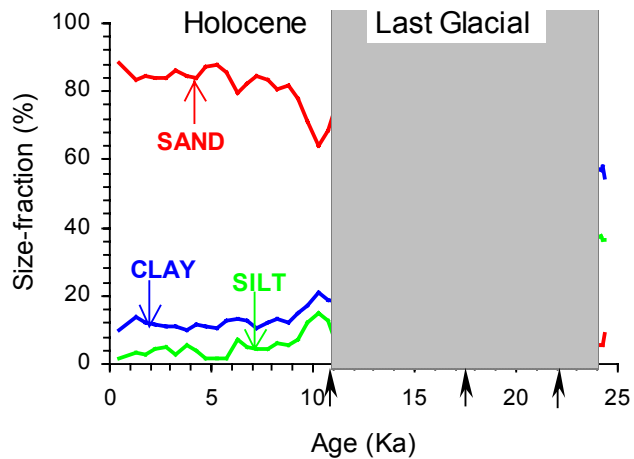
Figure 6: Temporal variation of the three sediment fractions in southern-EAS continental slope core (SK129/CR04). Note the opposite trends in the silt and sand variation. The block arrow indicates that the MIS6 continues beyond the core record. The vertical shaded bars with numbers are the glacial stages as defined by the age-model.



**SK117/GC02 (Figure 7):**

Except for few spikes around the beginning and closure of the LGP, the sediment fractions exhibit smooth variation. The variation of sand fraction is exactly opposite to both silt and clay, which are strongly coherent with each other in the

Figure 7: The Last Glacial to Holocene variation in the sediment fractions of the SK117/GC-02 core. Note the alternating dominance of coarse (sand) and fine (silt & clay) fractions at around the beginning of the LGP and the Holocene. The upward arrows on the age-axis indicate prominent events of coarse-fine reversals.



core. The Holocene section exhibits highest content of sand (~80 %) and reaches the lowest of <5 % at ~11 Ka. At the commencement of the LGP, the sand content is very low (<10 %) and drastically increases between ~21 Ka and ~18 Ka (i.e., around

LGM) to as high as >60 %. On the other hand, the lowest silt and clay contents are recorded during the Holocene followed by during the early part of the LGP (~22 Ka-~18 Ka), which overtake the sand dominance at ~18 Ka until ~11 Ka. The overall clay fraction is higher (~12 %) than the silt (~3 %) in the Holocene interval. Whereas, during the LGP the clay and silt contents are nearly equal and vary between 20 % and 40 %.

#### 5.4. Time-series record of sedimentary inorganic components

##### 5.4.1. Calcium carbonate

###### SK117/GC08 (Figure 8):

The calcium carbonate (henceforth only carbonate) content varies from 18 % to 49 %. There are four elevated carbonate intervals in the core, which are at around the latest Holocene, mid-LGP, early-MIS3 and MIS5.3. A fifth peak of ~35% carbonate is at MIS5.1, which is formed due to two lowest content (<20 %) troughs of carbonate at the commencement of MIS4 and at the MIS5.2. The former peaks exhibit nearly constant carbonate content of ~45 %. The other characteristics of the carbonate distribution in this core are, a) a drastic increase through the Holocene and MIS4, and marginal variation (within  $\pm 5$  %) during the LGP through MIS3 time-slice, and b) extreme variations (~20 % to ~45 %) through MIS4 and in MIS5.



Figure 8: Temporal variation of calcium carbonate in the SK117/GC08 core. Note the distinctly elevated carbonate in the post-MIS4 period, which begins to increase from ~20% at the commencement of MIS4 and reaches a high of ~45 % in the earliest MIS3. The largest variation is found during the MIS5 period.

**SK-129/CR04 (Figure 9):**

The average carbonate content in the core is ~50 % with a minimum at ~72 Ka. The Holocene through MIS3 section exhibits relatively narrow variation within  $\pm 5$  % around an average of 55 %. The carbonate content shows a monotonous increase through the MIS4 from ~25 % at the commencement to ~50% at the closure. The MIS5 section on the other hand contains three high carbonate peaks separated by three low carbonate troughs. The structure of the carbonate variation during the MIS5 though appears to resemble the stadial-interstadial pattern recognized in the oxygen isotope curves, but do not exactly correspond to their timings. The high-low carbonate events are rather located at the transition of stadial-interstadial events in MIS5. A common feature in carbonate variation during all the three glacial events is that of increasing trend through the glacial period towards the succeeding warm intervals.

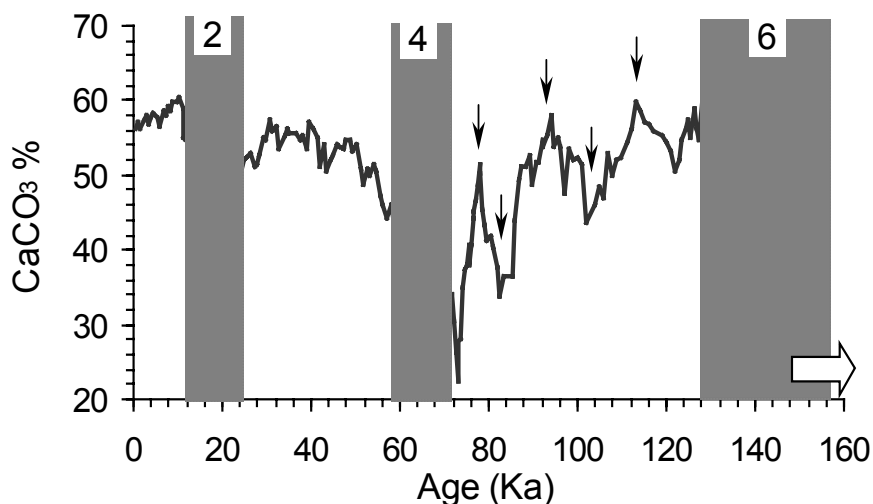


Figure 9: Temporal variation in carbonate content of the SK129/CR04 core from the southern-EAS region. Note the drastic increase of carbonate content through the MIS4 and the typical stadial and interstadial type structure in the MIS5 (downward arrows). Block arrow indicates that the MIS6 continues further down-core. The shaded bars are the glacial periods numbered at the top.

**SK117/GC02 (Figure 10):**

The Holocene average carbonate content is ~80 % without significant variations except for a rise at ~5 Ka. On the other hand, the LGP section records extreme variation. The LGP begins with a drastic increase from 20 % (at ~ 24 Ka) reaching to 60 % (at ~ 22 Ka) (i.e., 40 % increase in 2 kyr span). The rise continues gradually up to a maximum of ~70 % at ~17 Ka. During the latest part of the LGP (15 Ka onwards) the carbonate content gradually decreases to ~55 % at its termination.

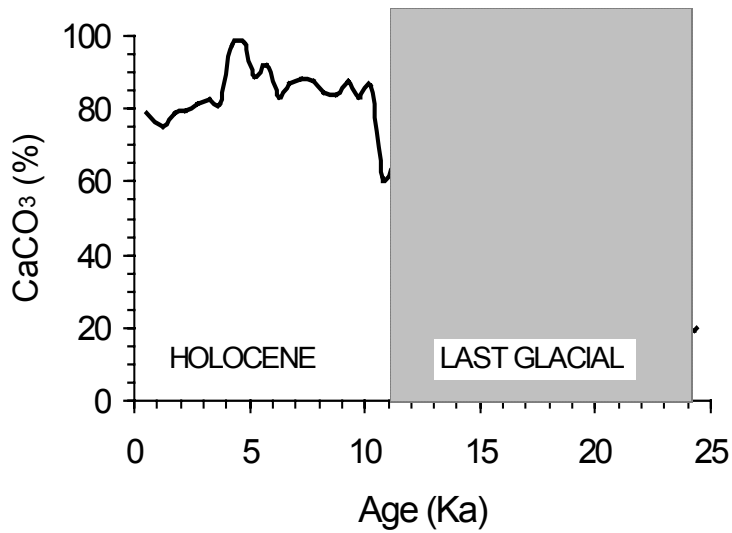


Figure 10: The carbonate variation during the LGP through the Holocene recorded in SK117/GC02 core. Note a drastic increase (from ~20 % to as high as 60 %) in the carbonate content during beginning of the LGP.

#### 5.4.2. Particulate-Mn and scavenged-Al variation (Figure 11):

The particulate Mn-oxide and the detrital silicate unsupported-Al (scavenged-Al) could be the indicators of water column redox conditions and surface water productivity respectively (Banakar et al., 1998; Dickens and Owen, 1994; Murray and Leinen, 1993). The core exhibits highest  $Mn_{excess}$  (~250 ppm) in the earliest part of the LGP decreasing to ~40 ppm at around 15 Ka. Further later, it increases to ~100 ppm in the latest part of the LGP, followed by monotonous decrease to 50 ppm through the Holocene. The  $Al_{excess}$  variation in this core is nearly similar to that of the  $Mn_{excess}$ . The lowest concentration troughs in the time-series are centred ~17 Ka.

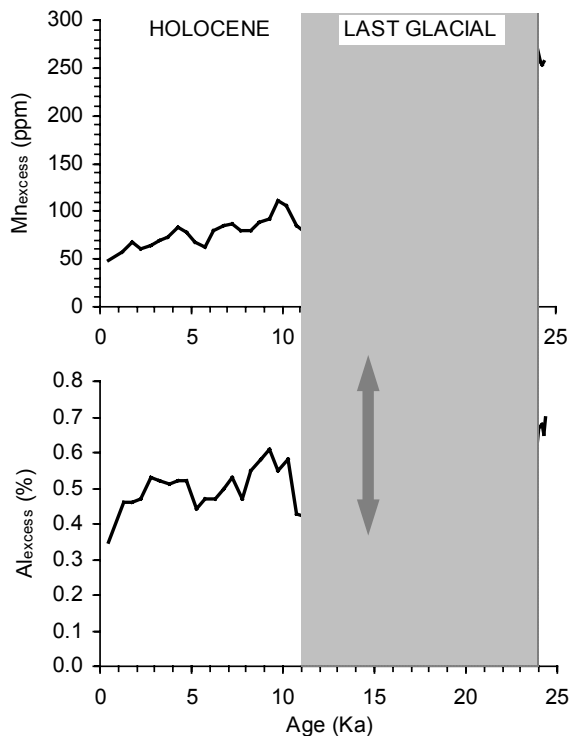


Figure 11: Sedimentary  $Al_{excess}$  and  $Mn_{excess}$  variation in continental shelf core (GC02). The shaded area is the time period covered by the LGP. The double head arrow marks the beginning of increase in excess Al & Mn around the beginning of deglaciation.

#### 5.5. Time-series records of sedimentary organic components:

The data of sedimentary organic components comprising organic carbon ( $C_{org}$ ), total nitrogen ( $N_{tot}$ ), and alkenones was obtained for only one deep-water core (GC08) due to certain analytical constraint. I am aware of this limitation because modern biogenic-flux across the deep Arabian Sea greatly varies in space (Haake et

al., 1993; Nair et al., 1989). Nevertheless, the present data-set for the GC-08 forms the nearly complete climate proxy record and hence should be able to provide important clues regarding EAS responses to past climate variability.

### 5.5.1. Sedimentary organic carbon and nitrogen (Figure 12):

The temporal variation of  $C_{org}$  and  $N_{tot}$  exhibit strictly similar trends as normally expected for the unaltered marine organic matter (Peters et al., 1978). The carbon is enriched nearly by an order of magnitude than the nitrogen. The  $C_{org}$  ranges from 0.5 to 1.8 %, while the  $N_{tot}$  varies between 0.06% and 0.21% in the core. During the major part of the LGP and MIS3 both these components are distinctly higher than the mean contents of 1% and 0.13% respectively in the core. In the MIS3 section the  $C_{org}$  and  $N_{tot}$  attain highest concentrations (up to 1.8% and 0.21% respectively). The  $C_{org}$  content in the Holocene is not only less than the core average, but also is the second lowest average content (~0.8%). Through the MIS4, both the components gradually decrease from ~1.2% and 0.15% to 0.5 % and 0.07 % respectively. The MIS5 stadial exhibits higher  $C_{org}$  and  $N_{tot}$  (~1.2% and 0.16% respectively) than the interstadials (~0.5% and 0.06%). The  $C_{org}$  and  $N_{tot}$  in the LGP are distinctly higher than the Holocene.

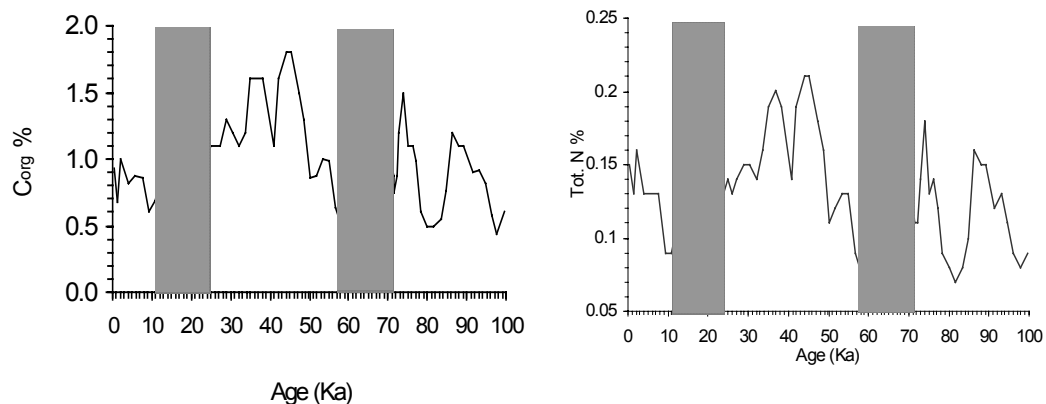


Figure 12: The temporal variation of the sedimentary organic-carbon and total-nitrogen in GC08. The replicated behaviour of these components suggests negligible fractionation. The carbon content is nearly 8 times higher than the nitrogen, nearly in accordance with the Redfield Ratio for marine organic matter (~7).

### 5.5.2. Alkenone variation during the LGP to Holocene (Figure 13):

The temporal variation of the  $\Sigma$ alkenones (sum of di- and tri-unsaturated ketones C37, C38 and C39) exhibit extremely low content in the Holocene section (<0.1 ppm) as compared to very high concentrations up to 1.6 ppm in the LGP. The Holocene-  $\Sigma$ alkenones show nearly constant value (<0.1 ppm), while in the LGP the content ranges between 0.6 ppm (~18 Ka) to ~1.5 ppm (~20 Ka & ~14 Ka). The average  $\Sigma$ alkenones content in the LGP (~1 ppm) is higher by an order of magnitude than the Holocene. The actual rise in  $\Sigma$ alkenones appears to begin around the commencement of the LGP and reaches the peaked concentration at the beginning of the deglaciation.

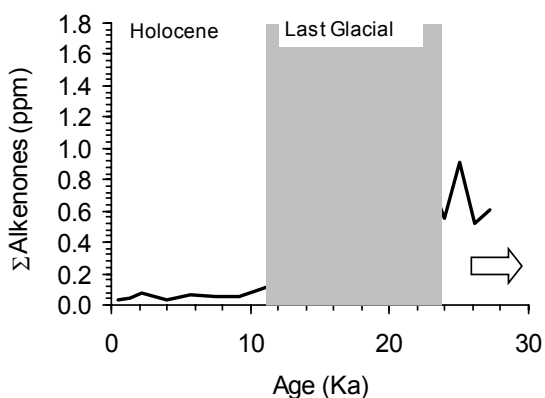


Figure 13: Temporal variation of  $\Sigma$ alkenones during the last 27 Ka in GC08. The concentrations in the LGP sections are enriched by an order of magnitude compared to the concentrations in the Holocene. The block arrow indicates that the MIS3 continues further down-core. The shaded vertical bar is the LGP.

### 5.5.3. Time-series record of organic carbon isotopes ( $\delta^{13}\text{C}_{\text{org}}$ ) (Figure 14):

The temporal variation of sedimentary carbon<sub>org</sub> isotopes is within  $-19\text{‰}$  and  $-17\text{‰}$ . The most depleted  $\delta^{13}\text{C}_{\text{org}}$  are evident around the latest Holocene, mid-MIS3, commencement of MIS4, and at MIS5.2 with a value of  $\sim -19.3\text{‰}$ . The enriched  $\delta^{13}\text{C}_{\text{org}}$  is evident at the commencement of the Holocene ( $\sim -17.7\text{‰}$ ) and at around MIS5.1 ( $\sim -18.1\text{‰}$ ). The  $\delta^{13}\text{C}_{\text{org}}$  curve exhibits steep slopes leading to rapid peak and



troughs. The most prominent and largest excursion of around 2.4 ‰ is noticed in the Holocene section, where the  $\delta^{13}\text{C}_{\text{org}}$  with  $\sim -17$  ‰ at the beginning of the Holocene

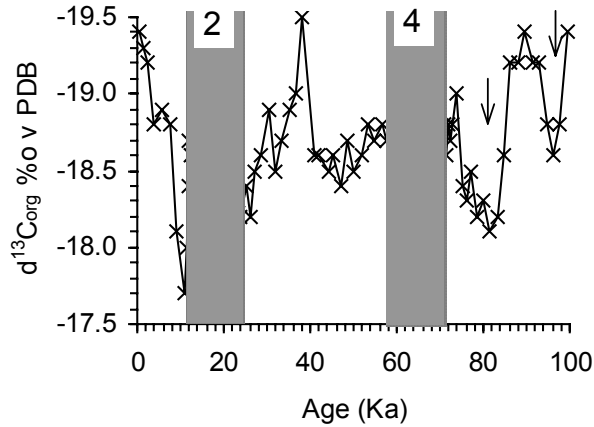


Figure 14: The  $\delta^{13}\text{C}_{\text{org}}$  variation during the last 100 Ky recorded in GC08 core. Equally depleted  $\delta^{13}\text{C}_{\text{org}}$  events are evident at the latest Holocene, mid-MIS3, early-MIS4, and mid-MIS5. The downward arrows indicate higher  $\delta^{13}\text{C}_{\text{org}}$  around the MIS5 interstadials (5.1 & 5.3) than during the stadal (5.2).

decreases to  $\sim -19.5$  ‰ in the latest Holocene (core top) section. Both the interstadials of MIS5 exhibit distinctly enriched  $\delta^{13}\text{C}_{\text{org}}$  than the stadal.

#### 5.5.4. Time-series record of sedimentary nitrogen isotopes ( $\delta^{15}\text{N}$ ) (Figure 15):

The sedimentary nitrogen isotopes ( $\delta^{15}\text{N}$ ) show distinct alternating enrichment and depletion during the last 100 Ky. Similar to the sedimentary organic-

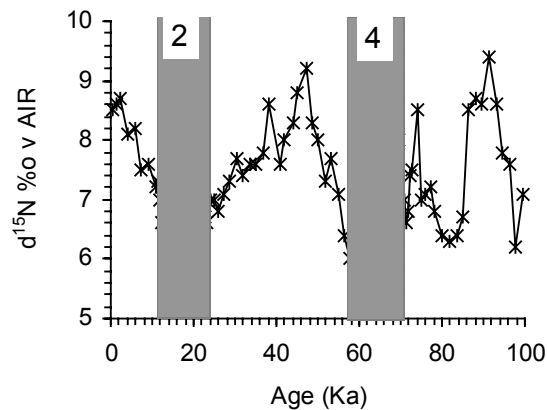


Figure 15: The temporal record of the sedimentary nitrogen isotopes in GC08 core. The variation defines several enrichment and depletion events.

carbon isotopes, the LGP section exhibits near uniform concentration of the  $\delta^{15}\text{N}$  ( $\sim 7$  ‰). Prominent peaks and troughs are evident throughout the pre-LGP period. The lowest  $\delta^{15}\text{N}$  (5.8 ‰) is evident in MIS4 followed by MIS5.1 and MIS5.2 interstadials.

The MIS5.1 and MIS5.2 low  $\delta^{15}\text{N}$  events are separated by a maximum enrichment (9.4 ‰) event centred on MIS5.2. The MIS3 section also contains a prominent peak of enriched  $\delta^{15}\text{N}$  (~9.2 ‰) at ~45 Ka. Through the Holocene the  $\delta^{15}\text{N}$  increases from ~7 ‰ at its commencement to 8.5 ‰ in the recent most (core-top) section. Another important aspect of the  $\delta^{15}\text{N}$ -temporal record is that the enrichment events appear to have spaced at about 45 Ky intervals, if relatively less prominent intruding peak at ~72 Ka is ignored.

#### **5.6. Time-series record of *G. sacculifer* carbon isotopes (Figure 16):**

The temporal record of the calcite carbon isotopes obtained from the skeletons of the *G. sacculifer* exhibit large scatter. Nevertheless, few distinct trends are noticeable. Therefore, to bring-out those trends the data is smoothed by two point running averages.

In the GC-08 core (panel A) the  $\delta^{13}\text{C}_{G.sacculifer}$  variation exhibits a decreasing trend through both the glacial stages (LGP and MIS4), where it decreases from ~1.1‰ at their commencement to ~0.6 ‰ at their closure. A monotonous increase from 0.6 ‰ to 1.05 ‰ is evident through the MIS3. However, during the Holocene and the MIS5 the  $\delta^{13}\text{C}_{G.sacculifer}$  fluctuations are rather gentle (within  $\pm 0.3$  ‰) around an average of 0.9 ‰. These minor fluctuations within both the warm periods do not exhibit any discernible trends. The lowest  $\delta^{13}\text{C}_{G.sacculifer}$  are evident around 13 Ka and 56 Ka.

The  $\delta^{13}\text{C}_{G.sacculifer}$  variation in CR04 core (Panel B) is more complex. The fluctuations through the last ~100 Ky are within a narrow margin of  $\pm 0.3$  ‰ around an average of ~1.2 ‰. The MIS4 exhibits minimum variation of <0.2 ‰ as compared to the rest of the 100 Ky time-span. The most interesting and the prominent feature in this core is a major positive shift from ~0.6 ‰ at ~128 Ka, to ~1.3 ‰ at ~100 Ka. This 0.7 ‰ shift is nearly double than those recorded in other time-slices in the core

and marks a major event in the last 150 Ky  $\delta^{13}\text{C}_{G.sacculifer}$ -record. Prior to this shift, in the latest part of the MIS6, the  $\delta^{13}\text{C}_{G.sacculifer}$  remains  $\sim 0.8$  ‰ with a fluctuation of  $\pm 0.3$ ‰. Thus there are two levels of  $\delta^{13}\text{C}_{G.sacculifer}$  trends in the core, viz., the enriched  $\delta^{13}\text{C}$ -trend ( $\sim 1.2$  ‰) during post-100 Ka period, and depleted  $\delta^{13}\text{C}$ -trend (0.8 ‰) prior to the Glacial Termination 2 (GT2) (or the commencement of MIS5 warm period). Thus the GT2 marks a major positive shift in the calcite carbon isotopes.

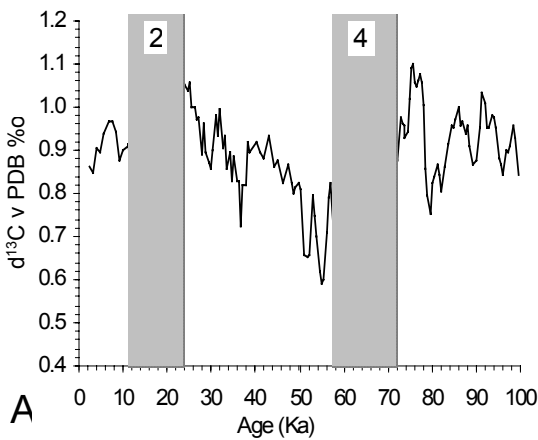
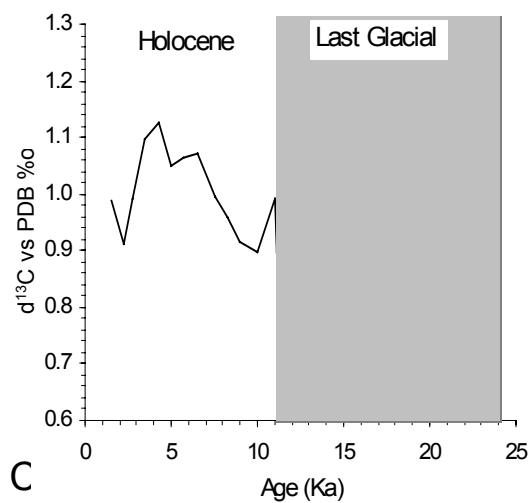
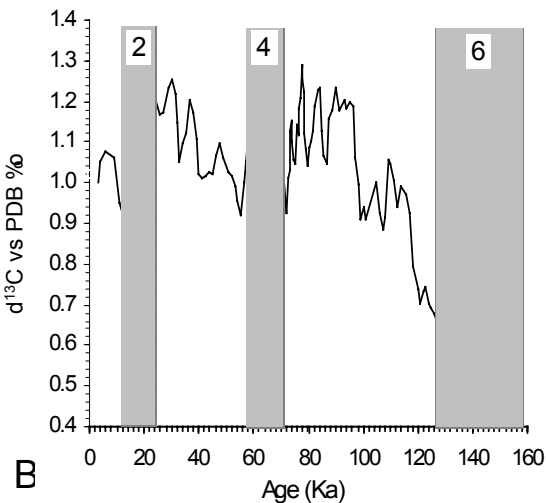


Figure 16: Time-series *G.sacculifer* calcite- $\delta^{13}\text{C}$  record in the Eastern Arabian Sea sediment. The two long-term records of the deep-water cores (A & B) exhibit nearly comparable temporal variation suggesting robustness of the carbon-isotopic record despite large fluctuations. The last glacial fluctuations appear more complex than during the Holocene in the high-resolution record of the GC02 core. Note a major positive shift of the  $\delta^{13}\text{C}_{G.sacculifer}$  at the Glacial Termination 2 through the MIS5 in the CR4 (B). Panel A = GC08, Panel B = CR04 and Panel C = GC-02.



The high-resolution  $\delta^{13}\text{C}_{G.sacculifer}$  curve in GC02 core does not exhibit any distinct variations (Panel C). The overall range of variation is between 0.8 ‰ and 1.2 ‰ with an average of 1 ‰. The Holocene record contains a gradual change with only one  $\delta^{13}\text{C}_{G.sacculifer}$ -enriched event of ~1.1 ‰ at ~5 Ka flanked by two -depleted events of 0.9 ‰ at ~2 Ka and ~10 Ka. The later half of the LGP (17-11 Ka) contains high frequency fluctuations of  $\pm 0.4$  ‰. In contrast the earlier half of the LGP shows a gradual variation within  $\pm 0.2$  ‰.

## 6. Discussion

In this section, sedimentary responses of the Holocene-Glacial period are presented first, as this record is available for all the three sediment cores, followed by the discussion on long-term responses based on the two deep-water cores (GC08 & CR04). As mentioned in the previous section, the multi-proxy data of the GC08 core are considered as the central evidences for the cumulative response of the EAS to climate change. The emphasis is given on themes of coupled responses rather than discussing each core individually based on each proxy, as the present cores provide an opportunity for a comprehensive understanding of changes in the entire EAS. The relevant data is provided at the end as Appendix. To extract the information on past changes in local E-P or salinity, the  $\delta^{18}\text{O}$ -correction required for subtracting the global ice-volume (or global sea level) effect from the composite calcite- $\delta^{18}\text{O}$ , the presently available most precise sea level reconstruction by Shackleton (2000) (Figure 17) has been used.

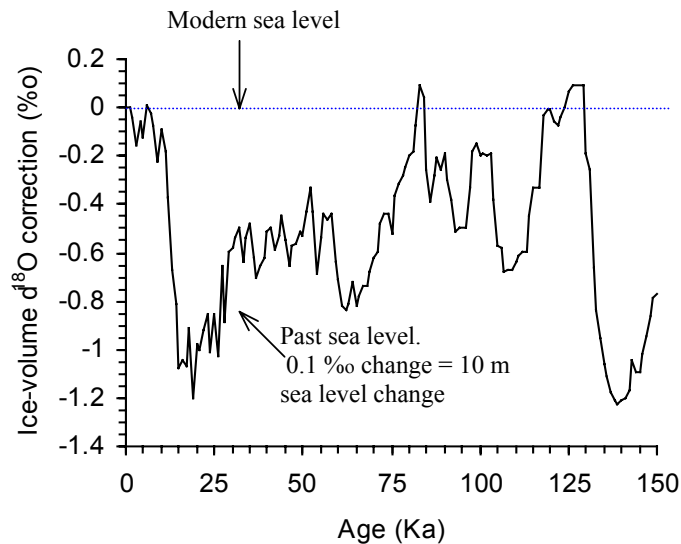


Figure 17: The seawater  $\delta^{18}\text{O}$  variation due to global ice-volume or sea level variation through time (Shackleton, 2000). This curve was used for correcting the *G.sacculifer*  $\delta^{18}\text{O}$  data for global ice effect.

### 6.1. $\delta^{18}\text{O}_{G. \text{ sacculifer}}$ , salinity, and monsoon linkage:

Variations in the Indian summer monsoons produce dramatic changes in sea surface salinity (hereafter salinity) structure because the salinity adjustment between the high-salinity Arabian Sea and low-salinity BOB largely depends upon the seasonally reversing monsoon system (Prasad, 2001; Prasannakumar and Prasad, 1999; Shetye et al., 1991). Therefore, the salinity budget of those two basins is dependent upon the annual variation of the E-P (Prasad, 2001). Irrespective of the mode of salt-exchange between the two basins such as, complex cross-equatorial mode of exchange through cross-equatorial cell (Jensen, 2001; 2003), or straightforward exchange between the two basins by reversing rhythmic monsoon surface circulations (Shankar et al., 2002; Shetye et al., 1991), the summer precipitation and winter evaporation largely determine the salt-budget in the region.

On one hand, the Quaternary monsoon system of the Arabian Sea was shown to have responded to the changing solar radiation or insolation pattern that has caused the glacial-interglacial cycles (Prell, 1984); on the other hand, the variation in the monsoon associated tropospheric aerosols derived from the Asian and the Arabian continents are believed to have played a major role in triggering the Dansgaard-Oeschger type rapid climate fluctuations recorded in the Greenland ice-cores (see Overpeck et al., 1996). The connection between the Greenland climate fluctuations and the Arabian Sea monsoon climate has been identified beyond reasonable doubt (Schulz et al., 1998; Hong et al., 2003). These studies indicate the importance of the Indian monsoons as a feedback for the global climate oscillations.

The planktonic foraminifera calcite oxygen isotopes have been the main source of information generated so far on the past variations in Indian monsoons in response to climate change (see Duplessy, 1982; Naidu and Malmgren, 1996; Niitsuma et al., 1991; Kutzbach et al., 2000; Rostek et al., 1997; Sarkar et al., 2000a & b, and references therein). The  $\delta^{18}\text{O}$  of foraminiferal calcite secreted in equilibrium with the ambient seawater contains three climatic signals (details in Methods

section). They are, changes in the volume of global continental ice, local-SST and local-salinity (Epstein et al., 1953; Shackleton and Opdyke, 1973). The effect of global ice volume remains uniform throughout the world oceans. Where as, the SST and salinity largely depend upon the local processes. Urey (1946) estimated a change of 0.2 ‰ calcite- $\delta^{18}\text{O}$  for every 1°C change in ambient water temperature, which has been confirmed by several subsequent culture experiments. On the other hand, the salinity and calcite- $\delta^{18}\text{O}$  relationship appears more complex and region specific (Delaygue et al., 2001; Duplessy, 1982; Rostek et al., 1993). However, the salinity and the seawater- $\delta^{18}\text{O}$  in general are directly related (Delaygue et al., 2001). When the ice-volume effect is global in nature and the past-SST variation in the EAS region is nearly uniform (Cayre and Bard, 1999; Sonzogni et al., 1998; Rostek et al., 1997), then the time-series planktonic calcite- $\delta^{18}\text{O}$  corrected for global ice volume should be able to reflect the local salinity variation over the time covered by the present sedimentary records. Even though the off-Goa cores (GC-02 and GC-08) do not exactly represent the northern-EAS, for convenience and clarity they are considered as northern cores in relative sense with the southern-EAS core (CR-04) (Figure 1).

The modern salinity in the GC-02 and CR-04 locations is nearly similar ~34.8 psu, while at the GC-08 location is ~35.8 psu (Levitus and Boyer, 1994 and NOAA Web, 2002). Where as, the annual average SST is similar at all the three locations (~28°C). In such a surface hydrographic set-up the core-top  $\delta^{18}\text{O}_{G.sacculifer}$  should also reflect an agreement with the local salinity. The former two core-top  $\delta^{18}\text{O}_{G.sacculifer}$  are nearly similar (-1.83 ‰ and -1.82 ‰ respectively), and lighter than the core-top value of the GC-08 (-1.37 ‰; Figure 18 A and 2, 3, 4) suggesting low-salinity regime in the former two core locations and high-salinity regime in the latter location in accordance with the modern salinity set-up. Therefore, the time-series  $\delta^{18}\text{O}_{G.sacculifer}$  difference (contrast) between these cores may effectively demonstrate the changes

in salinity regime through time. Thus, the ice-corrected (hereafter 'residual')- $\delta^{18}\text{O}_{G.sacculifer}$  would reasonably depict the local salinity changes. The EAS experiences in general, mixing of two salinity end-members in the upper mixed layer. They are, the high salinity end-member ASHSW originating due to excess evaporation (>E-P) in the northernmost Arabian Sea, and the low salinity end-member BOB-water originating in the northern BOB due to excess freshwater flux. The presence of these two end-members spreading in opposite directions as two distinct salinity fronts (Prasannakumar and Prasad, 1999; Shetye et al., 1993) result over 2 psu salinity difference between the northernmost and southernmost Arabian Sea (Figure 1). The low salinity BOB-water advected in to the EAS by the PCC is dominant source of freshening the modern EAS. The PCC is also responsible for sharply deflecting the zonally (E-W) trending isohalines towards north in the EAS (see Wyrki, 1973; Prasannakumar and Prasad, 1999; Duplessy, 1982, and references there in) (Figure 1). The northward deflection of the isohalines is the characteristic of the EAS. Therefore, any shift in the salinity pattern in the EAS should have a direct link with the relative importance of ASHSW and BOB-fresh water input (PCC) in maintaining the salinity balance in the region.

The full-Holocene/LGP averaged residual- $\delta^{18}\text{O}_{G.sacculifer}$  contrasts in the three cores is  $0.7 \pm 0.1$  ‰, wherein the northern-EAS deep-water core GC-08 shows highest contrast of 0.8 ‰ and southern-EAS deep-water core CR-04 shows lowest contrast of 0.6 ‰ (Figure 18 B) suggesting that the northern region has witnessed relatively higher salinity change than the southern region during the last 24 Ka. When the Holocene-peak and LGM-peak are considered, that contrast is much larger (>1‰). The inter-location (i.e., between the cores) residual- $\delta^{18}\text{O}_{G.sacculifer}$  contrasts during the past relative to the present can be used to understand the EAS-characteristic isohaline shift. To appreciate the following discussion, it may be necessary to characterize the locations of the sediment cores.



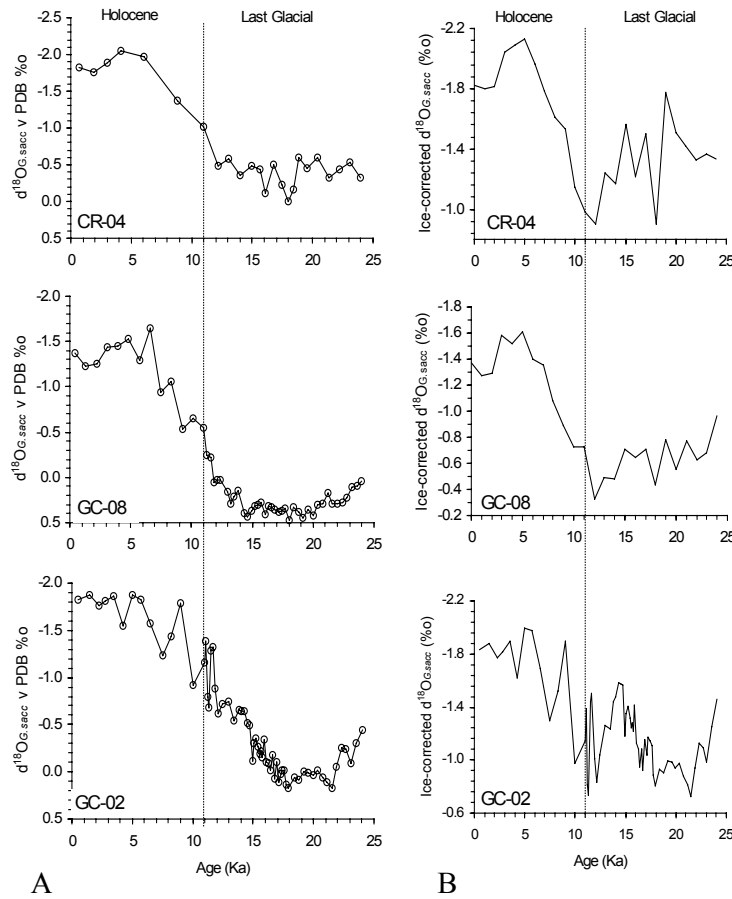


Figure 18: Holocene-Last Glacial Period variation of  $\delta^{18}O$  in three EAS sediment cores (A), and their respective global ice-volume corrected patterns (B). The ice-volume corrected  $\delta^{18}O$  would provide the record of the relative changes in the local salinity, when the modern SST and its past variations are considered to be nearly uniform in the region.

The CR04 and the GC02 are located in the southern and northern portion of the low-salinity tongue respectively. The GC08 is located around 200 km west of the GC02 and comes under the influence of southward spreading ASHSW. Though it is very difficult to isolate the GC08 totally from the influence of the low-salinity tongue, the salinity structure of the basin suggests that its location has dominant influence of the ASHSW than the influence of the low salinity tongue. These location-characteristics are clearly reflected in the relatively heavier  $\delta^{18}O_{G.sacculifer}$  in GC08 core-top than the nearly similar  $\delta^{18}O_{G.sacculifer}$  in CR04 and GC02 core-tops (Figure 18A). The full-Holocene residual- $\delta^{18}O_{G.sacculifer}$  contrast between northern-EAS deep- and shallow-water cores (GC08 & GC02 respectively) and northern- and southern-EAS deep-water cores (GC08 & CR04 respectively) are similar  $\sim 0.45$  ‰. Whereas, that difference between the northern-EAS shallow-water (GC-02) and southern-EAS

deep-water (CR-04) cores is minimum ( $\sim 0.1$  ‰). These differences in  $\delta^{18}\text{O}_{G.sacculifer}$  clearly suggest that the location of GC08 is under high salinity regime and the locations of CR04 and GC02 are under the low salinity regime throughout the Holocene. That is, the PCC effect is distinctly visible all along the near-coast region of the EAS through the entire Holocene. These Holocene residual- $\delta^{18}\text{O}_{G.sacculifer}$  patterns change during the LGP. The differences between the northern deep-water (GC08) and southern deep-water (CR04) cores increases to  $\sim 0.8$  ‰ and the northern shallow-water (GC02) and southern deep-water (CR04) cores increases to  $\sim 0.3$  ‰ (Figure 18 B). These shifts in residual- $\delta^{18}\text{O}_{G.sacculifer}$  contrasts towards higher values between northern and southern regions probably indicate that the northward deflection of the isohalines in the EAS has reduced during the LGP and they were mostly in east-west direction aligning with the general zonal trend across the Arabian Sea. In the northern-EAS continental shelf core (GC02), the signals of fresh water input from the Deccan Rivers might have also been incorporated. Therefore, the emphasis is given to the changes observed in the two deep-water cores because their locations are considerably away from the direct influence of the Deccan River discharge. Additionally, these two cores are well suited to understand the relative variation between two salinity end-members viz., ASHSW (high salinity northern end-member) and PCC activity (low-salinity southern end-member).

After having recognized the overall changes in the salinity regime through residual- $\delta^{18}\text{O}_{G.sacculifer}$  contrasts during the Holocene-LGP, a salinity contrast curve for the past 100 Kyr utilizing northern- and southern-EAS deep-water cores (GC-08 & CR-04 respectively) is constructed. This curve may help understanding the changes in salinity structure in the EAS due to variations in inter-basin communication through characteristic SMC and WMC-PCC circulation driven by the climate sensitive Indian monsoon system.

The  $\delta^{18}\text{O}_{G.sacculifer}$  of both the cores were first interpolated to 1 Ky time-scale to match the Shackleton's (2000) ice-volume correction curve (Figure 17). Then the ice-volume correction was applied to each interpolated data-point of both the cores to obtain residual- $\delta^{18}\text{O}_{G.sacculifer}$  (Figure 19).

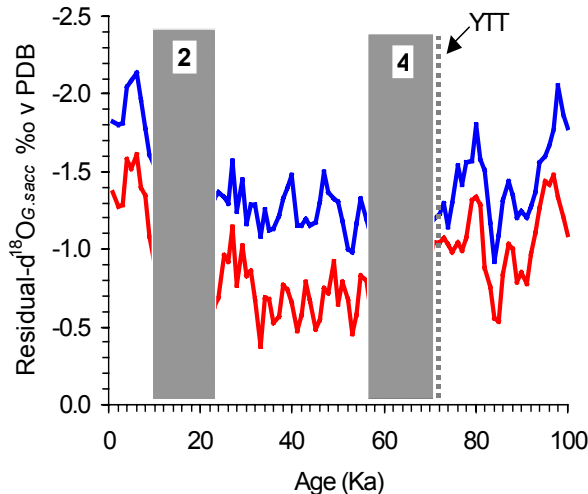


Figure 19: The ice-volume corrected (residual)- $\delta^{18}\text{O}_{G.sacculifer}$  curves for the northern (GC-08: red) and southern (CR-04: blue) sediment cores. The consistently heavier isotopic curve of the northern core than the southern core clearly indicates high-salinity regime in the former location throughout the last 100 Ky than in the latter location. Therefore, the time-series contrast between these two records should be able to demonstrate the changes in past-salinity gradient in the EAS region.

The time-series residual- $\delta^{18}\text{O}_{G.sacculifer}$  records (Figure 19) are comparable to the palaeosalinity curves reconstructed for the southern-EAS (see Rostek et al., 1993) and the BOB (see Kudrass et al., 2001). This similarity suggests that, a) the time-series residual- $\delta^{18}\text{O}_{G.sacculifer}$  variations in the present cores are largely the responses of regional salinity changes in the past, and b) the differences in past-SSTs in space and time within the EAS were not significantly different (Sonzogni et al., 1998), hence uniform effect of the site-specific SST component on  $\delta^{18}\text{O}_{G.sacculifer}$  of the EAS. Additionally, the residual- $\delta^{18}\text{O}_{G.sacculifer}$  in the northern-EAS remains heavier than in the southern-EAS throughout the last 100 Kyr suggesting that the former location has been perennially under high-salinity than the latter location.

The residual- $\delta^{18}\text{O}_{G.sacculifer}$  in the northern-EAS is  $-1.6\text{‰}$  at around the peak-Holocene ( $\sim 6\text{ Ka}$ ) and  $-0.4\text{‰}$  at around the LGM, while the southern-EAS records  $-2.1\text{‰}$  and  $-1\text{‰}$  respectively (Figure 19), i.e., a contrast of  $\sim 1.1\text{‰}$ . This contrast, in addition to local salinity change contains the LGM-SST drop of  $\sim 2^\circ\text{C}$  particularly in the vicinity of our core locations (Cayre and Bard, 1999; Sonzogni et al., 1998; Rostek et al., 1997). A similar lowered SST of  $\sim 2\text{ }^\circ\text{C}$  during the LGM was also obtained by  $\text{U}_K^{37}$  - thermometry for the northern-EAS core (GC-08).

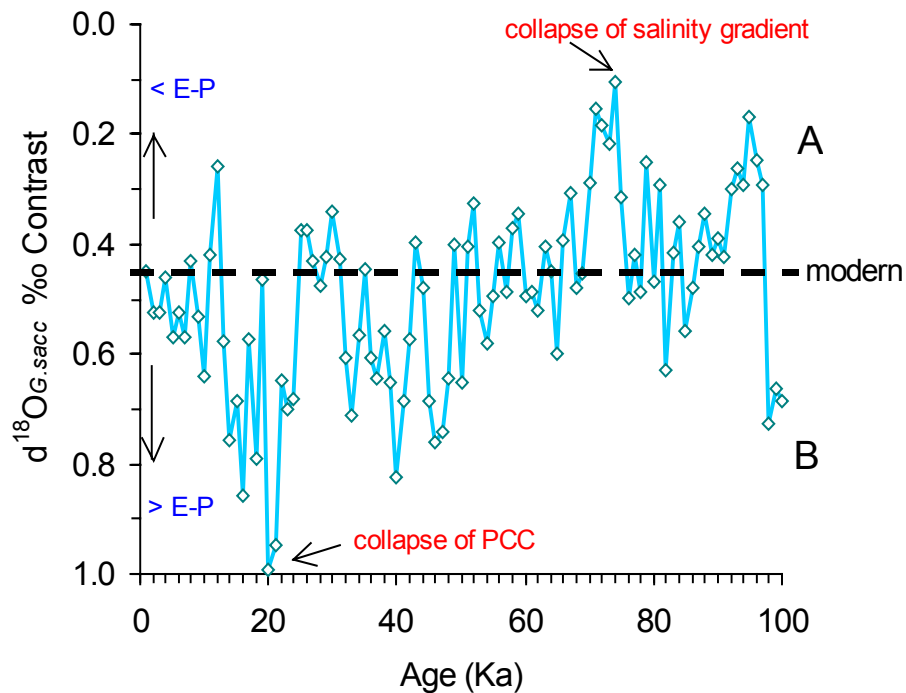


Figure 20: Residual- $\delta^{18}\text{O}_{G.sacculifer}$  contrast between northern- and southern -EAS derived using GC08 & CR04 sediment cores. The horizontal dashed-line indicates the modern contrast as recorded by the core-top sections. The lower sector 'B' marks the increased E-P (or reduced summer monsoon rains), and the upper sector 'A' marks the reduced E-P (or increased summer monsoon rains) than the modern conditions in the region.

A  $2^\circ\text{C}$  SST drop during the LGM would increase the *G. sacculifer* calcite- $\delta^{18}\text{O}$  by  $\sim 0.4\text{‰}$  (Duplessy et al., 1981). Subtracting this SST-effect from the residual- $\delta^{18}\text{O}_{G.sacculifer}$  contrasts yields a remainder of  $\sim 0.7\text{‰}$  accountable for the Holocene-LGM local salinity change. The  $\delta^{18}\text{O}_{G.sacculifer}$  contrast of  $\sim 0.45\text{‰}$  between the two

core tops (see Figure 20) can be considered as a measure of modern salinity difference of ~1 psu between those two corresponding locations. Then, a 0.7 ‰ Holocene-LGM contrast would translate in to ~1.5 psu salinity change at both the locations, which approximately in agreement with the overall salinity increase of ~2 psu during the LGM in the only available past-salinity record from the entire Arabian Sea region (MD900963 from the southern-EAS: Rostek et al., 1993, see Figure 1). This general agreement between the present averaged isotopic records and the previously published salinity reconstructions indicates the level of confidence with which the present residual- $\delta^{18}\text{O}_{G.sacculifer}$  could represent the past salinity variation in the study region.

Considering the surface hydrography in the EAS, the fluctuations in the north-south residual- $\delta^{18}\text{O}_{G.sacculifer}$  contrast can be associated with the relative variations in the intensity ASHSW and BOB-freshwater influx (PCC strength), in turn the monsoon intensity. Because, the northern Arabian Sea origin ASHSW and the southern Arabian Sea origin low salinity tongue caused by the BOB-water influx are solely responsible for the salinity structure of the EAS. Hereafter, the residual- $\delta^{18}\text{O}_{G.sacculifer}$  contrast is often referred as the 'salinity contrast' for clarity, because the SST variations in the past over the region are assumed to be nearly uniform (Cayre and Bard, 1999; Rostek et al., 1997; Sonzogni et al., 1998), which have contributed regionally more or less similar temperature sensitive signals.

The average salinity-contrast is highest for the LGP ( $\delta^{18}\text{O}_{contrast} \sim 0.7 \text{ ‰}$ ), high for the Holocene and MIS3 ( $\delta^{18}\text{O}_{contrast} \sim 0.5 \text{ ‰}$ ), moderate for the MIS4 and MIS5.2 ( $\delta^{18}\text{O}_{contrast} \sim 0.4 \text{ ‰}$ ) and lowest for MIS5.1 and MIS5.3 ( $\delta^{18}\text{O}_{contrast} \sim 0.2 \text{ ‰}$ ), which translate in to overall variation within ~1.5 psu in the last 100 Ky, considering the core-top contrast of 0.45 ‰ as an equivalent of the modern salinity difference of ~1 psu between those locations. In other words, the geographical salinity contrast between northern- and southern-EAS during the LGP was highest ~1.5 psu, while

during the interstadials of MIS5 was nearly half of the modern contrast, suggesting at the outset a largest salinity gradient during the former period and smallest gradient during latter period. However, the time-series salinity-contrast profile contains much larger amplitude oscillations ( $\delta^{18}\text{O}_{\text{contrast}}$  of 0.1 ‰ to 1 ‰) on shorter time-scales (<5 ky: Figure 20), suggesting rapid and much greater changes in the past salinity gradient in the EAS region accounting for an order of magnitude fluctuations (i.e., the salinity gradient varied between a minimum of ~0.2 psu and a maximum of ~2.2 psu as compared today's ~1 psu).

Before invoking the probable causes for fluctuations in the salinity-contrast between northern- and southern-EAS, it is necessary to identify the dominant contributing factors to the salinity changes at each of those two locations. Assuming nearly uniform effect of overhead precipitation due to vigorous surface circulations in the region, the northern location salinity change can be influenced largely by both the ASHSW and PCC. On the other hand, the variation in the intensity of WMC-PCC carrying BOB-low salinity water alone can affect the salinity change in the southern location, since the influence of ASHSW on the surface salinity structure gradually diminishes due to gradual sinking along with its southward advection. By the time the ASHSW reaches the southern-EAS region its influence is limited to the depth beyond the mixed layer (see Prasannakumar and Prasad, 1999). Keeping this modern hydrographic set-up as a framework, the changes in the geographical salinity-contrast between northern- and southern-EAS (within the low-salinity tongue), therefore could be the result of relative changes in the activity of two salinity end-members viz., ASHSW (high-salinity end-member) and WMC-PCC (low salinity end member).

The north-south salinity-contrast in the EAS would increase when the northern location comes under enhanced influence of ASHSW, and the contrast would decrease when it comes under the enhanced influence of PCC. The alternative combinations, which hypothetically can produce the changes in the

salinity-contrast are, 1) increased influence of ASHSW on northern location and WMC-PCC on southern location would increase the contrast, and 2) decreased influence of ASHSW on northern location and WMC-PCC on southern location would reduce the contrast. The simultaneously increased or decreased influence of the ASHSW on northern location and PCC on southern location at a given time is not possible considering the hydrographic set-up in the EAS, because, they operate in opposite sense to reduce the effect of each other on the northern location. In that an increased PCC would automatically reduce the influence of ASHSW on northern location. On the other hand, the intensified ASHSW will not have any significant influence in southern location mixed layer. Intensified PCC means the strengthening of the low salinity tongue, is associated with the intensified summer monsoons. Therefore, when the ASHSW intensifies (reduced freshwater flux or  $>E-P$ ) the north-south salinity-contrast in the EAS is increased and when the WMC-PCC is intensifies (increased freshwater flux or  $<E-P$ ) the contrast is decreased. This concept provides the preamble for understanding the past variation in the summer monsoon intensity utilizing the salinity-contrast between northern and southern regions of the EAS.

Presently the annular evolution of the summer monsoon is the main force driving almost all circulation changes in the northern Indian Ocean, where weak winter monsoons have less significant role (see Shankar et al., 2002). However, the Indian monsoons have witnessed dramatic changes during the LGP. For example, a) mean position of the summer monsoons is believed to have shifted southward resulting in reduced time-span of summer monsoons (Sirocko et al., 1991), and b) the CLIMAP-GCM models when forced with glacial boundary conditions such as reduced SST, increased continental albedo, and decreased atmospheric  $CO_2$ -level, resulted over 30% reduced southerly wind velocity and summer monsoon precipitation (Prell and Kutzbach, 1992), suggesting significantly weakened summer monsoons. The additional supports for weakened summer monsoons during the glacial periods emerge from, 1) large scale climate models for the modern conditions have

suggested that an intense winter and extended snow cover over the Tibet and Himalayas during the spring (generally expected scenario of glacial climate) delays and weakens the following summer monsoon (Yang, 1996), and 2) minimum surface water- $\delta^{18}\text{O}$  contrast between the Arabian Sea and the BOB during the LGP (Duplessy, 1982) suggested greatly reduced fresh water transfer from the Arabian Sea to the Indian sub continent (Schulz et al., 1998). Within the LGP sections of the sedimentary records from the northern Indian Ocean, the indications of enhanced sea surface salinity based on faunal analysis (Cullen, 1981) and oxygen-isotope based reconstructions (Rostek, 1993), and dominant Mediterranean type pollens characteristic of arid climate (Van Campo et al., 1982) strongly suggest either the intensification of winter monsoons or winter monsoons were the only dominant seasonal feature.

The increased salinity contrast between the northern and southern region of the EAS during the LGP appears to have associated therefore with greatly diminished fresh water input from the BOB and Deccan Rivers responsible for freshening the northern region. Near disappearance of the low salinity tongue along the west coast of India during the LGM (see 18 Ka salinity gradient for the Arabian Sea in Duplessy, 1982) not only supports the above interpretation but also suggests broken communication between the Arabian Sea and the BOB. All these evidences are clearly in contrast with the previously hypothesised intensification of low-salinity BOB water transfer into the Arabian Sea during the LGM (Sarkar et al., 1990). The southward shift of the summer monsoon mean-axis during the LGM (Sirocko et al., 1991) appears to have still maintained low salinity regime in the southern region of the EAS despite the collapse of inter-basin communication but by summer monsoon overhead precipitation. The southward shift of the summer monsoon axis also potentially has to result in significant increase of E-P in the northern region by reduced precipitation there. Such variation through time may have been responsible for maintaining the observed high-salinity regime in the northern EAS and the low-



salinity regime in the southern EAS. In fact, the CLIMAP models have shown that the western equatorial Indian Ocean has received increased precipitation during most of the glacial periods of the last 150 Ky (Prell and Kutzbach, 1987). The present study and previous models indicate that in spite of weakened summer monsoons during climate cooling cycles affecting both the basins and Indian subcontinent, the sustained equatorial precipitation has kept the CR04 core location in the southern-EAS out of the freshwater drought unlike in GC08 core location.

The dominant winter monsoon winds during the glacial periods are expected to enhance the formation of the ASHSW in the northern Arabian Sea due to increased E-P. The cumulative effect of such meteorological and hydrographic changes is to enhance the salinity build-up in the northern-EAS as compared to the southern-EAS. The increased salinity contrast during the LGM therefore was due to reduced freshening of the Arabian Sea and BOB due to weakened summer monsoon precipitation. The alongshore pressure gradient in the EAS (Shetye et al., 1991) might have decreased due to weakened summer monsoons during the LGM resulting in the diminished low-salinity tongue (or PCC) due to reduced flow of low-salinity BOB water (Shankar et al., 2002; Shetye et al., 1990; 1991). The diminished low-salinity tongue of the LGM thus not only rendered the northern-EAS to come under the increased influence of the intensified ASHSW, but also reduced the northward deviation of the isohalines in the region (see Duplessy, 1982).

The strengthening of the summer monsoon should result in reduced salinity contrast between northern- and southern-EAS. This reasoning is in agreement with both the summer monsoon influence on circulation of the Arabian Sea and the glacial-interglacial monsoon variations. During the interglacial periods both the basins were well connected and the BOB was significantly fresher than the glacial periods, hence an enhanced increase of the salinity in southern location relative to northern-EAS is not at all feasible. These observations and reasoning provide a clear scenario for the EAS that, the north-south salinity contrast fluctuations within the low-

salinity tongue of the EAS through time have been the summer monsoon forced changes in the intensity of ASHSW and PCC at the northern location. Therefore, the variation in the geographical salinity contrast of the EAS region has monitored the past changes in the Indian summer monsoon intensity, in that intense summer monsoons resulted in reduced salinity-contrast, while the weakened summer monsoon resulted in increased salinity-contrast. The high-frequency high-amplitude fluctuations in the salinity-contrast observed within the main climate events prior to the Holocene (Figure 20) might be indicative of the instability of the past summer monsoons.

Various palaeoceanographic records and models suggest that the Asian monsoon system was established by the late Miocene when the Himalayan mountains attained half of their present height probably following the main boundary thrust at ~10 Ma (Banakar et al., 2003) to induce characteristic monsoon circulations (Filippelli, 1997; Prell and Kutzbach, 1992). Even though the monsoons established long before, their unstable nature appears to be rather a rule than exception because most of the last 100 ky time period covered under this study has witnessed highly irregular summer monsoons on millennial time-scale. However, the Holocene period is devoid of such high frequency-high amplitude oscillations in the salinity-contrast variation (Figure 20) suggesting significantly stabilized monsoon regime since it's beginning. Considering the coherent behaviour of the summer monsoons with the D-O type Greenland Climate fluctuations (see Leuschner and Sirocko, 2000; Schulz et al., 1998), the observed instability in the pre-Holocene salinity-contrast further may lend a support for the above link. However, it is not possible to identify those individual D-O type high-frequency climate events in the present sedimentary record of the salinity-contrast due to poor time-resolution.

From Figure 20 it is also evident that on several occasions during the last 100 kyr EAS has witnessed more intense summer monsoons than the Holocene. The closing of the last warm period (MIS5: ~73 Ka) appears to have forced near collapse of the

salinity gradient in the EAS as evident in lowest salinity-contrast ( $\delta^{18}\text{O}_{\text{contrast}} \sim 0.1 \text{ ‰}$ , i.e., equivalent to just over 0.2 psu salinity contrast), probably due to very intense summer-monsoons, and vigorous PCC than today, i.e., greatly intensified and significantly expanded low-salinity tongue in the EAS. The warmest MIS5 and the coldest LGM ( $\sim 20 \text{ Ka}$ ) mark two extreme summer monsoon scenarios in the EAS as evident in respectively lowest and highest salinity-contrasts ( $\delta^{18}\text{O}_{\text{contrast}} : \sim 0.1 \text{ ‰}$  and  $1 \text{ ‰}$ ). The latest intensification of the summer-monsoon precipitation and strengthening of the PCC has taken place with commencement of the Holocene evident in the reduced salinity-contrast ( $\delta^{18}\text{O}_{\text{contrast}}$  from  $\sim 1 \text{ ‰}$  at LGM to  $\sim 0.3 \text{ ‰}$  at  $\sim 11 \text{ Ka}$ ; i.e, from  $\sim 2.2 \text{ psu}$  to  $\sim 0.6 \text{ psu}$  (Figure 20). As mentioned earlier the fully developed Holocene (since  $\sim 8 \text{ Ka}$ ) has experienced more stable summer monsoons and the PCC activity as evident in marginal variation of the salinity-contrast within  $< 0.4 \text{ psu}$  (i.e., residual- $\delta^{18}\text{O}_{\text{contrast}} < 0.15 \text{ ‰}$ ). This observation appears to be in disagreement with the earlier studies, which have invoked large fluctuations in the strength of the summer-monsoon precipitation during the Holocene (Thamban et al., 2001), and E-P (Sarkar et al. 2000). However, unless some kind of quantification of the relative changes in the monsoon precipitation and the corresponding salinity-contrast variation in the EAS is achieved, it may be difficult to assess the actual variation in the past summer monsoon intensity. It is interesting to note from Figure 20 that after the collapse of the salinity gradient in the EAS due to extremely intense summer monsoons at the interstadial MIS5.1 ( $\sim 73 \text{ Ka}$ ) has quickly re-established to the modern level within around 5 Ky (i.e., the commencement of MIS4). The near collapse of the salinity gradient during the last warm period (MIS5) may also suggest exceptionally vigorous surface water exchange between the Arabian Sea and the BOB. The period between  $\sim 73 \text{ Ka}$  and  $\sim 25 \text{ Ka}$  has witnessed moderate fluctuations in the summer monsoon intensity as evident in moderate variations in the salinity-contrast. Most of the last glacial cycle (LGP+MIS3+MIS4) has witnessed weaker

summer monsoons than the Holocene. (See the cartoon on next page for the likely scenario of the salinity structure in the EAS with varying PCC or the low-salinity tongue)

## **6.2. Silicate-detritus in sediment and summer rains on land:**

In the previous section a relationship of past salinity-contrast fluctuations in the EAS with the summer monsoon intensity is brought out. The summer monsoon rains on the Indian peninsula feed large network of seasonal rivers rapidly draining the Deccan Mountains, which discharge considerable amount of fresh water and silicate-detritus in to the EAS (over 73 km<sup>3</sup>/y: Rao, 1979). Therefore, it is possible to understand the past changes in the summer monsoon intensity utilizing the strength of the Deccan Rivers as means. The variation in the intensity of the Deccan Rivers can be assessed by their ability to erode the drainage area. In other words, the abundance of the coarse silicate material they transport to the continental shelf region depends on their strength. By monitoring the sediment grain-size variation through time at a location of the continental shelf in the proximity of discharge point of any Deccan Rivers, one can qualitatively assess the past variation in the strength of those rivers. Here, utilizing the time-series variation in volumetric changes of grain-size of the GC02 core in three size-windows (2 μm, 10 μm, and 100 μm), an attempt is made to reconstruct the past erosion strength of the Deccan rivers vis-à-vis summer monsoon intensity. One such river couple, viz., Mandovi-Zuari, which discharges around 1.3 km<sup>3</sup>/y of freshwater in to the EAS off Goa, is considered as the representative of the Deccan Rivers. The GC02 core is located about 200 km off the discharge point of these rivers and hence is under the direct influence of those rivers as far as fluvial sediment input is concerned. Moreover, the core-site is far isolated from the major dust source such as Arabia and hence the contribution of the aeolian material is not significant (Sirocko et al., 1991). The Indus sediment influence (Prins and Weltje, 1999) at this location may be ignored because of the shallow water continental shelf set-up. Therefore, the relative variation in the coarse and fine

grain-sizes would reasonably suggest the changes in the strength of Deccan River network in-turn the intensity of the summer monsoon rains on the Indian peninsula.

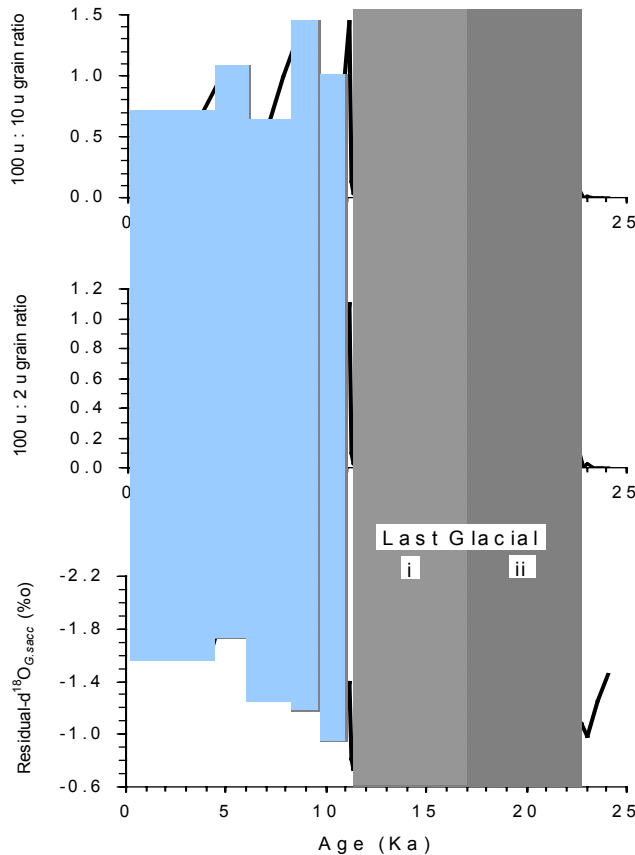


Figure 21: Residual- $\delta^{18}\text{O}_{G.saccullifer}$  record compared with the grain-size variation in continental shelf core GC-02. The blue shaded bars indicate correspondence between the coarse to fine grain ratios and residual- $\delta^{18}\text{O}_{G.saccullifer}$  during the Holocene, in which the decreased  $\delta^{18}\text{O}_{G.saccullifer}$  events invariably correspond with the dominance of larger grain-size suggesting higher erosion of the Deccan Mountains due to relatively intense summer monsoon rains on land (increased freshwater flux). On the other hand, the grey shaded bars in the LGP section exhibit opposite relationship to the Holocene. In that, during the Event-I, the decreased  $\delta^{18}\text{O}_{G.saccullifer}$  overlaps the lowest coarse grain abundance, probably due to melt-water input from the Himalayan glaciers during the deglacial episode (16 Ka to 11 Ka). The Event-II probably marks the period of intense aridity and strong winter winds around the LGM due to which the coarser grain abundance increased with concurrent increase in  $\delta^{18}\text{O}_{G.saccullifer}$ .

The geographical salinity-contrast in the EAS covering last 25 Ka (Figure 20), suggests that the summer monsoons were as intense as today at ~4 Ka and ~8 Ka but were more intense at around commencement of the Holocene (12-11 Ka). These events are separated by slightly weakened monsoon periods ~2-3 Ka, 5-7 Ka, and ~10 Ka. The events of increased summer monsoons recorded by the salinity-contrast must also reflect as the decreased residual- $\delta^{18}\text{O}_{G.saccullifer}$  events in the GC02 core, if the Deccan Rivers have responded to those events. In fact, they are evident in the residual- $\delta^{18}\text{O}_{G.saccullifer}$  record but with certain mismatched timings (Figure 21). This mismatch is acceptable because, a) the salinity-contrast was based on interpolated time-scale of 1 Ky of two deep-water cores, but the GC02 residual-

$\delta^{18}\text{O}_{G.sacculifer}$  profile is based on high-resolution data, and b) differences in water-depths at different core locations might have induced some uncertainty in their age comparison. I restrict the discussion on the age-uncertainty only to the observed marginal miss-match, due to non-availability of the  $^{14}\text{C}$ -dates. Nevertheless, when the residual- $\delta^{18}\text{O}_{G.sacculifer}$  of the GC02 are averaged on 1 ky time-scale then all the lowered salinity-contrast and the decreased residual- $\delta^{18}\text{O}_{G.sacculifer}$  events (depicting stronger summer monsoon associated high freshwater flux) show good agreement.

The increased summer monsoon rains are expected to increase the coarser to finer grain-ratios in the shelf sediment. The 100  $\mu\text{m}$  : 10  $\mu\text{m}$  and 100  $\mu\text{m}$  : 2  $\mu\text{m}$  grain-ratio in the core particularly during the Holocene do exhibit significant increases occurring at 11 Ka, 9 Ka and 5 Ka (Figure 21) in concordance with the increased summer monsoons recorded as salinity-contrast events in the EAS. The observed relationship between decreased residual- $\delta^{18}\text{O}_{G.sacculifer}$  and the increased coarse-versus fine grain-ratios clearly suggests that the Mandovi-Zuari river couple was relatively intense at around those times. This relationship drastically reverses during the LGP (24 Ka -11 Ka). The 100  $\mu\text{m}$  : 10  $\mu\text{m}$  and 100  $\mu\text{m}$  : 2  $\mu\text{m}$  grain-ratios surprisingly exhibit sympathetic relationship with the residual- $\delta^{18}\text{O}_{G.sacculifer}$  during the LGP in contrast to that observed during the Holocene. From 15 Ka to 12 Ka, the decreased 100  $\mu\text{m}$  : 10  $\mu\text{m}$  and 100  $\mu\text{m}$  : 2  $\mu\text{m}$  grain-ratio correspond to decreased residual- $\delta^{18}\text{O}_{G.sacculifer}$ , while the increased 100  $\mu\text{m}$  : 10  $\mu\text{m}$  and 100  $\mu\text{m}$  : 2  $\mu\text{m}$  grain-ratio between 22 Ka and 17 Ka correspond to increased residual- $\delta^{18}\text{O}_{G.sacculifer}$  (Figure 21). The decreased residual- $\delta^{18}\text{O}_{G.sacculifer}$  event at ~15 Ka is also evident in other two deep-water cores (Figure 20) suggesting that the event is robust and occurs in the entire EAS.

The decreased residual- $\delta^{18}\text{O}_{G.sacculifer}$  at ~15 Ka should have been associated with the increase in the 100  $\mu\text{m}$  : 10  $\mu\text{m}$  and 100  $\mu\text{m}$  : 2  $\mu\text{m}$  grain-ratio in the core, if that signal was due to increased fresh water flux as a result of intensified summer

monsoon rains. But the minima in  $100 \mu\text{m} : 10 \mu\text{m}$  and  $100 \mu\text{m} : 2 \mu\text{m}$  grain-ratios during this time period (Figure 21) suggest rather significantly weakened Mandovi-Zuari river couple indicating weakened summer monsoon rains in the region. Overall LGM has witnessed greatly reduced summer monsoons (Duplessy, 1982; Prell and Kutzbach., 1987; Sirocko et al., 1991; Naidu et al., 1996; Sarkar et al., 2001; Rostek et al., 1997; Kudrass et al., 2001; Shimmield et al., 1990, and references therein). The higher geographical salinity-contrast at  $\sim 15$  Ka in the EAS (Figure 20) also indicates weaker summer monsoons ( $> E-P$ ). The western Indian continental shelf (EAS-region) sediment properties in fact have suggested weakened summer monsoons around that time than the Holocene (Nair and Hashimi, 1980). Therefore, the decreased residual- $\delta^{18}\text{O}_{G.sacculifer}$  at  $\sim 15$  Ka is not associated with the intensified summer monsoon precipitation. Nevertheless, that period has significance in terms of melt water pulses (MWP). The period between 10.5 Ka and 14.5 Ka  $^{14}\text{C}$ -ages has witnessed four deglacial MWP events in the north Atlantic (Keigwin et al., 1991). The 14.5 Ka and 10.5 Ka events have been identified as major MWPs producing global signals (Bard et al., 1990; Brunnberg, 1995). Even though, the GC02 chronology lacks the  $^{14}\text{C}$ -dating, the decreased residual- $\delta^{18}\text{O}_{G.sacculifer}$  at  $\sim 15$  Ka associating with minimum coarse to fine grain ratios might be the result of MWPs, particularly from the Himalayan Glaciers during the LGM-Holocene deglaciation. If the Bølling interstadial ( $\sim 14$  Ka), which followed the Antarctic warming (Wilson et al., 2000) had the global effect, then there is a possibility of increased melting of the Himalayan ice, feeding mega-rivers such as Indus, Ganges, Brahmaputra (in turn Arabian Sea and BOB) with ice-locked extremely low  $\delta^{18}\text{O}$  freshwater even in the absence of stronger summer monsoon rains. It is interesting in this context to note that the southern-EAS deep-water core (CR-04) and the northern-EAS continental shelf core (GC02) contain signals of reduced residual- $\delta^{18}\text{O}_{G.sacculifer}$  at  $\sim 15$  Ka (Figure

18). A precise chronology based on  $^{14}\text{C}$ -dating would help resolve and confirm these MWP signals in the EAS, which until then would remain speculative.

The period around 20 Ka is marked by the intense dry climate as evident in the significant increase in the north-south salinity-contrast (or E-P) in the EAS region (Figure 20). This period was globally significant for the lowered sea level by  $\sim 120$  m due to extensive waxing of the continental ice sheets (Shackleton, 2000; Fairbanks, 1989). The observed heaviest residual- $\delta^{18}\text{O}_{G.sacculifer}$  in the entire EAS (Figure 18) is in accordance with such climate scenario, but surprisingly the coarse- to fine-grain ratios exhibit increased values in the shelf region (Figure 21). A significant increase in silt content in both northern-and southern-EAS deep-water cores (Figure 5 and 6) and sharp increase in sand content of northern-EAS shelf core (Figure 7) during most part of the LGP provide support to the above grain-ratio variation. Such increase in the coarser-grain abundance is not expected either in the shelf core or in the deep-water cores during the time of weakened summer monsoons during arid-LGP, because the Deccan Rivers' erosion ability should have been diminished significantly.

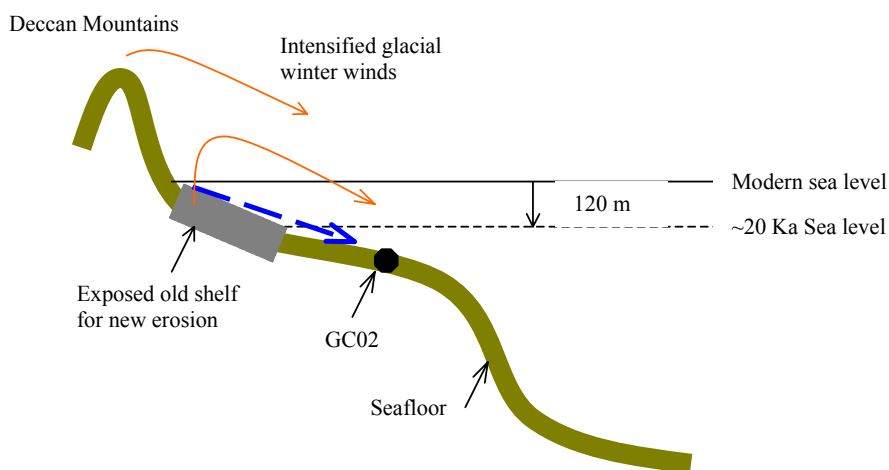


Figure 22: Cartoon drawing showing the exposed continental shelf during the lowered sea level, which could have acted as a source of coarse grain sedimentary material to the GC02 site.



The increased coarse to fine grain-ratios around the LGM (~20 Ka) can be explained alternatively by invoking the exposed continental shelf due to lowered sea-level (see Figure 22). The lowering of the sea level by ~120 m during the LGM must have exposed the modern inner shelf and hence the modern outer shelf (GC02 location at 225 m depth) was converted in to shallow inner shelf around that time. Thus the coarse-grain dominant detritus deposited on the palaeo-inner shelf prior to ~20 Ka ought to have subjected to new erosion regime. Therefore, the subsequent erosion by then intensified winter winds of the LGP (Rostek et al., 1997; Riechart et al., 1998 and references therein) and to certain extent further seaward extended river activity, though had greatly weakened, might have transferred the relict coarse sedimentary material to the GC02 location. The possibility of enhanced transport of the Deccan Mountain erosion products by strengthened winter winds also might have contributed to the increased coarse grain material in the sediment deposited during the LGP. Thus the coarse-grained material supply to the EAS has increased during the LGP in spite of the diminished fluvial activity due to reduced summer monsoons.

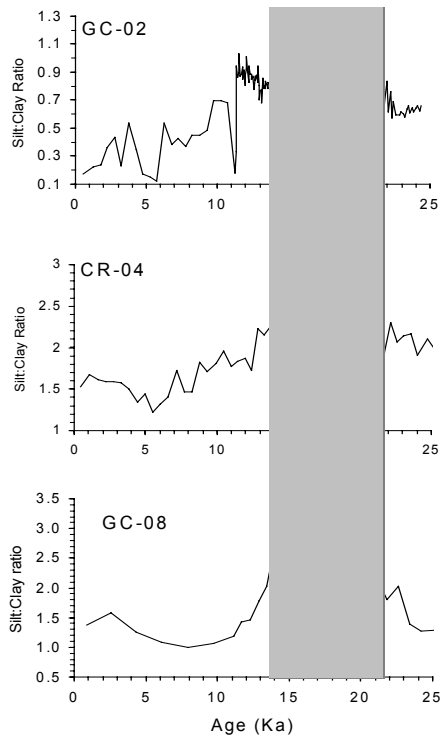


Figure 23: Increased silt:clay ratios during the last glacial period (shaded) in all the three sediment cores from the EAS suggest increased transport of continental weathered products by stronger winter winds blowing towards the Arabian Sea.

The silt : clay ratios calculated using the sedimentary fraction contents (Figures 5, 6 & 7) in all the three cores from the EAS also exhibit increased trends between 15 Ka and 20 Ka (Figure 23). Such near concordant increase of the coarser material in the sediment all over the EAS region strengthens the above views invoking intensified glacial winter winds and exposed continental shelf resulting in the enhanced coarse material transport further off in to the sea. Presently unavailable detrital grain morphology would be able to resolve the exact mode of material transport to the sea during the LGP. Therefore, the sediment cores from the EAS provide interesting clues for the past linkage between monsoon precipitation, Deccan River strength, and continental erosion in response to the climate variation.

### **6.3. Past-monsoon driven productivity changes in the EAS**

#### **6.3.1. The Controversy:**

The strong winds of summer monsoons promote mixing of water in offshore regions leading to entrainment of the deep nutrient rich waters to the surface resulting in the development of intense upwelling zones along the coasts of Somalia, Oman and India (Banse and McClain, 1986; Currie et al., 1973; Haake et al., 1993; Rao et al., 1989; Wyrski et al., 1973). The moderate upwelling has been observed in the northern and eastern Arabian Sea during the winter monsoons also (Banse, 1987; Brock et al., 1991; Qasim, 1982). The monsoon wind driven upwelling induces increased productivity. The seasonal productivity is highest in the western region, gradually reducing eastward during the summer monsoons, whereas, the EAS experiences high productivity during the winter monsoons in addition to the summer monsoon peaked productivity (Haake et al., 1993).

I have already mentioned briefly in the introduction chapter about the contrasting views on monsoon driven productivity patterns across the Arabian Sea on glacial-interglacial time-scales. In the sedimentary records of the western Arabian Sea upwelling region, interglacial high- and glacial low-productivity trends have been observed previously. The interglacial high productivity in the western region (Emeis et al., 1995; Naidu and Malmgren, 1996; Shimmield et al., 1990; Spaulding and Oba, 1992), as well as in the southeastern region of the Arabian Sea (Pattan et al., 2003) have been suggested based on various proxies. The increased water column denitrification during the interglacial periods was interpreted as indicative of intense OMZ due to elevated productivity across the Arabian Sea (Altabet et al., 1999). As the strong summer monsoon winds drive upwelling and associated productivity in the western region where the winter monsoons do not have much influence, the interglacial high productivity may be in accordance with the Indian monsoon dynamics. But the entire Arabian Sea in general or southeastern region in particular showing the elevated productivity only during the interglacial is debatable because

the summer monsoon driven upwelling cells are largely develop off Somalia and Oman but not over the entire Arabian Sea.

The enhanced glacial productivity in the EAS indicated by the past OMZ reconstructions and biomarkers (Cayre and Bard, 1999; Rostek et al., 1997; Schulte et al., 1999) questioned the views suggesting in general high productivity in the interglacial Arabian Sea as a whole. This interglacial high-productivity coupling may not hold good to the EAS region as it also comes under the direct influence of the northeasterlies, which can induce upwelling during the winter. The east-west difference in present day productivity has already been observed in the Indo-FRG sediment trap experiments, which clearly demonstrated a productive EAS during the winter-monsoons also, unlike only a summer maximum biogenic-flux in the western region (Haake et al., 1993). The recently conducted sediment trap experiments by the National Institute of Oceanography, in the continental shelf to upper continental slope regions of the EAS covering the present day OMZ (200 m - 1100 m) have brought out very interesting observation that suggest seasonally independent organic matter flux within the experimental depth range (Paropkari et al., 2003, personal communication). This experiment strongly argues that, in spite of the modern weak winter winds compared to the summer monsoon winds, effect of the former on the productivity is distinct in the EAS region and forces to recognise the importance of the winter monsoons in determining the average annual biological activity of the region. Therefore, increased glacial productivity in the EAS (Cayre and Bard, 1999; Rostek et al., 1997; Schulte et al., 1999) that largely hinges on the hypothesis that invokes intensified winter monsoon and weakened summer monsoon during the LGP (Duplessy, 1982) is well justified. In the following sections the multiple proxies are used to evaluate the EAS productivity in response to oscillated monsoon dynamics.

### 6.3.2. Biogenic calcite and productivity:

The accumulation of biogenic calcium carbonate on the seafloor mainly depends on surface water productivity, dissolution through the water column and on the seafloor, and dilution by the non-carbonate fraction such as terrigenous matter. The carbonate-flux (carbonate mass-accumulation rate) at the seafloor has been extensively used as a reconnaissance for marine productivity. But, its application is valid only if the preservation is complete. It has been shown by several workers that the past climate induced variations in the preservation of carbonate complicated the approach. Berger et al. (1982) and Curry and Cullen (1997) have demonstrated that the progressive dissolution of foraminiferal calcite leads to the weakening and fragmentation of their tests, i.e., the loss of skeletal-calcite. The increased corrosiveness of the deep-waters during the climate cooling cycles has been shown to dissolve the biogenic calcite to great extent (Gröger et al., 2003 and references therein). Such preservation problems may lead to the underestimation of the productivity. Therefore, it becomes mandatory to examine the planktonic calcite tests to confirm the proper preservation before utilizing it for productivity interpretations. The coarse-fraction of the studied cores at all the intervals were carefully examined under the microscope. The shell-damage and fragmentation due to dissolution were not significant. Particularly, the *Gr. menardii* tests were intact and the abundance of keel (indicating destroyed shell walls) and fragmentation were rare in almost all the sections suggesting insignificant dissolution and good preservation (Ku and Oba., 1978). However, mechanical fragmentation caused due to processing of the sample was noticed and can be differentiated from the shell damage process. Additionally, the seafloor depths (<3000 m) at the studied core locations are much shallower than the carbonate lysocline in the region (~4000 m).

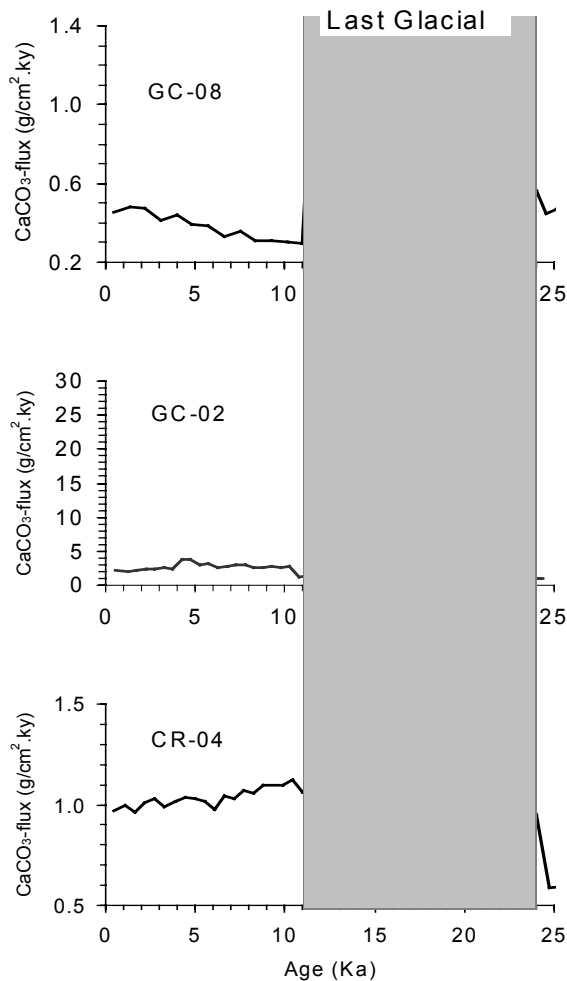


Figure 24: Holocene-LGP carbonate-flux variation in the EAS. The northern-EAS cores (GC02 & GC08) exhibit distinctly higher flux during most of the LGP, whereas, the southern core (CR04) records nearly uniform flux since the beginning of the last glaciation.

The possibility of aeolian dust carbonate from the Arabian Deserts may be ruled out in the study region because the dust input to the EAS has been shown to be negligible compared to the western and central regions (Sirocko et al., 1991). Therefore, calcium carbonate variations in the EAS region represent the productivity changes related to monsoon intensity.

The Holocene sections in the two northern-EAS cores (GC08 and GC02) exhibit almost similar trends, while the southern-EAS core (CR04) shows nearly uniform carbonate-flux since the commencement of the LGP (Figure 24). There is rapid increase in the productivity in the northern-EAS at around the LGM as evident

in the sharp increase of  $\text{CaCO}_3$ -flux in GC02 (from 7 to 25  $\text{g/cm}^2\cdot\text{ky}$ ) and GC08 (0.7 to 1.3  $\text{g/cm}^2\cdot\text{ky}$ ). Where as, the productivity has remained constant through the LGP-Holocene in the southern-EAS region as evident by the nearly unchanged flux recorded in the CR04 core ( $\sim 1.0 \text{ g/cm}^2\cdot\text{ky}$ ). Both the northern-EAS cores exhibit peaked production at  $\sim 16 \text{ Ka}$ . Thus at the outset it appears that the surface water biological productivity was distinctly higher during the LGP in the EAS. Even though the southern-EAS core exhibits nearly uniform productivity signal through the LGP and the Holocene, the increase appears to have commenced at the closure of the previous period (MIS3) (Figure 24), suggesting that the increase in productivity has in fact begun with the commencement of the LGP, but well-sustained through the Holocene in the southern-EAS.

The long-term productivity changes recorded in two deep-water sediment (GC08 and CR04) exhibit almost similar trend from the MIS3 through MIS5 (Figure 25). A nearly uniform  $\text{CaCO}_3$ -flux during the MIS3 is evident in both the cores. The last warm period (MIS5) however, exhibits higher productivity roughly around the colder-stadial. The later part of the penultimate glacial period (MIS6) recorded in the CR04 exhibits distinct maximum of  $\text{CaCO}_3$ - flux ( $\sim 2 \text{ g/cm}^2\cdot\text{ky}$  as against  $\sim 1 \text{ g/cm}^2\cdot\text{ky}$  of the LGP-Holocene) (Figure 25) suggesting significantly higher productivity during the penultimate glacial period (MIS6) than during the warm periods.

The higher productivity during the LGM is also evident in the time-series  $\text{Al}_{\text{excess}}$  that exhibits elevated content between 25 Ka and 19 Ka. The corresponding  $\text{Mn}_{\text{excess}}$  on the other hand shows well-oxygenated waters in the shelf region at the beginning of the LGM (24-22 Ka) (Figure 11). The high-oxygenation during the early part of the LGM suggests a possibility of weaker OMZ in spite of high productivity. This particular issue is addressed in the Section 6.3 dealing with the denitrification. However, the observations based on the  $\text{Mn}_{\text{excess}}$  and  $\text{Al}_{\text{excess}}$  need to be considered with caution because the GC-02 core is from a shallow water where rapid changes in

geochemical cycling of the scavenged metals is common due to high very high export production and large supply of terrigenous matter.

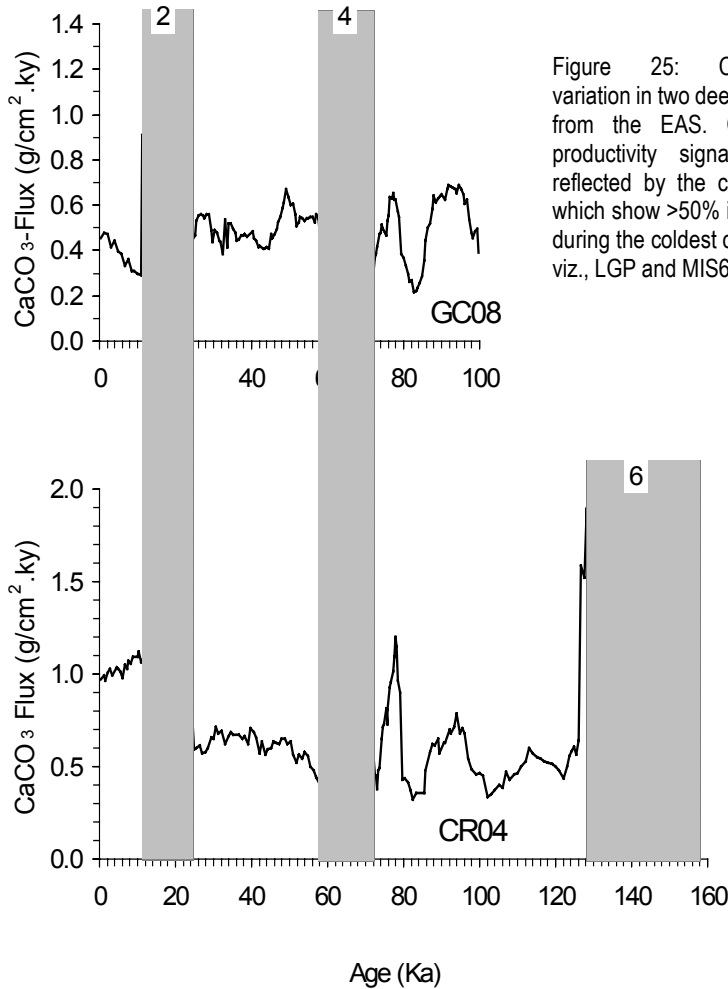


Figure 25: Carbonate-flux variation in two deep-water cores from the EAS. Glacial high-productivity signals are well reflected by the carbonate-flux, which show >50% increased flux during the coldest climate events viz., LGP and MIS6.

### 6.3.3. Sedimentary organic matter and productivity:

Variation in the intensity of summer- and winter-monsoons on glacial-interglacial time-scale has influenced the productivity in the EAS as evident in the carbonate-flux changes. The high carbonate-flux during the coldest MIS6 and LGP (Figure 25) warrants detailed assessment of the past productivity in the EAS region with the help of other widely used organic matter (OM) proxies. Because, the present results are not in agreement with the general view suggesting increased productivity



during the warm and wet interglacial periods, when the summer monsoons were intense and winter-monsoons were weak.

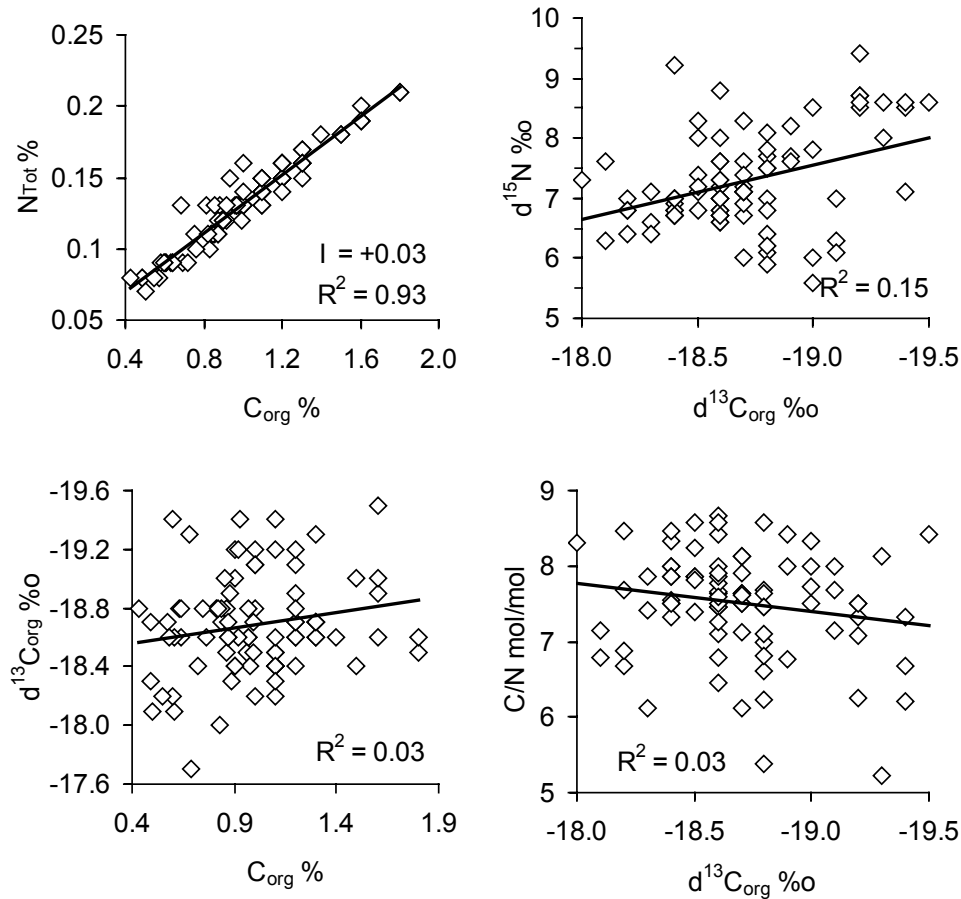


Figure 26: The association between various productivity proxies of the organic matter. The  $R^2$  values tending towards 1 suggest increasing coherency in mutual variation of the proxies concerned due to increasing dominance of one process governing the variation.

Before considering the sedimentary-OM as palaeo-productivity indicator, it is necessary to demonstrate that the preservation of the OM in the sediment of the study region is adequately satisfactory. A good preservation of OM in the EAS region may be reasonably assumed based on the following observations, a) a previous study from the southern-EAS (sediment core: MD900963) has yielded excellent correlations between the  $C_{org}$  and various refractory biomarkers (Schulte et al., 1999); and b) the presence of poorly oxygenated ( $\sim 1$  ml/lit  $O_2$ ) Indian Central Water

in the intermediate depth (Olson et al., 1993) may not favour degradation of OM. The close association of the biomarkers with the  $C_{org}$  clearly indicates that the OM in the EAS sediment is rather unaltered. Nevertheless, it is necessary to establish the fidelity of the present OM-based proxies. For this purpose few simple inter-relationships between the different proxies (Figure 26) are evaluated.

The Redfield ratio of C/N for marine-OM is  $\sim 7$  and for terrestrial-OM is  $\sim 35$  (Ikehara et al., 2000; Reichart, 1997; Walsh et al., 1981). In the present core the C/N ratios vary around 7 indicating dominance of the marine-OM. The C/N ratios however can vary greatly depending upon the degree of preservation and mixing with high C/N terrestrial-OM. The C/N ratios as high as 30 in the OM dominated by marine origin have been found to be the result of diagenesis (Walsh et al., 1981). If the diagenesis has altered the OM content of the present sediment, then the C and N should vary randomly yielding very poor mutual association because the latter element fractionates during the settling- and burial-diagenesis (Walsh et al., 1981). A very strong linear positive association ( $R^2=+0.93$ ) between those two elements (Figure 26) and their ratios lower than 9 (Figure 27e) rule-out any such alterations and confirm good preservation of the OM. The marginally higher C/N ratios ( $>7$ ) and the offset in the intercept of the best-fit (0.03 % on N-axis: Figure 26) may suggest the presence of small amount of terrestrial-OM in the sediment. Using the C/N ratios of the marine- and terrestrial-OM ( $\sim 7$  and  $\sim 35$  respectively) as two end-members of the mixing line, a maximum of 9 % of terrestrial-OM can be expected in the core. This would affect the carbon- and nitrogen-isotopic ratios in the OM to a maximum of 0.2 ‰, which is within the analytical uncertainty. The additional support for good preservation and purity of the marine-OM can be obtained by its isotopic relationships.

- a) If the varying proportion of terrestrial-OM of significantly lighter-C and –N isotopes and higher C/N ratio has altered the marine-OM of significantly heavier-C and –N isotopes and lower C/N ratio, then such alteration should produce a sympathetic relationship between  $\delta^{13}\text{C}$  and  $\delta^{15}\text{N}$  and inverse relationship between  $\delta^{13}\text{C}$  and C/N ratios (see Ganeshram et al., 2000).
- b) According to Rayleigh's fractionation kinetics, the diagenetic alteration should result in the preferential loss of  $^{12}\text{C}$  and  $^{14}\text{N}$  of the sedimentary-OM leaving behind the residual-OM enriched with  $^{13}\text{C}$  and  $^{15}\text{N}$ . Therefore, if the decreased OM content in the sediment was due to the diagenetic breakdown, then the decreased OM should correlate with the increased  $\delta^{13}\text{C}$ , and the  $\delta^{13}\text{C}$  and  $\delta^{15}\text{N}$  should correlate sympathetically (Ganeshram et al., 2000; Kienast et al., 2001).

None of the above inter-relationships are evident in Figure 26 and hence are indicative of near pristine nature of the OM in the EAS and the studied cores in fact have recorded the changes in marine production with remarkable fidelity. The distinguishing isotopic features of the well-preserved, non-contaminated sedimentary-OM such as significantly heavier  $\delta^{13}\text{C}$  and  $\delta^{15}\text{N}$  of the tropical marine-OM (~-20 ‰ and ~5 ‰ respectively) as compared to the terrestrial C3-OM (~-27 ‰ and ~2 ‰ respectively) (see Figure 27c & d: and Altabet et al., 1999; Fontugne and Duplessy, 1981; Jasper and Gogosian, 1990; Rau et al., 1989; Sigman et al., 1997; Sweeney and Kaplan, 1980) provide further confirmation in favour of well-preserved sedimentary-OM inventory in studied core.

The phytoplankton preferentially fractionates  $^{12}\text{C}$  during the synthesis of the organic matter leaving the surface ocean  $\Sigma\text{CO}_2$  enriched with  $^{13}\text{C}$  (Kroopnick, 1985) and the plankton-calcite precipitated in equilibrium with that water should preserve the enriched  $^{13}\text{C}$  signal. Therefore, enhanced marine productivity at a given time is expected to associate with increased  $\delta^{13}\text{C}$  in the planktonic foraminifera calcite. The

vital effects modifying the expected equilibrium are assumed to remain uniform for the time-slice covered by the core. Therefore, the fluctuations in  $C_{\text{org}}$ -flux and the  $\delta^{13}\text{C}_{\text{calcite}}$  together should be able to represent the past changes in productivity. The upwelling may alter the  $\delta^{13}\text{C}$  inventory of the surface water and hence the  $\delta^{13}\text{C}$  composition of both the organic matter and calcite. However, the organic-inorganic fractionation mechanism still remains the same and hence would not affect the relative changes on glacial-interglacial time-scales.

It is evident from the co-varying  $C_{\text{org}}$ -flux and  $\delta^{13}\text{C}_{\text{calcite}}$  (Figure 27a & b) that the productivity in general was highest during the LGP, higher during MIS3 through MIS4, and stadial of MIS5 than the Holocene. The  $\Sigma$ alkenones in the LGP section exhibit nearly three-times higher content than at the closure of MIS3 and over an order of magnitude higher content than in the Holocene (Figure 28). The alkenones are highly refractory for diagenetic alterations and hence are faithful indicators of the marine productivity (Brassell, 1993). Therefore, the enrichment of the  $\Sigma$ alkenones in the LGP time-slice than the two adjacent warm periods demonstrates distinctly increased productivity in the EAS during that time.

The productivity minima have occurred during the terminations of the last two glacial periods (LGP and MIS4) and at the interstadials of MIS5 (i.e., ~80 Ka and ~97 Ka) (Figure 27). This observation implies that the climate warming episodes appear to have commenced when the marine productivity has reached its ebb. The association of high productivity largely with the cold events supports the previously proposed hypothesis of increased nutrient injection in to the photic zone of the EAS due to strengthened winter monsoons (Cayre and Bard, 1999; Rostek et al., 1997; Schulte et al., 1999; Thamban et al., 2001).

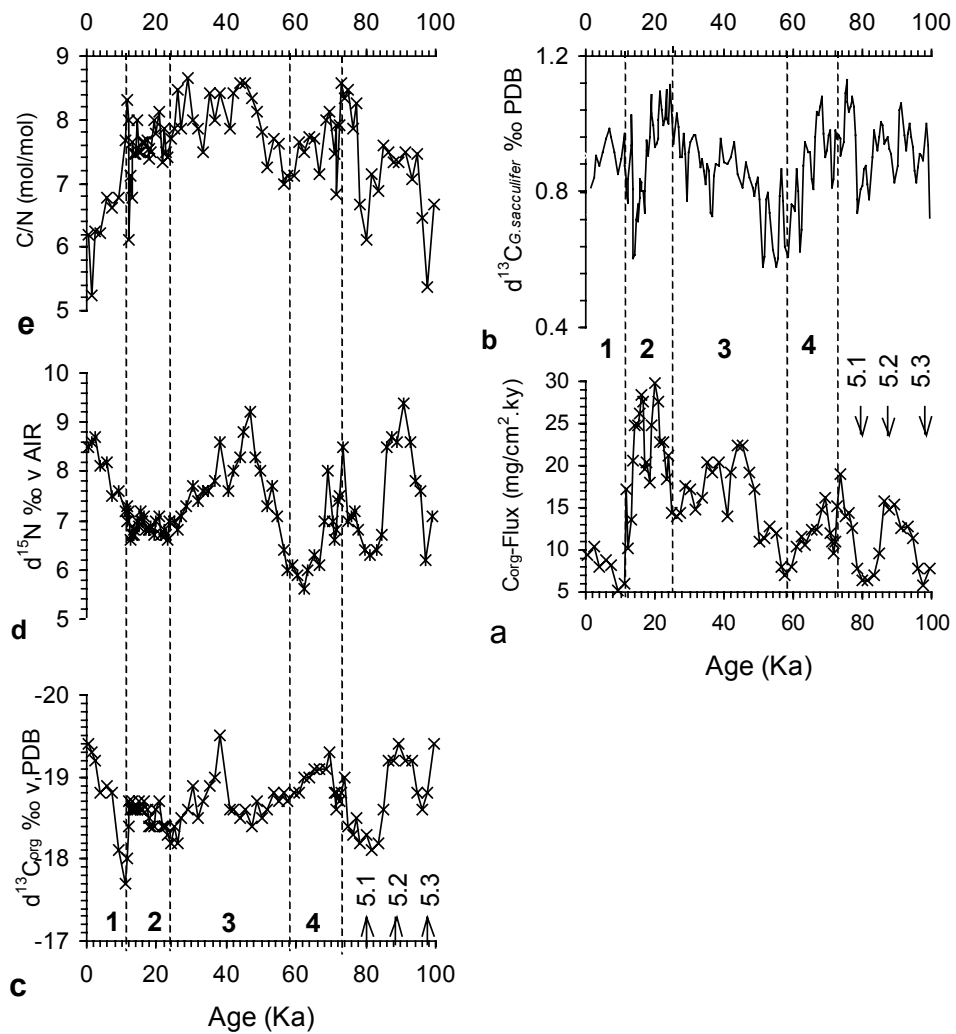


Figure 27: The time-series variation of the various organic and inorganic proxies of the marine productivity. The proxies invariably suggest higher marine production during cold climate, despite the presence of certain amount of terrestrial organic matter in the sediment of the EAS.

Weakening of the WMC and PCC during the glacial times (i.e., reduced low-salinity water flux in to the EAS from the BOB) appear to have weakened the surface layer stratification facilitating injection of the deep-water nutrient in to the euphotic zone. Additionally, the intensified winter-monsoon winds blowing over the Indian peninsula towards the EAS (see Figure 1) might have enriched the photic waters of

the Indian margin with Fe-rich dust derived from the basaltic and lateritic terrains of the Deccan enhancing the possibility of complete utilization of the injected nutrients (Martin, 1990), thus greatly increasing the glacial productivity.

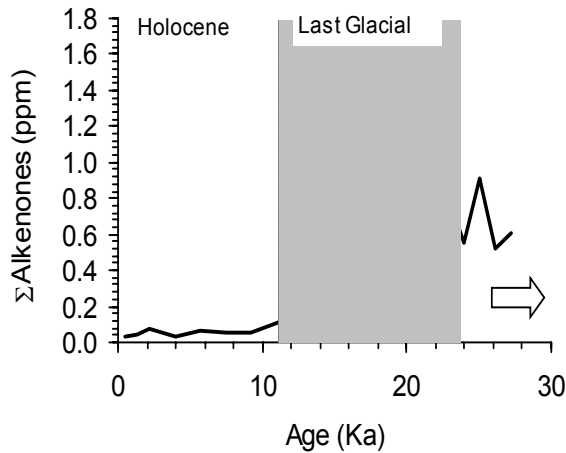


Figure 28: The alkenones synthesized by the prymnesiophyta group of algae are refractory to the post-burial diagenesis. Therefore, alkenone content in the sediment is most reliable proxy for the marine productivity. Distinctly higher content of the total-alkenones in the Glacial-EAS sediment strengthens the view based on other proxies suggesting higher Glacial-productivity.

This interpretation is supported by, a) elevated particle flux to the deep-EAS during the coldest SSTs of 1988/89 associated with strongest winter monsoons, and b) the definite role of winter monsoons in the inter-annual variability of the particle fluxes in the EAS unlike the western region, which is governed by the strength of summer monsoons (Haake et al., 1993). Interestingly, the recent study from the Oman Margin sedimentary records have provided new clues for well-sustained high productivity even during the LGM climate due to strengthened winter monsoons (Tamburini et al., 2003), which probably have intensified the winter cooling and deep-winter mixing (Madhupratap et al., 1996; Reichart et al., 1998). The marginally higher C/N ratios (>7) during the last glacial cycle (~72 Ka - ~11 Ka: Figure 27e) suggesting relatively increased transfer of the terrestrial-OM to the EAS region perhaps may be indicative of intensified glacial cycle winter winds.

#### **6.4. Eastern Arabian Sea productivity vis-à-vis global climate:**

The strengthened biological pump has been considered most important mechanism that lowered the atmospheric-CO<sub>2</sub> leading into the cold and dry glacial periods from the warm and wet interglacials (see Sigman and Boyle, 2000). In the last decade the southern ocean sector primary productivity emerged as the driver of the global climate variability in general and atmospheric-CO<sub>2</sub> in particular. However, this view was challenged with the help of biogenic-opal and calcite-carbon and sedimentary-nitrogen isotope evidences, which rather indicated that the primary productivity was lower during the LGP than during the Holocene (Shemesh et al., 1993). The role of oceanic productivity in sequestering the atmospheric-CO<sub>2</sub> (i.e., climate variability) in to the deep-oceanic sedimentary reservoir is rather unquestionable considering the size of oceanic carbon reservoir. If the primary productivity was lower in the southern ocean during the LGP, then there must be some oceanic regions elsewhere, which must have regulated the biological pump with amazingly rhythmic toggle. In this regard it is tempting to suggest that the oceanic areas such as the EAS, where the preliminary evidences in support of strengthened biological pump during the LGP brought-out in this study, may have played an important role in regulating the global climate! It may be necessary to investigate the marginal seas of the tropical regions to assess whether the glacial high productivity was specific to the EAS alone, or the marginal seas of the glacial tropics have witnessed high productivity in general. If the latter is true, then the mechanism regulating the global climate is located right within the tropical region, where the high latitudes might have merely responded to the tropical climate forcing during the glacial cooling. This view needs to be tested with several other records from the global oceans, until then it remains a speculation.

### 6.5. Denitrification and past-productivity: a mismatch?

The water column denitrification records preserved in the sediment can be useful in understanding the past productivity. The present day Arabian Sea has an intense OMZ due to basin-wide high productivity and low oxygen intermediate water feeding the OMZ (Olson et al., 1993), making it one of the worlds largest marine denitrification regions (Codispoti, 1995; Naqvi, 1987). The bacterially mediated denitrification in the ocean is a process by which marine nitrate is reduced to gaseous species. Marine denitrification produces significant enrichment of  $\delta^{15}\text{N}$  in subsurface nitrates (Codispoti and Christensen, 1985), and is reflected in the sinking organic particulates (Altabet et al., 1995). Therefore, the sedimentary- $\delta^{15}\text{N}$  record may provide an additional tool to understand past changes in the productivity if the intermediate water oxygenation has remained unaltered. However, this relationship is not straightforward as different processes may be involved in controlling the denitrification. For example, recently Ganeshram et al., (2002) suggested that the glacial productivity was low due to altered Redfield ratios of phosphorous and nitrogen in spite of increased nutrient- or iron-supply. On the other hand, Altabet et al., (2002) have shown that the denitrification and productivity go hand-in-hand even on millennial time-scale. As there is little isotopic fractionation associated with the sedimentary denitrification (Brandes and Devol, 1997), the sedimentary  $\delta^{15}\text{N}$  should be able to faithfully preserve the record of water column denitrification.

The time-series  $\delta^{15}\text{N}$  record of the EAS obtained from GC-08 core (Figure 27) accurately superimposes the  $\delta^{15}\text{N}$  records of the western Arabian Sea (Altabet et al., 1995) and closely resembles the only other available  $\delta^{15}\text{N}$  record from the EAS (Ganeshram et al., 2000). Similar structure in time-series  $\delta^{15}\text{N}$  profiles with similar range of values (6-9 ‰) (Figure 29 and also see Altabet et al., 1999, Ganeshram et al., 2000) across the Arabian Sea suggest the basin-wide homogeneity in the  $\delta^{15}\text{N}$  signals irrespective of greatly differing upwelling and productivity intensity (Haake et



al., 1993). The observed regional homogeneity across the basin renders the link between productivity and denitrification a complex issue especially for the EAS in light of the increased glacial productivity. The glacial increase in the productivity should have produced increased enrichment of the  $\delta^{15}\text{N}$ , had the intermediate water redox conditions remained uniform throughout. The glacial decreases ( $\sim 6\text{‰}$ ) and interglacial increases ( $\sim 8\text{‰}$ ) in the  $\delta^{15}\text{N}$  of the EAS (Figure 27 & also see Ganeshram et al., 2000; Suthhof et al., 2001) can be explained by significant change in mid-water oxygenation feeding the OMZ-depth during the glacial periods.

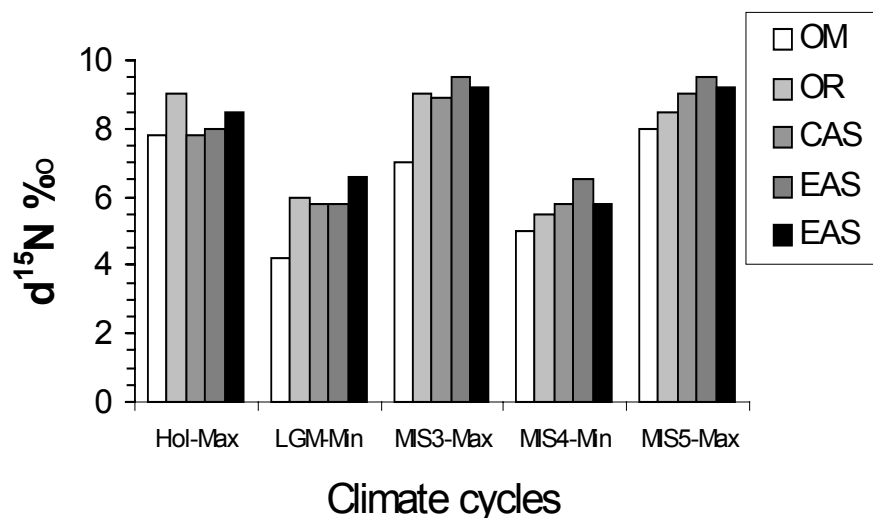


Figure 29: The sedimentary  $\delta^{15}\text{N}$  records of the Arabian Sea. Note the marginal differences in the averaged peak- $\delta^{15}\text{N}$  events across the basin in spite of differing productivity pattern. OM=Oman Margin, OR=Owen Ridge, CAS=Central Arabian Sea, EAS=Eastern Arabian Sea. The black bar is the present data.

The Arabian Sea intermediate water presently consists of Persian Gulf Water with  $\sim 2.6\text{ ml/L O}_2$  (2 Sv: sill-depth= $\sim 60\text{ m}$ ), Red Sea Water with  $\sim 3.5\text{ ml/L O}_2$  (0.5 Sv; Sill-depth= $\sim 140\text{ m}$ ), and Indian Central Water with  $\sim 1\text{ ml/L O}_2$  (6 Sv) (Olson et al., 1993; Wyrski, 1973). Only the Indian Central water fed the OMZ of the LGM-EAS, as the Persian Gulf was desiccated and Red Sea water greatly reduced due to drop in sea level. This hydrographic condition coupled with the increased productivity during the LGP should further intensify and expand the OMZ in the EAS leading to an intensified denitrification rather than observed collapse of the OMZ (see Figure 27d).

Unless there was a perennial existence of the well-oxygenated water in the intermediate depths, the observed productivity-denitrification decoupling in the high productive glacial-EAS is simply not possible. The remarkably improved mid-water oxygenation during the time of isolation of the Persian Gulf and Red Sea probably has resulted by either the enhanced advection of oxygen rich southerly ventilated water (Wyrski, 1973), or the intensified ASHSW and deep winter mixing. The deep winter mixing has already been invoked to explain the collapse of glacial-OMZ in the northern Arabian Sea (Reichart et al., 1998). The former possibility is unlikely, because by the time the southern source water penetrates in to the Arabian Sea, its oxygen is expected to deplete beyond the required level to diminish the OMZ. The intensified ASHSW in the northern Arabian Sea and its southward advection associating with enhanced deep winter mixing due to strengthened winter monsoons during the cold periods appear to have resulted effective ventilation of the mid-depth water in the EAS. Such vigorous ventilation could have satisfied the increased demand of oxygen due to elevated glacial-productivity and hence reduced the denitrification. Therefore, the latter hypothesis is a plausible mechanism to explain the reduced denitrification in the EAS in spite of increased productivity during the LGP. The reduced denitrification resulting in increased nitrate- and intensified winter monsoons increasing the Fe supply to the photic zone appear to have led to the complete utilization of increased nutrients.

The OMZ-oxygenation in the EAS could be evaluated with the help of particulate Mn-oxide or  $Mn_{\text{excess}}$  in the shelf core (GC02) because the present day OMZ sweeps over this region. The  $Mn_{\text{excess}}$  variation (Figure 11) is nearly similar to the alkenone variation in the GC08 (Figure 13), wherein both of them show very high values in the early part of the LGP. Interestingly, the  $Al_{\text{excess}}$  also shows similar variation (Figure 11) indicating high productivity (Banakar et al., 1998). This in fact supports the interpretation of decoupled productivity and denitrification, where the OMZ-depth might have remained well oxygenated (high  $Mn_{\text{excess}}$ ) due to excellent

ventilation during the LGP. However, in absence of such records from the other parts of the EAS, the above interpretation based on the similarity between GC02 and GC08 may remain speculative.

The most weakest denitrification events are evident during the moderately cold-MIS4 and warm-MIS5.1 and -MIS5.3 interstadials (Figure 27d) further complicating the generally believed denitrification and productivity linkage. If the Arabian Sea was more productive during the warm and wet climate periods than during the cold and dry periods as envisaged in many previous works based on the western Arabian Sea sediments, then why the denitrification intensity was weakest during both those type of climates? Why the milder cold period MIS4 shows lowest denitrification or practically non-existing OMZ than compared to the coldest-LGM, if the mid-depth oxygenation was improved only during the cold climates? Even though it is not a easy task to address these complexities with the aid of very limited data, at the out-set it is possible to suggest that, at several occasions in the past either the denitrification-productivity must have been decoupled or the basin-wide homogenisation process in the Arabian Sea due to highly vibrant thermocline might have modified the region and climate specific signals of the water column denitrification. The above-discussed conditions in the Arabian Sea hydrography probably have led to the observed mismatch between the sedimentary denitrification records and the climate-forced productivity changes.

## 7. Conclusions

The Eastern Arabian Sea bordering western India appears to be unique with respect to its response to the past climate change. In that, it shows quite contrasting features as compared to its western counter part. Few important interpretations derived from the present multi-proxy study are summarised below. These observations have significance in understanding the response of the Eastern Arabian Sea biogeochemical processes to the past climate change.

1. **The** north-south salinity gradient variation in the Eastern Arabian Sea, productivity patterns, and sedimentary properties reconstructed for the last 100,000 years provide a fairly consistent record of the biogeochemical responses of the region to the climate forced monsoon variations.
2. **The** salinity-gradient reconstruction based on the geographical contrast in the planktonic calcite- $\delta^{18}\text{O}$  has yielded higher gradient of  $\sim 2.2$  psu for the last glacial maximum as compared to the present  $\sim 1$  psu gradient between the studied locations. Nearly doubled salinity-gradient indicates that the poleward coastal current, which is responsible for maintaining the low-salinity in the study region, appears to have collapsed during that time. The collapse of this winter-spring circulation in the region possibly was the result of broken communication between the Bay of Bengal and the Eastern Arabian Sea. The greatly diminished summer monsoons during the last glacial period appear to have resulted in the broken communication between those two basins.
3. **The** events of lowest salinity gradient of  $\sim 0.2$  psu during the last warm period (MIS5) clearly indicate that much stronger summer monsoons than the Holocene existed in the past, which have driven the coastal currents more vigorously. The vigorous coastal currents appear to have led to the disappearance of the salinity gradient in the Eastern Arabian Sea.

4. **The** salinity-gradient during the pre-Holocene period exhibits high-frequency large amplitude fluctuations as compared to the marginal variations in the Holocene time. This may be due to the fact that, the Holocene monsoon system has been considerably stable than the preceding period.
5. **The** coarse grain silicate detritus transport to the continental shelf by the Deccan Rivers was high during most of the Holocene as compared to the last glacial period indicating stronger summer-monsoons during the former period. On the other hand, the increased proportion of the coarse grains in the sediment during the early part of the last glacial period when the Deccan Rivers were weaker suggests that the relict material was transported further off from the exposed continental shelf at the time of lowered sea level stand.
6. **The** productivity in the Eastern Arabian Sea was significantly higher during the last glacial period than the Holocene and the last warm period (MIS5). The isotopic proxies of the productivity exhibit maxima at the commencement of the climate cooling events (glacial) and reach the minima around their termination. Such productivity patterns have significance because the beginnings of the climate warming episodes coincide with the ebbs in marine productivity.
7. **The** glacial-high productivity in the study region can be explained by the combination of enhanced deep-water nutrient supply to the photic zone and the adequate availability of limiting-micronutrient iron. Intensified injection of the deep-water nutrients into the surface water might have taken place when the fresh water flux in the region has greatly reduced (due to broken communication between Bay of Bengal and Eastern Arabian Sea) leading to weakening of upper water stratification. The large supply of iron must have been possible when the winter winds blowing from the Indian continent towards the Eastern Arabian Sea were intense. Such glacial scenario might

have led to the complete utilization of nutrients injected in to the surface layer and hence significantly increased glacial productivity.

8. **As** the biogenic opal and carbon-isotope evidences from the Southern Ocean sediment have revealed reduced primary productivity during the last glacial period, the increased tropical marine productivity gains importance. In that, the biological pump elsewhere than the Southern high latitudes must have to be strengthened to account for the glacial drop in the atmospheric carbon dioxide. In light of convincing evidences for the glacial high productivity in the Eastern Arabian Sea, it may be feasible to suggest that the tropical continental-margin environment have played crucial role in regulating glacial climate through strengthened biological pump.
9. **The** sedimentary record of nitrogen-isotopes suggests that the water column denitrification in the Eastern Arabian Sea was almost collapsed (i.e., the oxygen minimum zone disappeared) during the last glacial period. This region showing high productivity during the glacial time, the evidence for reduced denitrification is intriguing. However, the reduced denitrification may be a reason for increased nutrient availability to the photic zone from OMZ-depth. Secondly, the ventilation of the OMZ-water might have been very vigorous during the glacial time due to intensified deep-winter mixing that has resulted in satisfying the oxygen demand of increased export production. Therefore, the exceptionally excellent OMZ-depth ventilation during the last glacial period when the winter monsoons were intense might have led to great reduction in the water column denitrification.

## 8. References

- Altabet, M.A., Francois, R., Murray, D.W. and Prell, W.L., 1995. Climate related variations in denitrification in the Arabian Sea from sediment  $^{15}\text{N}/^{14}\text{N}$  ratios. *Nature*, 373: 506-509.
- Altabet, M.A., Murray, D.W. and Prell, W.L., 1999. Climatically linked oscillations in Arabian Sea denitrification over the past 1 my: implications for the marine N cycle. *Paleoceanography*, 14: 732-734.
- Banakar, V.K., Galy, A., Sukumaran, N., Parthiban, G. and Volvaiker, A.Y (Chodankar, A.R)., 2003. Himalayan sedimentary pulses recorded by silicate detritus within a ferromanganese crust from the Central Indian Ocean. *Earth and Planetary Science Letters*, 205: 337-348.
- Banakar, V. K., Parthiban, G., Pattan, J. N. and Jauhari, P., 1998. Chemistry of surface sediment along a north-south transect across the equator in the Central Indian Basin: an assessment of biogenic and detrital influences on element burial on the seafloor. *Chemical Geology*, 147: 217-132.
- Banse, K., 1987. Seasonality of plankton chlorophyll in the Central and northern Arabian Sea. *Deep Sea Research*, 34: 713-723.
- Banse, K. and McClain, C.R., 1986. Winter blooms of phytoplankton in the Arabian Sea as observed by the Coastal Zone Colour Scanner. *Marine Ecology Progress. Ser*, 34: 201-211.
- Bard, E., Hamelin, B., Fairbanks, R.G. and Zinder, A., 1990a. Calibration of the  $^{14}\text{C}$  timescale over the past 30,000 years using mass spectrometric U-Th ages from Barbados corals. *Nature*, 345: 405-410.
- Bard, E., Hamelin, B. and Fairbanks, R.G., 1990b. U-Th ages obtained by mass spectrometry in corals from Barbados: Sea level during the last 130,000 years. *Nature*, 346: 456-458.
- Bassinot, F.C., Beaufort, L., Vincent, E., Labeyrie, L.D., Rostek, F., Müller, P.J., Quidelleur, X., Lancelot, Y., 1994. Coarse fraction fluctuations in pelagic carbonate sediments from the tropical Indian Ocean: A 1500-kyr record of carbonate dissolution. *Paleoceanography*, 9: 579-600.

- Berger, W.H., Bonneau, M.-C., Parker, F.L., 1982. Foraminifera on the deep-sea floor: Lysocline and dissolution rate. *Oceanol. Acta*, 5: 249-258.
- Bhattacharya, G.C., Murty, G.P.S., Srinivas, K., Choubey, A.K., Sudhakar, T. and Nair, R.R., 1994. Swath bathymetric investigations of seamounts located in the Laxmi Basin, Eastern Arabian Sea. *Mar. Geodesy*, 17: 169-182.
- Bond, G.C., Broecker, W.S., Johnsen, S.J., McManus, J.F., Labeyrie, L., Jouzel, J. and Bonani, G., 1993. Correlations between climate records from North Atlantic sediments and Greenland ice. *Nature*, 365: 143-147.
- Bradley, R.S. and Eddy, J.A., 1991. Records of past global changes. In: Global Changes of the Past (R.S. Bradley, ed.). Boulder: University Corporation for Atmospheric Research, p.5-9.
- Brandes, J.A. and Devol, A.H., 1997. Isotopic fractionation of oxygen and nitrogen in coastal marine sediment. *Geochimica et Cosmochimica Acta*, 61: 1793-1801.
- Brassell, S.C., 1993. Applications of biomarkers for delineating marine paleoclimatic fluctuations during the Pleistocene. In: Organic Geochemistry Principles and Applications. Engel, M.H. and Macko, S.A. (Eds), Plenum Press, New York and London, pp, 699-738.
- Brassell, S.C., Eglinton, G., Marlowe, I.T., Pflaumann, U. and Sarnthein, M., 1986. Molecular stratigraphy: a new tool for climate assessment. *Nature*, 320:129-133.
- Broecker, W.S., 1991. The great ocean conveyor. *Oceanography*, 4:79-89.
- Brunnberg, L., 1995. The Baltic Ice Lake. *Quaternary International*, 28: 177-178.
- Cadet, D. and Reverdin, G., 1981. Water vapour transport over the Indian Ocean during summer. *Tellus*, 33: 476-487.
- Calvert, S.E., Pederson, T.F. and Thunell, R.C., 1993. Geochemistry of surface sediments of the Sulu and South China Seas. *Marine Geology*, 114: 207-231.
- Calvert, S.E., Pedersen, T.F., Naidu, P.D. and Von Stackelberg, U., 1995. On the organic carbon maximum on the continental slope of eastern Arabian Sea. *Journal of Marine Research*, 53:269-296



- Calvert, S.E., Douglas, F., Cowie, G.L., Schubert, C., Von Rad, U., Schulz, H., Berner, U. and Erlenkeuser, H., 1996. Late Pleistocene record of organic carbon accumulation in the northeastern Arabian Sea. *International Symposium on Geology and Geophysics of the Indian Ocean, Goa (Abstract)*, pp. 60-61.
- Cayre, O. and Bard, E., 1999. Planktonic foraminiferal and alkenone records of the last deglaciation from the eastern Arabian Sea. *Quaternary Research*, 52: 337-342.
- Chaisson, W.P. and Ravello, A.C., 2000. Pliocene development of the east-west hydrographic gradient in the equatorial Pacific. *Paleoceanography*, 15: 497-505.
- Chodankar, A. R., Banakar, V. K. and Oba, T., 2003. Past-salinity gradient variations in the eastern Arabian Sea: reconstructions from the sedimentary  $\delta^{18}\text{O}_{G.sacculifer}$  records. Internat. Young Scientists Global Change Conf., Triesty, Italy, 16-19 Nov. p.27.
- Clemens, S. and Prell, W.L., 1990. Late Pleistocene variability of Arabian Sea summer monsoon winds and continental aridity; eolian records from the lithogenic component of deep-sea sediments. *Paleoceanography*, 5 (2): 109-145.
- Clemens, S., Prell, W.L., Murray, D., Shimmield, G.B. and Weedon, G., 1991. Forcing mechanism of the Indian Ocean Monsoon. *Nature*, 353: 720-725.
- Codispoti, L.A., 1995. Biogeochemical cycles: Is the ocean loosing nitrate? *Nature*, 376: 724-727.
- Codispoti, L.A. and Christensen, J.P., 1985. Nitrification, denitrification, nitrous oxide cycling in the eastern tropical south pacific ocean. *Marine Chemistry*, 16:277-300.
- Cullen, J.L., 1981. Microfossil evidence for changing salinity pattern in the Bay of Bengal over the last 20000 years. *Palaeogeography Palaeoclimatology Palaeoecology*, 35: 315-356.
- Currie, R. I., Fisher, A. E. and Hargreaves, P. M., 1973. Arabian Sea Upwelling. In: *The biology of the Indian Ocean*, B. Zeitzschel (ed),. Springer, Berlin, pp. 37-52.
- Curry, W.B. and Cullen, J.L., 1997. Carbonate production and dissolution in the western equatorial Atlantic during the last 1 m.y. *Proc. ODP Sci. Results*, 154, 189-199.

- Dansgaard, W., Johnsen, S.J., Clausen, H.B., Dahl-Jensen, D., Gundestrup, N. and Hammer, C.U., 1984. North Atlantic climatic oscillations revealed by deep Greenland ice cores. In: *Climate Processes and climate sensitivity. Geophysical Monograph 29, Maurice Ewing Volume 5*, edited by J.E. Hansen and T. Takahashi, American Geophysical Union, Washington D.C., pp. 288-298.
- Dansgaard, W., Johnsen, S.J., Clausen, H.B., Dahl-Jensen, D., Gundestrup, N.S., Hammer, C.U., Hvidberg, C.S., Steffensen, J.P., Sveinbjörnsdóttir, A.E., Jouzel, J. and Bond, G., 1993. Evidence for general instability of past climate from a 250-kyr ice-core record. *Nature*, 364: 218-220.
- Delaygue, G., Bard, E., Rollion, C., Jouzel, J., Steivenard, M., Duplessy, J.-C., 2001. Oxygen isotope/salinity relationship in the northern Indian Ocean. *J. Geophys. Res.*, 106: 4565-4574.
- Demaison, G. and Moore, G. T., 1980. Anoxic environments and oil source bed genesis. *American Association of Petroleum Geologists Bulletin*, 64: 1179-1209.
- Dickens, G. R. and Owen, R.M., 1994. Late Miocene-Early Pliocene manganese redirection in the central Indian Ocean: Expansion of the intermediate water oxygen minimum zone. *Paleoceanography*, 9: 169-181.
- Dodge, R.E., Fairbanks, R.G., Benninger, L.K. and Maurrasse, F., 1983. Pleistocene sea levels from raised coral reefs of Haiti. *Science*, 219: 1423-1425.
- Duplessy, J.-C., 1982. Glacial to interglacial contrast in the northern Indian Ocean. *Nature*, 295: 494-498.
- Duplessy, J.-C., Bè, A.W.H., Balnk, P.L., 1981. Oxygen and carbon isotopic composition and biogeographic distribution of planktonic foraminifera in the Indian Ocean. *Paleogeography Paleoclimatology Paleoecology*, 33: 9-46.
- Emeis, K-C., Anderson, D.M., Doose, H., Kroon, D., Schulz-Bull, D., 1995. Sea-surface temperatures and history of monsoon upwelling in the northwest Arabian Sea during the last 500,000 years. *Quaternary Research*, 43: 355-361.
- Emiliani, C., 1955. Pleistocene temperatures. *Journal Geology*, 63: 538-578.
- Epstein, S., Buchsbaum, R., Lowenstan, H.A., Uray, H.C., 1953. Revised carbonate-water isotopic temperature scale. *Bull. Geological Society of America*, 64: 1315-1325.

- Fairbanks, R.G., 1989. A 17000-year glacio-eustatic sea level record: influence of glacial melting rates on younger Dryas event and deep ocean circulation. *Nature*, 342: 637-642.
- Filippelli, G.M., 1997. Intensification of the Asian monsoon and a chemical weathering event in the late Miocene-early Pliocene: Implications for late Neogene climate change. *Geology*, 25: 27-30.
- Folk, R.L., 1968. Petrology of sedimentary rocks, *Hemphills, Austin*. 177 pp.
- Fontugne, M.R. and Duplessy, J.-C., 1981. Organic carbon isotopic fractionation by marine plankton in the temperature range-1°C-31°C. *Oceanologica Acta*, 4: 85-89.
- Ganeshram, R.S., Pederson, T.F., Calvert, S.E., McNeill, G.W., Fontugne, M.R., 2000. Glacial-interglacial variability in denitrification in the world oceans: causes and consequences. *Plaeoceanography*, 15: 361-376.
- Gröger, M., Henrich, R. and Bickert, T., 2003. Glacial-interglacial variability in lower North Atlantic deep water: inference from silt grain-size analysis and carbonate preservation in the western equatorial Atlantic. *Marine Geology*, 201: 321-332.
- Haake, B., Ittekkot, V., Rixon, T., Ramaswami, V., Nair, R.R., Curry, W.B., 1993. Seasonality and inter-annual variability of particle fluxes to the deep Arabian Sea. *Deep-Sea Research Part-I*, 40: 1323-1344.
- Haake, B., Rixen, T., Reemtsma, T., Ramaswamy, V. and Ittekkot, V. D., 1996. Process determining seasonality and interannual variability of settling particle fluxes to the deep Arabian Sea. In: V. Ittekkot et al. (Eds.), *Particle fluxes in the ocean*. John Wiley and Sons, pp: 251-270.
- Hasternath, S. and Greischar, L., 1991. The monsoonal current regimes of the tropical Indian Ocean: Observed surface flow fields and their geostrophic and wind-driven components. *Journal of Geophysical Research*, 96: 12619-12633.
- Hays, J.D., Imbrie, J. and Shackleton, N.J., 1976. Variations in the Earth's orbit: Pacemaker of the ice ages. *Science*, 194: 1121-1132.
- Heinrich, M., 1988. Origin and consequences of cyclic ice rafting in the northeast Atlantic Ocean during the past 130,000 years. *Quaternary Research*, 29: 143-152.

- Hemleben, C., Spindler, M., Anderson, R.O., 1989. Modern planktonic foraminifera. *Springer-Verlag, NY.*, p. 363.
- Hoefs, J., 1997. Stable isotope geochemistry. Springer-verlag, Germany, p. 201.
- Hong, Y.T., Hong, B., Lin, Q.H., Zhu, Y.X., Shibata, Y., Hirota, M., Uchida, M., Leng, X.T., Jiang, H.B., Xu, H., Wang, H. and Yi, L., 2003. Correlation between Indian Ocean summer monsoon and north Atlantic climate during the Holocene. *Earth and Planetary Science Letters*, 211: 371-380.
- Imbrie, J., Hays, J.D. Martinson, D.G., McIntyre, A., Mix, A.C., Morley, J.J., Pisias, N.G., Prell, W.L., Shackleton, N.J., 1984. The orbital theory of Pleistocene climate: support from a revised chronology of the marine  $\delta^{18}\text{O}$  record. In: A. Berger et al (Eds.). *Milankovitch and climate, Part-I, Plenum-Reidel*, pp. 269-305.
- Ikehara, M., Kawamura, K., Ohkouchi, N., Kimoto, K., Murayama, M., Nakamura, T., Oba, T. and Taira, A., 1997. Alkenone sea surface temperature in the Southern Ocean for the last two deglaciations. *Geophysical Research Letters*, 24: 679-682.
- Ikehara, M., Kawamura, K., Ohkouchi, N., Murayama, M., Nakamura, T. and Taira, A., 2000. Variations of terrestrial input and marine productivity in the Southern Ocean (48°S) during the last two deglaciations. *Paleoceanography*, 15: 170-180.
- Jasper, J. P and Gogosian, R. B., 1990. The sources and deposition of organic matter in late Quaternary Pigmy Basin. *Geochimica et Cosmochimica Acta*, 54: 1117-1132.
- Jensen, T.G., 2001. Arabian Sea and Bay of Bengal exchange of salt and tracers in an ocean model. *Geophysical Research Letters*, 28: 3967-3970.
- Jensen, T.G., 2003. Cross-equatorial pathways of salt and tracers from the northern Indian Ocean: Modelling results. *Deep Sea Research-II*, 50: 2111-2127.
- Kabanova, Y. G., 1968. Primary production in the northern part of the Indian Ocean. *Oceanology*, 8: 214-225.
- Keigwin, L.D., Jones, G.A., Lehman, S.J. and Boyle, E.A., 1991. Deglacial meltwater discharge, North Atlantic deep circulation and abrupt climate change. *Journal of Geophysical research*, 96C: 16811-16826.

- Keinast, M., 2000. Constant nitrogen isotopic composition of organic matter in the South China Sea during the last climatic cycle: Global implications. *Paleoceanography*, 15(2): 244-253
- Kienast, M., Calvert, S. E., Pelejero, C. and Grimalt, O., 2001. A critical review of marine sedimentary  $\delta^{13}\text{C}$ - $p\text{CO}_2$  estimates: New palaeorecords from the South China Sea and a revisit of other low latitude  $\delta^{13}\text{C}$ - $p\text{CO}_2$  records. *Paleoceanography*, 15: 113-127.
- Kroopnick, P.M., 1985. The distribution of  $\delta^{13}\text{C}$  of  $\Sigma\text{CO}_2$  in the world oceans. *Deep Sea Research*, 32: 57-84.
- Kudrass, H.R., Hofmann, A., Doose, H., Emeis, K. and Erlenkeuser, H., 2001. Modulation and amplification of climatic changes in the northern hemisphere by the Indian summer monsoon during the past 80 k.y. *Geology*, 29: 63-66.
- Ku, T-L. and Oba, T., 1978. A method for quantitative evaluation of carbonate dissolution in deep-sea sediments and its application to paleoceanographic reconstruction. *Quaternary Research*, 10: 112-129.
- Leuschner, D. K. and Sirocko, F., 2000. The low-latitude monsoon climate during Dansgaard-Oeschger cycles and Heinrich Events. *Quaternary Science Reviews*, 19: 243-254.
- Levitus, S. and Boyer, T.P., 1994. World Ocean Atlas-1994. vol 5, Salinity, NOAA Atlas NESDIS 3, 99p, U.S. Govt. Print. Off. Washington DC.
- Madhupratap, M., Kumar, S.P., Bhattatri, P.M.A., Kumar, M.D., Raghukumar, S., Nair, K.K.C. and Ramaiah, N., 1996. Mechanism of the biological response to winter cooling in the northeastern Arabian Sea. *Nature*, 384: 549-552.
- Martin, J.H., 1990. Glacial-interglacial  $\text{CO}_2$  change: the iron hypothesis. *Paleoceanography*, 5: 1-13.
- Milankovitch, M. M., 1941. Canon of insolation and the ice-age problem. Beograd: Koniglich Serbische Akademie. (English translation by the Israel Program for Scientific Translations, published for the US Department of Commerce, and the National Science, Foundation, Washington, DC (1969).)
- Murray, R.W., Leinen, M., 1993. Chemical transport to the seafloor of the equatorial Pacific Ocean across the latitudinal transect at 135oW: tracking the sedimentary major, trace and REE element fluxes at the equator and intertropical convergence zone. *Geochimica et Cosmochimica Acta*, 57: 4141-4163.

- Muller, P. J., Schneider, R. and Ruhland, G., 1994. Late Quaternary  $PCO_2$  variations in the Angola Current: evidence from organic carbon  $\delta^{13}C$  and alkenone temperatures. In: Zahn, R., Pedersen, T. F., Kaminski, M. A., Labeyrie, L. (Eds.). *Carbon Cycling in Glacial Ocean: Constraints on the Ocean's Role in Global Change*. NATO ASI Series, Vol 17, Springer, Berlin Heidelberg New York, pp 343-366.
- Naidu, P. D. and Malmgren. B.A., 1999. Quaternary carbonate record from the equatorial Indian Ocean and its relationship with productivity changes. *Marine Geology*, 161: 49-62.
- Naidu, P.D. and Malmgren. B.A., 1996. A high-resolution record of late Quaternary upwelling along the Oman margin, Arabian Sea based on planktonic foraminifera. *Paleoceanography*, 11: 129-140.
- Nair, R.R. and Hashmi, N.H., 1980. Holocene climatic inferences from sediments of the western Indian continental shelf. *Proc. Indian Academy of Science*, 89-A: 299-315.
- Nair, R.R., Ittekkot, V., Manganini, S.J., Ramaswami, V., Haake, B., Degens, E.T., Desai, B.N., Honjo, S., 1989. Increased particle flux to the deep ocean related to monsoon. *Nature*, 338: 749-751.
- Naqvi, S.W.A., 1987. Some aspects of the oxygen deficient conditions and denitrification in the Arabian Sea. *Journal of Marine Research*, 45: 1049-1072.
- Ninkovitch, D., 1979. Distribution, age, and chemical composition of western Indonesia. *Journal of Volcanology and Hydrothermal Research*, 5: 67-86.
- Niitsuma, N., Oba, T. and Okada, M., 1991. Oxygen and carbon isotope stratigraphy at Site 723, Oman margin. In: W. L. Prell et al (eds), *Proceedings of ODP Scientific Results*, 117, College Station, Tx., 321-341.
- Oeschger, H., Beer, J., Siegenthaler, U. and Stauffer, B., 1984. Late glacial climate history from ice cores. In: *Climate Processes and Climate Sensitivity* (J.E. Hansen and T. Takahashi, eds.). Washington, DC: American Geophysical Union, pp. 299-306.
- Olausson, E., 1965. Evidence of climatic changes in deep-sea cores, with remarks on isotopic palaeotemperature analysis. *Progress in Oceanography*, 3: 321-352.
- Olson, D.B., Hitchcock, G.L., Fine, R.A. and Bruce, A.W., 1993. Maintenance of low oxygen layer in the central Arabian Sea. *Deep Sea Research Part-II*, 40: 673-685.

- Overpeck, J., Rind, D., Lacy, A.C. and Healy, R., 1996. Possible role of dust induced regional warming in abrupt climate change during the last glacial period. *Nature*, 384: 447-449.
- Paropkari, A. L., Babu, C. P. and Mascarenhas, A., 1992. A critical evaluation of depositional parameters controlling the variability of organic carbon in Arabian Sea sediments. *Marine Geology*, 107:213-226.
- Pattan, J.N., Shane, P., Banakar, V.K., 1999. New occurrence of Youngest Toba Tuff in abyssal sediment of the Central Indian Basin. *Marine Geology*, 155: 243-248.
- Pattan, J.N., Masuzawa, T., Naidu, P.D., Parthiban, G., Yamamoto, M., 2003. Productivity fluctuations in the southeastern Arabian Sea during the last 140 Ka. *Palaeogeography Palaeoclimatology Palaeoecology*, 193: 575-590.
- Pedersen, T. F. and Calvert, S. E., 1990. Anoxia Vs. Productivity: What controls the formation of organic carbon-rich sediments and sedimentary rocks? *American Association of Petroleum Geologists Bulletin*, 74: 454-466.
- Pedersen, T. F., Shimmiel, G. B. and Price, N. B., 1992. Lack of enhanced preservation of organic matter in sediments under the oxygen minimum in the Oman margin. *Geochimica et Cosmochimica Acta*, 56: 545-551.
- Peters, K. E., Sweeney, R. E. and Kaplan, I. R., 1978. Correlation of carbon and nitrogen stable isotope ratios in sedimentary organic matter. *Limnology Oceanography*, 23: 598-604.
- Pettijohn, F.J., Potter, P.E. and Siever, R., 1972. Sand and Sandstones. Springer, New-York, p.618.
- Prasad, T.G., 2001. Formation and seasonal spreading of water masses in the Arabian Sea based on Data Analysis and Modelling. Ph. D. Thesis, Hokkaido Univ., Japan. p. 131.
- Prasanna Kumar, S. and Prasad, T.G., 1999. Formation and spreading of Arabian Sea high-salinity water mass. *Journal of Geophysical Research*, 104: 1455-1464.
- Prahl, F. G. and Wakeham, S. G., 1987. Calibration of unsaturation patterns in long-chain ketone compositions for paleotemperature assessment. *Nature*, 330: 367-369.

- Prahl, F. G., Muehlhausen, L. A. and Zahnle, D. L., 1988. Further evaluation of long-chain alkenones as indicators of paleoceanographic conditions. *Geochimica et Cosmochimica Acta*, 52: 2303-2310.
- Prahl, F.G., de Lange, G.J., Lyle, M. and Sparrow, M.A., 1989. Post depositional stability of long-chain alkenones under contrasting redox conditions. *Nature*, 341: 434-437.
- Prell, W.L. and Kutzbach, J.E., 1992. Sensitivity of the Indian monsoon to forcing parameters and implications for its evolution. *Nature*, 360: 647-652.
- Prell, W.L. and Kutzbach, J.E., 1987. Monsoon variability over the past 150,000 years. *Journal of Geophysical Research*, 92 (D7): 8411-8425.
- Prell, W.L., Hutson, W.H., Williams, D.F., Be, A.W.H., Geitzenauer, R. and Molino, B., 1980. Surface circulation of the Indian Ocean during the last interglacial maximum, approximately 18,000 yr B.P. *Quaternary Research*, 14: 309-336.
- Prins, M.A. and Weltje, G.J., 1999. End-member modeling of siliciclastic grain-size distributions: The late quaternary record of eolian and fluvial sediment supply to the Arabian Sea and its paleoclimatic significance in: Harbaugh et al., (eds), Numerical experiments in stratigraphy: Recent advances in stratigraphic and sedimentologic computer simulations. SEPM (Society for Sedimentary Geology), Spl. Publ. 62, p. 91-111.
- Prins, M.A., Postma, G., Cleveringa, J., Cramp, A. and Kenyon, N.H., 2000. Controls on terrigenous sediment supply to the Arabian Sea during the late Quaternary: the Indus Fan. *Marine Geology*, 169: 327-349.
- Prins, M.A., Postma, G. and Weltje, G.J., 2000. Controls on terrigenous sediment supply to the Arabian Sea during the late Quaternary: the Makran continental slope. *Marine Geology*, 169: 351-371.
- Qasim, S.Z., 1977. Biological productivity of the Indian Ocean. *Indian Journal of Marine Sciences*, 6: 122-137.
- Qasim, S.Z., 1982. Oceanography of the northern Arabian Sea. *Deep Sea Research*, 29: 1041-1068.
- Rao, B. R. and Veerayya, M. 2000. Influence of marginal highs on the accumulation of organic carbon along continental slope off India. *Deep-Sea Research II*, 47: 303-327.



- Rao, K. L. 1979. India's water wealth: Its assessment, uses and projections. Orient Longman, pp. 261.
- Rao, R.R., Molinari, R.L. and Festa, J.F., 1989. Evolution of the climatological near-surface thermal structure of the tropical Indian Ocean. *Journal of Geophysical Research*, 94: 10801-10815.
- Rau, G. H., Takahashi, T. and Marais, D. J. D., 1989. Latitudinal variation in plankton  $\delta^{13}\text{C}$ : Implications for  $\text{CO}_2$  and productivity in past oceans. *Nature*, 341: 516-518.
- Reichart, G., 1997. Late Quaternary variability of the Arabian Sea monsoon and oxygen minimum zone. *Ph.D.Thesis*, Univ. Utrecht, p. 171.
- Reichart, G.J., Lourens, L.J., Zachariasse, W.J., 1998. Temporal variability in the northern Arabian sea oxygen minimum zone during the last 225,000 years. *Paleoceanography*, 13: 607-621.
- Reichart, G.J., Dulk, M. den., Visser, H.J., van der Weijden, C.H. and Zachariasse, W.J., 1997. A 225 kyr record of dust supply, paleoproductivity and the oxygen minimum zone from the Murray Ridge (northern Arabian Sea). *Paleogeography Paleoclimatology Paleoecology*, 134: 149-169.
- Rose, W. I. and Chesner, C. A., 1987. Dispersal of ash in the great Toba eruption. *Geology*, 15: 913-917.
- Rostek, F., Ruhland, G., Bassinot, F. C., Muller, P. J., Labeyrie, L. D., Lancelot, Y. and Bard, E., 1993. Reconstructing sea surface temperature and salinity using  $\delta^{18}\text{O}$  and alkenone records. *Nature*, 364: 319-321.
- Rostek, F., Bard, E., Beafort, L., Sonzogni, C. and Ganssen, G., 1997. Sea surface temperature and productivity records for the past 240 kyr in the Arabian Sea. *Deep Sea Research II*, 44: 1461-1480.
- Sarkar, A., Ramesh, R., Somayajulu, B. L. K., Agnihotri, R., Jull, A. J. T. and Burr, G. S., 2000. High resolution Holocene monsoon record from the eastern Arabian Sea. *Earth and Planetary Science Letters*, 177: 209-218.
- Sarkar, A., Ramesh, R., Bhattacharya, S. K. and Rajagopalan, G., 1990. Oxygen isotope evidence for a stronger winter monsoon current during the last glaciation. *Nature*, 343: 549-551.

- Schulte, S., Rostek, F., Bard, E., Rullkotter, J., Marchal, O., 1999. Variation of oxygen minimum and primary productivity recorded in sediments of the Arabian sea. *Earth Planetary Science Letters*, 173: 205-221.
- Schulz, H., von Rad, U. and Erlenkeuser, H., 1998. Correlation between Arabian Sea and Greenland climate oscillations of the past 110,000 years. *Nature*, 393: 54-57.
- Shackleton, N.J., 2000. A 100,000 year ice-age cycle identified and found to lag temperature, carbon-dioxide, and orbital eccentricity. *Science*, 289: 1897-1902.
- Shackleton, N. J., Opdyke, N. D., 1973. Oxygen isotope and palaeomagnetic stratigraphy of equatorial Pacific core V28-238: Oxygen isotope temperatures and ice volume on a 105 and 106 year-scale. *Quaternary Research*, 3: 39-55.
- Shackleton, N.J., 1967. Oxygen isotope analyses and Pleistocene temperatures re-assessed. *Nature*, 215: 15-17.
- Shankar, D., Vinayachandra, P. N. and Unnikrishnan, A. S., 2002. The monsoon currents in the north Indian Ocean. *Progress in Oceanography*, 52: 63-120.
- Sharma, G. S., 1977. Upwelling off the southwest coast of India. *Journal of Marine Sciences*, 7: 209-218.
- Shemesh, A., Macko, S.A., Charles, C.D. and Rau, G.H., 1993. Isotopic evidence for reduced productivity in the glacial Southern Ocean. *Science*, 262: 407-410.
- Shetye, S. R., Gouveia, A. D., Shenoi, S. S. C., Michael, G. S., Sundar, D., Almeida, A. M. and Santanam, M., 1990. Hydrography and circulation off the west coast of India during the southwest monsoon. *Journal of Marine Research*, 48: 359-378.
- Shetye, S.R., Gouveia, A.D., Shenoi, S.S.C., Michael, G.S., Sundar, D., Almeida, A.M. and Santanam, K., 1991. The coastal current off western India during the northeast monsoon. *Deep Sea Research*, 38: 1517-1529.
- Shimmield, G.B., Mowbray, S.R., Weedon, G.P., 1990. A 350 ka history of the Indian SW-monsoon: evidence from deep sea cores, northwest Arabian Sea. *Transactions of the Royal Society, Edinburgh, Earth Sciences*, 81: 289-299.

- Sigman, D.M. and Boyle, E.A., 2000. Glacial/interglacial variations in atmospheric carbon dioxide. *Nature*, 407: 859-869.
- Sirocko, F., Sarnthein, M., Lange, H. and Erlenkeuser, H., 1991. Atmospheric summer circulation and coastal upwelling in the Arabian Sea during the Holocene and last glaciation. *Quaternary Research*, 36: 72-93.
- Sirocko, F., Sarnthein, M., Erlenkeuser, H., Lange, H., Arnold, M. and Duplessy, J. -C., 1993. Century scale events in monsoon climate over the past 24,000 years. *Nature*, 364: 322-324.
- Sirocko, F., Garbe-Schonberg, D., McIntyre, A. and Molfino, B., 1996. Teleconnections between the subtropical monsoons and high-latitude climates during the last deglaciation. *Science*, 272: 526-529.
- Sirocko, F. and Sarnthein, M., 1989. Wind-borne deposits in the Northwestern Indian Ocean: record of Holocene sediments versus modern satellite data. In: *Paleoclimatology and Paleometeorology: Modern and Past Patterns of Global Atmospheric Transport*, Leinen, M. and Sarnthein, M. (Eds.). NATO ASI Series (282), Kluwer, Dordrecht-Boston-London, pp. 401-433.
- Slater, R. D. and Kroopnick., 1984. Controls on dissolved oxygen distribution and organic carbon deposition in the Arabian Sea. In: *Marine Geology and Oceanography of the Arabian Sea and Coastal Pakistan*, Haq, B. U. and Milliman, J. D. (Eds.). Van Nostrand Reinhold, New York, 305-313 pp.
- Smith, S. L., Banse, K., Cochran, J. K., Codispoti, L. A., Ducklow, H. W., Luther, M. E., Olson, D. B., Peterson, W. T., Prell, W. L., Surgi, N., Swallow, J. C. and Wishner, K., 1991. U. S. JGOFS: Arabian Sea Process Study, U. S. JGOFS Planning Report No. 13, Woods Hole Oceanographic Institution, Woods Hole, Massachusetts, 164 pp.
- Sonzogni, C., Bard, E., Rostek, F., 1998. Tropical sea surface temperatures during the last glacial period: a view based on alkenones in Indian Ocean sediment. *Quaternary science Reviews*, 17: 1185-1201.
- Spaulding, S.A., Oba, T., 1992. Association of late Pleistocene calcareous nonfossil assemblages and  $^{18}\text{O}$  and  $^{13}\text{C}$  isotopic changes, ODP Leg 117, Oman Margin, Arabian Sea. *Memoire Di Scienze Geology, Univ. Padova*, XLIII, 389-407.

- Suthhof, A. Ittekkot, V., Gaye-Haake, B., 2001. Millennial-scale oscillation of denitrification intensity in the Arabian Sea during the late quaternary and its potential influence on atmospheric N<sub>2</sub>O and global climate. *Global Biogeochemical Cycles*, 15, 637-649.
- Sweeney, R. E. and Kaplan, I. R., 1980. Natural abundance of <sup>15</sup>N as a source indicator of nearshore and marine sedimentary and dissolved nitrogen. *Marine Chemistry*, 9: 81-94.
- Tamburini, F., Föllmi, K. B., Adatte, T., Bernasconi, S. M. and Steinmann, F., 2003. Sedimentary phosphorous records from the Oman Margin: New evidence of high productivity during glacial periods. *Paleoceanography*, 18: 15-14.
- Thamban, M., Rao, P.C., Schneider, R.R., Grootes, P.M., 2001. Glacial to Holocene fluctuations in hydrography and productivity along the southwestern continental margin of India. *Palaeogeography Palaeoclimatology Palaeoecology*, 165: 113-127.
- Urey, H.C., 1947. The thermodynamic properties of isotopic substances. *Journal of Chemical Society*, 562-581.
- Van Campo, E., Duplessy, J.C. and Rossignol-Strick, M., 1982. Climatic conditions deduced from a 100 kyr oxygen isotope-pollen record from the Arabian Sea. *Nature*, 296: 56-59.
- Volkman, J. K., Eglinton, G., Corner, E. D. S. and Sargent, J. R., 1980. Novel unsaturated straight chain C37-C39 methyl and ethyl ketones in marine sediment and coccolithophore *Emiliana Huxleyi*. In: *Advances in organic geochemistry* (A.G. Douglas and J. R. Maxwell, Eds.). Pergamon, pp. 219-227.
- Wada, E.M. and Hattori, A., 1978. Nitrogen isotope effects in the assimilation of inorganic nitrogenous compounds. *Geomicrobiology Journal*, 1: 85-101.
- Walsh, J.J., Premuzic, E.T. and Whitedge, T.E., 1981. Fate of nutrient enrichment on continental shelves as indicated by C/N content of bottom sediments. In: *Ecohydrodynamics*. J.C.J. Nihoul (Ed). Elsevier, pp. 13-49.
- Wyrski, K., 1973. Physical oceanography of the Indian Ocean. In: *The biology of the Indian Ocean*. B. Zeitzschel (ed). Springer, Berlin, pp. 18-36.
- Yamamoto, M., Yamamura, M., Tada, R., 2000. Late Quaternary records of organic carbon, calcium carbonate, and biomarkers from Site 1016 off Point Conception, California margin. *ODP Scientific Results*, 167: 183-194.

- Yang, S., 1996. Snow-monsoon associations and seasonal-interannual prediction. *International Journal of Climatology*, 16: 125-134.
- You, Y. and Tomczak, M., 1993. Thermocline circulation and ventilation in the Indian Ocean derived from water mass analysis. *Deep Sea Research*, 40: 13-56.
- Zielinski, G.A., Mayewski, P.A., Meeker, L.D., Whitlow, S., Twickler, M.S. and Taylor, K., 1996. Potential atmospheric impact of the Toba mega-eruption ~71,000 years ago. *Geophysical Research Letters*, 23: 837-840.

## **APPENDIX**

(The following pages contain various data generated for this study. The depth-interval or the chronological data shall be made available if required for review. However, those details are presented in the age-models of the sediment cores for ready reference)

**G. *sacculifer* oxygen- and carbon-isotopes in the Eastern Arabian Sea sediment**

(on PDB scale)

Section No	SK129/GC02 core		SK129/GC08 core		SK117/CR04 core	
	$\delta^{18}\text{O} \text{‰}$	$\delta^{13}\text{C} \text{‰}$	$\delta^{18}\text{O} \text{‰}$	$\delta^{13}\text{C} \text{‰}$	$\delta^{18}\text{O} \text{‰}$	$\delta^{13}\text{C} \text{‰}$
1	-1.829	1.122	-2.065	2.844	-2.301	4.691
2	-1.879	0.857	-2.115	2.562	-2.351	4.392
3	-1.763	0.964	-1.999	2.673	-2.235	4.506
4	-1.810	1.022	-2.046	2.737	-2.282	4.576
5	-1.860	1.169	-2.096	2.895	-2.332	4.747
6	-1.542	1.080	-1.777	2.790	-2.013	4.623
7	-1.874	1.022	-2.110	2.739	-1.022	4.580
8	-1.826	1.106	-2.062	2.827	-2.298	4.672
9	-1.579	1.040	-1.814	2.748	-2.050	4.580
10	-1.227	0.950	-1.462	2.640	-1.698	4.453
11	-1.432	0.964	-1.667	2.662	-1.902	4.483
12	-1.785	0.864	-2.021	2.567	-2.257	4.394
13	-0.922	0.932	-1.156	2.611	-1.391	4.411
14	-1.157	1.053	-1.392	2.748	-1.627	4.566
15	-1.383	0.739	-1.618	2.419	-1.853	4.222
16	-0.789	1.245	-1.023	2.940	-1.258	4.758
17	-0.675	1.196	-0.909	2.884	-1.143	4.695
18	-1.285	1.005	-1.520	2.701	-1.755	4.520
19	-1.320	1.021	-1.555	2.718	-1.790	4.540
20	-0.884	0.800	-1.118	2.468	-1.353	4.257
21	-0.616	0.906	0.210	2.572	-0.023	4.324
22	-0.723	1.220	-0.957	2.912	-1.191	4.726
23	-0.738	0.954	-0.972	2.628	-1.206	4.423
24	-0.537	0.962	-0.771	2.630	-1.005	4.418
25	-0.656	0.883	0.370	2.549	0.138	4.293
26	-0.643	0.705	-0.877	2.359	-1.111	4.132
27	-0.641	0.959	-0.875	2.630	-1.109	4.422
28	-0.517	1.009	-0.751	2.679	-0.985	4.471
29	-0.493	0.884	-0.727	2.544	-0.961	4.326
30	-0.117	0.923	-0.350	2.574	-0.584	4.345
31	-0.299	1.036	-0.533	2.701	-0.766	4.486
32	-0.360	1.056	-0.594	2.724	-0.828	4.513
33	-0.264	1.118	-0.497	2.787	-0.731	4.577
34	-0.191	0.960	-0.424	2.616	-0.658	4.392
35	-0.217	1.109	-0.450	2.776	-0.684	4.564
36	-0.153	0.912	-0.386	2.563	-0.620	4.334
37	-0.344	0.810	-0.578	2.461	-0.812	4.232
38	-0.107	0.807	-0.340	2.449	-0.573	4.211
39	-0.092	1.067	-0.325	2.726	-0.558	4.506
40	-0.010	0.977	-0.243	2.628	-0.476	4.399
41	-0.177	0.960	-0.410	2.615	-0.644	4.390

42	0.071	0.959	-0.161	2.605	-0.395	4.372
43	-0.098	1.166	-0.331	2.833	-0.564	4.620
44	0.106	0.931	-0.127	2.574	-0.361	4.338
45	0.027	1.147	-0.206	2.808	-0.439	4.590
46	-0.013	1.056	-0.246	2.713	-0.479	4.489
47	-0.020	1.111	-0.253	2.771	-0.486	4.552
48	0.141	1.016	-0.092	2.664	-0.325	4.432
49	0.179	1.096	-0.054	2.748	-0.287	4.521
50	0.059	1.037	-0.173	2.689	-0.407	4.462
51	0.089	1.191	-0.143	2.853	-0.377	4.635
52	-0.002	0.971	-0.235	2.621	-0.468	4.391
53	0.012	1.004	-0.221	2.656	-0.454	4.428
54	0.035	1.066	-0.198	2.721	-0.431	4.496
55	-0.016	1.050	-0.249	2.706	-0.482	4.482
56	0.058	0.801	-0.174	2.437	-0.408	4.193
57	0.108	0.988	-0.125	2.636	-0.359	4.403
58	0.173	1.065	-0.060	2.716	-0.293	4.486
59	-0.052	0.925	-0.285	2.574	-0.518	4.342
60	-0.259	1.026	-0.492	2.689	-0.726	4.472
61	-0.238	0.997	-0.471	2.657	-0.705	4.437
62	-0.085	1.062	-0.318	2.721	-0.551	4.501
63	-0.308	0.940	-0.542	2.599	-0.775	4.377
64	-0.448	0.880	-0.682	2.539	-0.916	4.318
65			-0.233	1.584	-0.466	3.283
66			-0.233	1.584	-0.466	3.283
67			-0.233	1.584	-0.466	3.283
68			-0.233	1.584	-0.466	3.283
69			-0.233	1.584	-0.466	3.283
70			-0.233	1.584	-0.466	3.283
71			-0.233	1.584	-0.466	3.283
72			-0.233	1.584	-0.466	3.283
73			-0.233	1.584	-0.466	3.283
74			-0.233	1.584	-0.466	3.283
75			-0.233	1.584	-0.466	3.283
76			-0.233	1.584	-0.466	3.283
77			-0.233	1.584	-0.466	3.283
78			-0.233	1.584	-0.466	3.283
79			-0.233	1.584	-0.466	3.283
80			-0.233	1.584	-0.466	3.283
81			-0.233	1.584	-0.466	3.283
82			-0.233	1.584	-0.466	3.283
83			-0.233	1.584	-0.466	3.283
84			-0.233	1.584	-0.466	3.283
85			-0.233	1.584	-0.466	3.283
86			-0.233	1.584	-0.466	3.283
87			-0.233	1.584	-0.466	3.283
88			-0.233	1.584	-0.466	3.283
89			-0.233	1.584	-0.466	3.283



90	-0.233	1.584	-0.466	3.283
91	-0.233	1.584	-0.466	3.283
92	-0.233	1.584	-0.466	3.283
93	-0.415	1.584	-0.649	3.290
94	-0.233	1.584	-0.466	3.283
95	-0.233	1.584	-0.466	3.283
96	-0.233	1.584	-0.466	3.283
97	-0.233	1.584	-0.466	3.283
98	-0.233	1.584	-0.466	3.283
99	-0.233	1.584	-0.466	3.283
100	-0.233	1.584	-0.466	3.283
101	-0.233	1.584	-0.466	3.283
102	-0.233	1.584	-0.466	3.283
103	-0.233	1.584	-0.466	3.283
104	-0.233	1.584	-0.466	3.283
105	-0.233	1.584	-0.466	3.283
106	-0.233	1.584	-0.466	3.283
107	-0.233	1.584	-0.466	3.283
108	-0.233	1.584	-0.466	3.283
109	-0.233	1.584	-0.466	3.283
110	-0.233	1.584	-0.466	3.283
111	-0.233	1.584	-0.466	3.283
112	-0.233	1.584	-0.466	3.283
113	-0.233	1.584	-0.466	3.283
114	-0.233	1.584	-0.466	3.283
115	-0.233	1.584	-0.466	3.283
116	-0.233	1.584	-0.466	3.283
117	-0.233	1.584	-0.466	3.283
118	-0.233	1.584	-0.466	3.283
119	-0.233	1.584	-0.466	3.283
120	-0.233	1.584	-0.466	3.283
121	-0.233	1.584	-0.466	3.283
122	-0.233	1.584	-0.466	3.283
123	-0.233	1.584	-0.466	3.283
124	-0.233	1.584	-0.466	3.283
125	-0.233	1.584	-0.466	3.283
126	-0.233	1.584	-0.466	3.283
127	-0.233	1.584	-0.466	3.283
128	-0.233	1.584	-0.466	3.283
129	-0.233	1.584	-0.466	3.283
130	-0.233	1.584	-0.466	3.283
131	-0.233	1.584	-0.466	3.283
132	-0.233	1.584	-0.466	3.283
133	-0.233	1.584	-0.466	3.283
134	-0.233	1.584	-0.466	3.283
135	-0.233	1.584	-0.466	3.283
136	-0.233	1.584	-0.466	3.283
137	-0.233	1.584	-0.466	3.283

138	-0.233	1.584	-0.466	3.283
139	-0.233	1.584	-0.466	3.283
140	-0.233	1.584	-0.466	3.283
141	-0.233	1.584	-0.466	3.283
142	-0.233	1.584	-0.466	3.283
143	-0.233	1.584	-0.466	3.283
144	-0.233	1.584	-0.466	3.283
145	-0.233	1.584	-0.466	3.283
146	-0.233	1.584	-0.466	3.283
147	-0.233	1.584	-0.466	3.283
148	-0.233	1.584	-0.466	3.283
149	-0.233	1.584	-0.466	3.283
150	-0.233	1.584	-0.466	3.283
151	-0.233	1.584	-0.466	3.283
152	-0.233	1.584	-0.466	3.283
153	-0.233	1.584		
154	-0.233	1.584		
155	-0.233	1.584		
156	-0.233	1.584		
157	-0.233	1.584		
158	-0.233	1.584		
159	-0.233	1.584		
160	-0.233	1.584		
161	-0.233	1.584		
162	-0.233	1.584		
163	-0.233	1.584		
164	-0.233	1.584		
165	-0.233	1.584		
166	-0.233	1.584		
167	-0.233	1.584		
168	-0.233	1.584		
169	-0.233	1.584		
170	-0.233	1.584		
171	-0.233	1.584		
172	-0.233	1.584		
173	-0.233	1.584		
174	-0.233	1.584		
175	-0.233	1.584		
176	-0.233	1.584		
177	-0.233	1.584		
178	-0.233	1.584		
179	-0.233	1.584		
180	-0.233	1.584		
181	-0.233	1.584		
182	-0.233	1.584		
183	-0.233	1.584		
184	-0.233	1.584		

**Sediment texture data for the three cores of the Eastern Arabian Sea**

Section	SK129/GC02			SK129/GC08			SK129/CR04		
	Sand %	Silt %	Clay %	Sand %	Clay %	Silt %	Sand %	Clay %	Silt %
1	88.5	1.7	9.8	24.4	31.9	43.8	19.4	31.8	48.7
2	83.2	3.1	13.7	23.4	29.7	47.0	19.7	30.0	50.2
3	84.6	3.0	12.4	23.4	34.0	42.6	20.3	30.4	49.2
4	84.1	4.2	11.7	25.3	35.8	38.9	20.4	30.7	48.9
5	83.9	4.9	11.2	22.5	38.8	38.7	23.9	29.4	46.7
6	86.3	2.5	11.2	19.9	38.6	41.4	24.8	29.2	46.1
7	84.6	5.4	10.1	19.2	37.0	43.8	26.9	29.2	43.9
8	84.1	4.1	11.8	20.5	32.8	46.8	27.3	30.9	41.7
9	87.1	1.9	11.0	15.8	34.4	49.9	28.5	29.3	42.2
10	87.9	1.6	10.5	14.5	30.7	54.8	27.6	32.5	39.9
11	85.7	1.5	12.7	13.1	28.7	58.3	28.6	30.8	40.6
12	79.8	7.1	13.2	11.7	24.7	63.6	30.2	29.1	40.8
13	82.5	4.9	12.6	10.9	24.8	64.3	34.1	24.2	41.7
14	84.7	4.6	10.7	11.5	29.8	58.7	35.5	26.1	38.4
15	83.2	4.5	12.3	14.2	27.0	58.7	32.3	27.4	40.3
16	80.9	5.9	13.1	14.0	24.8	61.3	31.6	24.3	44.2
17	82.0	5.6	12.4	15.5	23.7	60.9	37.7	23.0	39.3
18	78.1	7.2	14.7	19.9	21.0	59.2	31.4	24.4	44.2
19	71.0	11.9	17.0	17.1	20.4	62.4	30.1	23.7	46.3
20	64.2	14.7	21.1	12.0	21.6	66.4	32.6	24.3	43.2
21	68.4	12.8	18.8	11.6	25.6	62.8	30.0	24.7	45.3
22	78.8	3.2	18.0	11.1	26.1	62.8	27.2	25.3	47.5
23	73.8	6.5	19.6	12.4	27.4	60.2	28.9	26.1	45.0
24	21.3	38.2	40.5	12.3	31.2	56.5	27.8	22.4	49.8
25	6.6	43.3	50.1	12.4	29.0	58.7	28.3	22.7	49.0
26	8.2	43.3	48.5	9.1	38.0	52.9	25.0	22.9	52.1
27	8.1	46.6	45.3	10.3	39.6	50.1	25.1	19.8	55.2
28	6.6	43.8	49.7	10.5	39.1	50.4	25.5	21.7	52.8
29	3.7	44.8	51.5	12.9	40.1	47.0	27.1	19.4	53.6
30	3.3	45.4	51.3	11.4	40.4	48.3	26.4	21.7	51.9
31	6.5	45.2	48.3	11.2	40.1	48.7	20.3	20.5	59.2
32	23.0	35.4	41.6	13.5	39.6	46.9	17.9	22.3	59.8
33	5.1	45.4	49.5	14.1	42.0	43.8	17.8	22.8	59.4
34	38.3	27.6	34.1	9.0	43.9	47.1	24.1	22.7	53.2
35	3.9	45.0	51.1	7.0	41.1	51.9	25.0	23.4	51.6
36	6.8	44.8	48.4	7.2	44.1	48.7	25.8	22.9	51.3
37	4.5	47.9	47.5	5.2	42.6	52.1	22.6	26.1	51.3
38	3.4	45.7	50.9	5.2	43.1	51.6	21.9	27.2	50.9
39	3.1	43.8	53.1	5.7	44.7	49.6	21.2	27.0	51.8
40	3.0	47.2	49.9	6.1	42.4	51.5	21.0	25.4	53.6
41	3.3	45.5	51.3	6.4	47.1	46.5	24.0	25.8	50.2
42	38.5	28.9	32.6	5.9	50.7	43.4	24.9	23.9	51.2
43	2.9	44.6	52.4	5.1	48.2	46.7	21.7	26.6	51.8
44	2.3	44.7	51.8	3.6	46.9	49.5	21.8	23.7	54.5

45	3.8	44.8	51.3	3.4	50.2	46.4	17.8	26.8	55.4
46	2.7	42.6	54.7	4.0	43.1	52.9	21.0	25.1	53.9
47	3.3	44.9	51.8	4.3	43.1	52.6	18.4	25.8	55.8
48	2.9	44.3	52.8	6.8	44.3	48.9	19.2	27.8	53.1
49	2.9	45.5	51.6	10.4	42.0	47.6	19.1	26.1	54.9
50	3.0	43.9	53.1	12.5	41.3	46.2	21.0	27.2	51.8
51	4.0	46.6	49.4	11.4	44.2	44.4	19.3	26.2	54.5
52	2.3	43.6	54.1	9.9	43.0	47.1	21.4	26.8	51.8
53	3.3	39.8	56.8	9.2	42.8	48.1	18.9	27.4	53.7
54	2.3	42.4	55.3	10.2	42.9	46.8	23.6	25.7	50.7
55	5.1	41.5	53.4	12.4	41.8	45.8	22.8	28.3	48.9
56	3.2	39.3	57.5	10.4	44.4	45.3	27.3	24.9	47.8
57	2.9	44.8	52.3	9.8	44.3	45.9	24.5	25.8	49.7
58	2.1	43.0	54.9	7.0	52.1	40.9	28.8	24.4	46.8
59	3.2	43.2	53.6	5.5	49.1	45.5	23.4	25.6	51.1
60	2.5	42.8	54.6	5.1	47.6	47.3	20.6	26.9	52.5
61	3.4	44.0	52.5	4.5	46.6	48.9	18.0	26.0	56.0
62	4.0	43.1	53.0	4.9	46.2	48.9	17.3	26.3	56.4
63	3.4	42.4	54.2	4.2	50.1	45.7	22.5	27.1	50.4
64	2.5	44.1	53.3	3.3	49.6	47.1	20.5	25.3	54.2
65	4.7	43.0	52.3	3.1	46.3	50.6	21.2	24.7	54.1
66	3.1	41.7	55.2	3.5	48.5	48.0	18.4	26.2	55.4
67	3.1	42.0	54.9	3.0	47.8	49.2	21.2	24.7	54.1
68	2.4	41.2	56.4	2.6	50.9	46.5	22.3	25.6	52.1
69	5.8	41.1	53.1	2.8	49.7	47.5	21.9	25.2	52.9
70	2.9	42.4	54.7	3.0	48.3	48.6	22.1	25.3	52.6
71	3.1	41.8	55.1	3.0	43.5	53.5	24.2	27.2	48.7
72	2.9	42.1	55.0	3.0	40.7	56.3	16.9	27.2	55.9
73	5.3	42.0	52.7	3.1	35.0	61.9	18.9	26.5	54.5
74	2.2	42.8	55.0	3.8	32.6	63.6	16.6	27.8	55.6
75	2.2	43.3	54.5	3.2	34.5	62.2	18.0	28.6	53.3
76	2.5	43.1	54.3	3.2	40.5	56.4	19.5	25.2	55.3
77	2.7	41.0	56.3	3.3	43.0	53.6	19.2	25.4	55.4
78	1.8	41.7	56.5	3.6	47.5	48.9	18.4	26.5	55.0
79	2.4	39.7	57.9	5.0	45.0	50.0	19.0	27.9	53.1
80	3.6	41.8	54.6	6.7	43.1	50.3	20.1	27.2	52.7
81	3.2	44.5	52.3	7.0	44.2	48.7	22.1	28.0	49.9
82	2.6	45.3	52.1	7.6	45.9	46.5	20.2	28.0	51.7
83	3.5	46.1	50.4	7.9	46.3	45.8	21.3	27.5	51.2
84	3.0	44.5	52.4	7.5	46.7	45.9	15.6	29.3	55.1
85	2.8	44.2	52.9	4.5	48.0	47.6	15.6	28.8	55.6
86	2.5	47.0	50.5	3.4	47.5	49.1	16.9	30.7	52.5
87	2.9	45.6	51.5	2.8	47.9	49.3	20.2	29.6	50.2
88	3.4	45.7	50.9	3.5	49.7	46.9	19.5	28.1	52.3
89	2.7	47.6	49.7	4.4	45.1	50.5	21.0	28.7	50.3
90	4.3	47.5	48.2	6.4	42.9	50.7	20.5	31.4	48.1
91	5.2	46.8	47.9	4.9	50.6	44.5	17.5	33.1	49.4
92	4.1	47.6	48.3	4.0	49.4	46.6	15.8	35.0	49.2
93	7.2	49.2	43.6	4.2	49.3	46.5	14.6	34.7	50.7

94	6.9	46.6	46.6	4.8	50.4	44.8	15.6	32.0	52.5
95	9.0	46.2	44.8	5.2	50.1	44.7	12.6	32.0	55.4
96	9.3	47.1	43.6	5.9	48.1	46.0	11.6	33.3	55.1
97	11.3	48.0	40.7	7.1	50.3	42.6	13.4	29.7	56.9
98	10.6	45.9	43.5	7.3	52.2	40.5	10.5	31.3	58.2
99	9.2	42.7	48.1	7.5	52.9	39.6	9.5	30.7	59.9
100	8.7	47.4	43.9	6.5	53.9	39.6	11.0	33.3	55.7
101	5.8	50.0	44.3	5.4	50.7	43.9	12.3	35.7	52.1
102	8.6	49.0	42.5	4.6	51.2	44.2	8.5	31.1	60.3
103	12.2	46.1	41.7				8.6	29.4	62.0
104	8.8	46.5	44.7				8.0	27.7	64.3
105	13.0	45.9	41.1				8.4	26.6	65.0
106	12.6	46.8	40.6				11.8	27.3	60.9
107	11.2	45.7	43.1				10.7	26.4	62.9
108	8.6	47.6	43.7				10.6	26.9	62.5
109	9.5	46.4	44.0				9.5	28.1	62.4
110	10.1	46.4	43.5				9.4	26.6	64.0
111	11.5	45.4	43.2				9.2	21.0	69.8
112	12.2	45.9	41.9				9.6	19.5	71.0
113	13.3	47.3	39.4				10.5	18.9	70.6
114	12.5	47.2	40.3				8.5	20.0	71.6
115	11.8	46.8	41.4				8.3	23.3	68.5
116	22.9	41.9	35.1				7.2	29.1	63.6
117	14.9	45.7	39.3				7.6	29.8	62.7
118	20.8	44.0	35.2				7.9	31.0	61.2
119	17.3	44.8	37.9				9.6	30.6	59.8
120	13.8	46.7	39.5				10.3	30.6	59.2
121	16.4	45.7	37.9				13.9	29.7	56.4
122	14.5	46.3	39.2				11.8	35.4	52.9
123	13.3	46.3	40.3				12.9	34.7	52.4
124	13.4	48.8	37.9				13.1	35.8	51.0
125	19.0	45.8	35.2				17.7	35.8	46.5
126	24.7	41.8	33.4				20.4	35.0	44.6
127	19.0	45.4	35.6				18.3	36.3	45.5
128	25.2	41.1	33.8				16.3	37.4	46.3
129	28.8	39.5	31.7				15.7	38.9	45.5
130	21.5	43.4	35.1				13.2	40.1	46.8
131	27.7	39.9	32.5				16.9	39.0	44.1
132	33.3	35.9	30.8				15.4	40.4	44.2
133	28.8	39.7	31.5				12.5	42.4	45.1
134	31.1	37.7	31.2				11.5	41.0	47.5
135	30.8	37.7	31.5				10.0	42.0	48.0
136	35.5	35.1	29.4				10.1	41.1	48.8
137	36.6	35.2	28.2				8.5	37.8	53.8
138	37.6	34.7	27.7				10.9	33.9	55.2
139	32.0	38.0	29.9				10.6	34.3	55.1
140	44.3	31.2	24.5				14.8	31.1	54.1
141	43.5	31.7	24.8				16.8	29.7	53.5
142	44.6	29.9	25.5				13.1	33.5	53.3
143	55.8	23.9	20.4				14.7	31.5	53.8

144	44.0	29.6	26.3	12.7	33.1	54.2
145	48.6	27.3	24.1	14.6	31.5	53.9
146	56.4	23.3	20.3	12.8	34.2	53.1
147	60.5	21.6	17.9	13.1	32.2	54.8
148	58.1	19.1	22.8	14.2	31.8	54.1
149	60.3	21.4	18.3	14.0	34.3	51.7
150	62.9	19.5	17.7	14.2	34.5	51.3
151	64.8	16.3	18.9	12.1	37.1	50.8
152	66.1	16.4	17.5	12.7	36.6	50.7
153	55.9	23.6	20.5	11.6	37.0	51.4
154	55.3	21.9	22.8	14.9	35.8	49.3
155	66.2	16.2	17.5	15.6	37.6	46.8
156	68.2	16.2	15.6	16.1	35.3	48.6
157	68.6	15.8	15.7	14.8	35.2	50.1
158	71.2	13.8	15.0	14.4	34.4	51.2
159	64.3	17.1	18.6	17.4	33.8	48.8
160	69.9	13.7	16.4	17.0	34.6	48.4
161	65.2	16.3	18.5	19.4	38.0	42.6
162	66.6	15.4	18.0	21.3	35.3	43.4
163	73.0	12.6	14.5	17.9	37.3	44.9
164	69.6	14.2	16.2	15.0	36.9	48.1
165	63.9	16.4	19.7	13.5	34.5	52.0
166	74.5	10.5	15.0	13.2	33.1	53.7
167	73.5	12.0	14.5	16.5	35.3	48.2
168	63.6	17.5	18.9	15.4	35.6	48.9
169	72.9	12.1	15.0	13.3	30.6	56.2
170	71.6	12.5	15.8	13.3	32.5	54.3
171	59.4	19.1	21.5	13.7	32.0	54.3
172	79.6	8.2	12.2	13.2	33.9	52.9
173	71.8	12.0	16.2	12.2	33.3	54.5
174	73.9	10.6	15.5	14.3	31.6	54.1
175	73.7	12.0	14.4	16.3	33.8	49.9
176	38.4	23.4	38.2	21.9	31.5	46.6
177	29.6	30.4	39.9	22.7	33.2	44.1
178	15.6	30.8	53.6	23.5	30.9	45.6
179	72.0	11.4	16.6	25.9	33.8	40.3
180	16.2	31.3	52.5	28.2	31.4	40.4
181	25.6	27.7	46.7	36.6	26.6	36.7
182	40.2	22.2	37.5	33.4	27.0	39.6
183	38.0	23.6	38.4	36.6	25.7	37.7
184	10.2	33.7	56.1	29.3	31.0	39.7
185	75.1	9.2	15.7	29.6	29.8	40.5
186	27.7	28.1	44.1	31.2	26.9	41.9
187	5.3	37.6	57.0	32.8	27.7	39.5
188	7.8	34.9	57.3	30.0	24.1	46.0
189	6.4	36.6	56.9	28.9	26.0	45.1
190	6.6	35.5	57.9	28.8	27.0	44.2
191	5.5	37.1	57.4	28.3	24.8	46.9
192	5.3	37.8	57.0	29.1	25.7	45.2
193	5.5	36.2	58.3	24.9	22.8	52.3

194	8.7	36.4	54.9	25.1	24.2	50.7
195				25.6	22.5	51.9
196				24.7	23.5	51.8
197				26.4	23.0	50.6
198				25.5	23.5	51.0
199				26.6	24.0	49.4
200				25.7	24.4	49.9
201				26.4	24.6	48.9
202				24.6	26.4	49.0
203				23.2	27.8	49.0
204				23.5	27.3	49.2
205				25.2	28.3	46.5
206				24.6	30.6	44.8
207				24.2	30.4	45.5
208				23.8	31.1	45.1
209				28.2	28.1	43.7
210				26.8	28.9	44.3
211				26.4	30.0	43.6
212				26.0	28.9	45.1
213				23.9	31.0	45.1
214				25.5	29.9	44.6
215				21.9	31.3	46.9
216				19.9	32.7	47.4
217				19.4	33.3	47.2
218				19.6	33.0	47.4
219				21.9	31.3	46.8
220				19.7	29.0	51.3
221				21.8	27.1	51.0
222				22.7	25.9	51.4
223				21.3	25.4	53.3
224				20.8	24.9	54.3
225				19.8	26.1	54.1
226				19.0	25.3	55.7
227				18.7	27.4	54.0
228				17.4	28.8	53.8
229				16.1	30.7	53.2
230				13.2	32.6	54.2
231				14.0	31.4	54.7
232				15.6	34.5	49.9
233				16.0	35.3	48.7
234				19.4	31.7	49.0
235				20.5	31.7	47.8
236				22.5	32.7	44.9
237				22.6	32.1	45.3
238				23.1	31.0	45.9
239				21.6	29.9	48.5
240				20.9	30.9	48.2
241				17.8	37.2	45.0
242				19.1	36.9	44.0
243				15.6	34.2	50.2

244	14.4	35.7	49.9
245	12.0	33.4	54.6
246	11.8	31.6	56.5
247	10.1	31.1	58.8
248	19.6	34.2	46.2
249	18.9	33.5	47.6
250	11.6	35.6	52.8
251	10.1	33.1	56.8

**Calcium carbonate, scavenged-Al, and particulate-Mn content in the sediment cores**

Section	SK129/GC02			SK129/GC08	SK129/CR04
	CaCO <sub>3</sub> (%)	Al (%)	Mn (ppm)	CaCO <sub>3</sub> (%)	CaCO <sub>3</sub> (%)
1	78.7	0.35	49	48.2	56.3
2	74.9	0.46	57	49.4	57.0
3	78.9	0.46	67	47.4	56.2
4	79.7	0.47	61	43.9	57.4
5	81.2	0.53	65	41.9	58.0
6	82.7	0.52	70	38.0	56.9
7	81.2	0.51	73	36.7	57.6
8	97.6	0.52	83	35.7	58.2
9	97.9	0.52	78	37.5	58.0
10	88.9	0.44	67	35.7	57.6
11	91.9	0.47	62	39.2	56.6
12	83.4	0.47	80	36.0	58.5
13	86.9	0.50	85	40.5	58.1
14	88.1	0.53	87	39.7	59.1
15	87.6	0.47	79	45.4	58.7
16	84.6	0.55	80	42.9	59.8
17	83.6	0.58	88	41.9	59.8
18	87.4	0.61	92	40.0	59.8
19	83.4	0.55	111	38.5	60.5
20	86.6	0.58	106	36.0	59.0
21	61.2	0.43	85	35.2	54.9
22	63.9	0.42	78	37.0	54.8
23	62.4	0.42	78	36.4	55.2
24	55.7	0.44	96	35.9	56.5



25	54.2	0.42	93	35.7	57.1
26	56.4	0.38	93	33.9	55.4
27	55.7	0.30	130	33.1	55.9
28	55.2	0.30	96	35.7	55.1
29	54.7	0.31	96	40.0	56.6
30	53.4	0.30	102	40.0	54.7
31	55.2	0.30	98	40.5	51.4
32	56.7	0.32	84	37.0	50.2
33	56.7	0.32	94	37.0	51.0
34	61.4	0.32	91	34.2	53.9
35	67.4	0.34	102	30.7	55.7
36	68.9	0.34	102	32.7	54.5
37	67.7	0.35	127	38.2	53.7
38	65.7	0.35	119	36.2	53.6
39	66.7	0.34	115	34.7	54.0
40	65.7	0.35	107	35.5	51.5
41	66.2	0.35	132	35.2	53.8
42	63.4	0.32	91	35.0	54.7
43	61.2	0.32	138	32.7	54.7
44	59.4	0.31	117	32.2	53.3
45	63.9	0.33	106	32.7	51.2
46	58.4	0.29	93	36.0	52.2
47	56.7	0.39	106	36.0	52.4
48	62.4	0.36	114	38.7	49.7
49	62.7	0.34	111	41.7	52.0
50	76.4	0.39	135	45.2	52.3
51	67.5	0.52	124	42.2	53.0
52	64.5	0.56	112	40.5	51.0
53	61.7	0.55	116	38.7	51.5
54	57.8	0.47	98	39.5	52.6
55	55.0	0.49	101	39.5	55.1
56	56.8	0.48	95	39.7	54.6
57	55.3	0.49	140	38.7	57.4
58	53.3	0.44	92	37.9	55.9
59	53.0	0.41	98	35.0	56.4
60	51.7	0.42	89	32.3	53.4
61	62.9	0.29	109	32.3	55.3
62	62.7	0.29	121	31.7	56.2
63	61.2	0.28	121	29.0	55.7
64	62.9	0.30	119	28.2	55.7
65	63.4	0.30	116	28.5	55.6
66	63.9	0.31	122	29.2	54.8
67	64.2	0.29	115	24.4	55.4
68	61.9	0.29	115	23.8	53.4
69	61.9	0.28	110	22.7	57.2
70	64.2	0.29	113	25.2	56.2
71	62.7	0.30	138	24.2	55.0
72	61.4	0.30	105	23.5	51.1

73	61.7	0.30	115	20.2	54.2
74	62.4	0.31	122	19.0	50.6
75	63.7	0.29	113	22.6	52.1
76	65.4	0.29	95	27.2	52.6
77	64.4	0.28	95	29.1	54.1
78	65.7	0.29	104	27.4	53.7
79	68.2	0.27	90	30.1	53.6
80	68.9	0.24	83	34.4	54.6
81	69.7	0.23	79	35.0	54.8
82	71.4	0.21	72	33.9	53.3
83	73.2	0.19	64	30.9	54.0
84	73.4	0.20	62	29.8	50.9
85	74.2	0.19	61	24.7	48.7
86	74.7	0.18	59	22.6	50.8
87	76.9	0.18	55	19.1	49.8
88	76.2	0.17	52	21.7	51.3
89	77.7	0.20	53	28.8	50.5
90	76.4	0.22	67	37.4	47.3
91	74.2	0.21	54	41.2	46.0
92	79.2	0.18	45	42.5	44.3
93	79.7	0.17	47	43.8	46.1
94	79.9	0.19	44	42.9	41.8
95	79.2	0.19	39	45.7	42.4
96	81.4	0.17	39	45.2	38.8
97	79.7	0.20	43	44.2	37.9
98	78.2	0.23	44	44.9	36.5
99	77.2	0.23	52	42.2	37.0
100	79.4	0.17	37	39.0	36.3
101	77.9	0.22	54	34.7	36.6
102	80.7	0.18	37	37.0	35.5
103	78.9	0.19	38		34.7
104	75.7	0.21	42		33.9
105	79.4	0.19	37		35.6
106	80.9	0.17	35		35.4
107	77.9	0.21	39		35.7
108	78.9	0.20	40		30.6
109	76.9	0.18	36		34.1
110	79.2	0.17	34		30.5
111	76.2	0.18	36		26.3
112	76.7	0.19	36		26.2
113	81.2	0.18	36		22.3
114	82.9	0.18	36		27.7
115	77.2	0.18	32		28.2
116	77.2	0.23	39		34.9
117	75.9	0.19	33		37.4
118	78.4	0.20	33		37.9
119	80.2	0.19	34		40.7
120	77.4	0.18	31		37.8

121	79.7	0.20	32	40.6
122	79.9	0.19	32	44.4
123	79.4	0.19	33	45.2
124	80.7	0.17	30	46.7
125	81.4	0.21	33	48.7
126	78.7	0.24	37	51.4
127	80.7	0.24	39	50.1
128	77.4	0.28	40	45.4
129	79.2	0.25	40	43.4
130	81.4	0.25	37	41.4
131	81.9	0.29	39	41.9
132	79.9	0.31	46	40.3
133	84.6	0.26	47	37.6
134	85.9	0.23	41	33.7
135	84.6	0.21	39	36.5
136	86.6	0.25	44	36.6
137	83.2	0.26	44	36.6
138	76.9	0.25	41	36.3
139	75.2	0.23	40	44.0
140	75.4	0.21	38	49.4
141	76.2	0.30	45	51.2
142	74.7	0.31	48	51.1
143	72.9	0.27	43	52.7
144	79.4	0.24	39	48.8
145	76.7	0.33	50	51.6
146	73.9	0.39	57	51.7
147	74.2	0.39	56	54.8
148	73.2	0.33	48	53.9
149	75.2	0.38	53	55.3
150	76.4	0.47	64	57.9
151	80.2	0.39	57	53.9
152	73.9	0.46	64	55.0
153	74.9	0.44	61	53.9
154	74.2	0.43	61	47.7
155	72.7	0.46	65	53.6
156	72.7	0.52	68	52.0
157	66.2	0.52	71	52.2
158	69.9	0.51	71	51.5
159	70.4	0.58	78	43.6
160	73.4	0.47	71	44.7
161	71.4	0.56	81	46.2
162	72.9	0.51	72	48.3
163	69.9	0.56	75	47.0
164	68.4	0.59	87	53.0
165	70.9	0.50	84	50.1
166	65.9	0.62	90	51.9
167	65.9	0.63	92	52.2
168	67.7	0.51	83	54.6

169	65.9	0.57	87	56.1
170	65.9	0.55	84	59.7
171	65.9	0.40	72	58.5
172	65.2	0.41	69	57.3
173	60.7	0.43	75	56.8
174	60.9	0.44	74	56.0
175	59.4	0.53	100	55.6
176	44.4	0.60	181	55.3
177	41.5	0.58	185	54.6
178	34.2	0.61	238	53.4
179	51.7	0.50	106	50.7
180	38.2	0.54	180	51.9
181	41.9	0.53	153	54.9
182	35.2	0.56	183	56.3
183	21.5	0.56	219	57.3
184	21.3	0.61	248	55.1
185	47.2	0.47	121	59.0
186	21.9	0.61	233	56.1
187	19.2	0.66	253	54.9
188	18.1	0.68	262	61.2
189	18.5	0.66	267	57.9
190	19.7	0.62	240	58.2
191	18.8	0.67	272	57.9
192	19.1	0.68	257	55.7
193	19.1	0.65	253	53.2
194	19.8	0.70	256	52.7
195				52.9
196				61.6
197				59.2
198				58.6
199				59.4
200				58.3
201				52.9
202				53.8
203				51.7
204				48.7
205				51.4
206				48.7
207				49.7
208				49.2
209				50.2
210				51.9
211				50.9
212				54.4
213				52.4
214				53.1
215				53.1
216				49.4

217	48.0
218	49.4
219	48.7
220	50.7
221	51.9
222	54.2
223	53.4
224	53.7
225	53.7
226	53.7
227	50.7
228	54.9
229	52.2
230	48.9
231	48.7
232	55.4
233	54.2
234	55.9
235	58.4
236	49.4
237	49.4
238	50.7
239	51.2
240	45.9
241	47.7
242	47.4
243	47.4
244	44.4
245	41.0
246	40.5
247	42.2
248	49.7
249	46.2
250	46.4
251	46.9

**Sedimentary organic components and their isotopes  
in deep-water core SK117/GC08**

Section	C <sub>org</sub> %	Tot-N %	C/N mol/mol	δ <sup>13</sup> C <sub>org</sub> ‰ PDB	δ <sup>15</sup> N ‰ Air	ΣAlkenone ppm
1	0.93	0.15	6.2	-19.4	8.5	0.033
2	0.68	0.13	5.2	-19.3	8.6	0.040
3	1.00	0.16	6.3	-19.2	8.7	0.075
4	0.81	0.13	6.2	-18.8	8.1	0.036
5	0.88	0.13	6.8	-18.9	8.2	0.068
6	0.86	0.13	6.6	-18.8	7.5	0.056
7	0.61	0.09	6.8	-18.1	7.6	0.050
8	0.69	0.09	7.7	-17.7	7.2	0.104
9	0.83	0.10	8.3	-18.0	7.3	0.131
10	0.72	0.09	8.0	-18.4	7.0	0.107
11	0.49	0.08	6.1	-18.7	7.2	0.269
12	0.64	0.09	7.1	-18.6	6.6	0.636
13	0.61	0.09	6.8	-18.6	6.7	0.969
14	0.84	0.11	7.6	-18.7	6.7	1.126
15	0.97	0.13	7.5	-18.6	6.8	1.446
16	0.97	0.13	7.5	-18.6	6.7	1.609
17	1.20	0.15	8.0	-18.6	7.0	1.200
18	1.20	0.16	7.5	-18.7	6.9	0.775
19	1.20	0.16	7.5	-18.6	7.2	1.066
20	1.30	0.17	7.6	-18.6	7.0	0.876
21	1.30	0.17	7.6	-18.7	7.1	0.719
22	0.92	0.12	7.7	-18.6	6.8	0.593
23	0.96	0.13	7.4	-18.5	6.8	0.538
24	0.98	0.13	7.5	-18.4	6.8	0.827
25	0.90	0.12	7.5	-18.4	6.9	1.311
26	1.20	0.15	8.0	-18.4	6.7	1.208
27	1.40	0.18	7.8	-18.6	7.0	0.928
28	1.30	0.16	8.1	-18.7	7.1	2.951
29	1.10	0.15	7.3	-18.4	6.7	0.938
30	1.10	0.14	7.9	-18.4	6.8	0.729
31	0.90	0.12	7.5	-18.4	6.7	0.556
32	0.89	0.12	7.4	-18.3	6.6	0.915
33	1.00	0.13	7.7	-18.2	7.0	0.520
34	1.10	0.14	7.9	-18.4	7.0	0.605
35	1.10	0.13	8.5	-18.2	6.8	
36	1.10	0.14	7.9	-18.5	7.1	
37	1.30	0.15	8.7	-18.6	7.3	
38	1.20	0.15	8.0	-18.9	7.7	
39	1.10	0.14	7.9	-18.5	7.4	
40	1.20	0.16	7.5	-18.7	7.6	
41	1.60	0.19	8.4	-18.9	7.6	

42	1.60	0.20	8.0	-19.0	7.8
43	1.60	0.19	8.4	-19.5	8.6
44	1.10	0.14	7.9	-18.6	7.6
45	1.60	0.19	8.4	-18.6	8.0
46	1.80	0.21	8.6	-18.5	8.3
47	1.80	0.21	8.6	-18.6	8.8
48	1.50	0.18	8.3	-18.4	9.2
49	1.30	0.16	8.1	-18.7	8.3
50	0.86	0.11	7.8	-18.5	8.0
51	0.87	0.12	7.3	-18.6	7.3
52	1.00	0.13	7.7	-18.8	7.7
53	0.99	0.13	7.6	-18.7	7.1
54	0.63	0.09	7.0	-18.8	6.4
55	0.57	0.08	7.1	-18.7	6.0
56	0.64	0.09	7.1	-18.8	6.1
57	0.84	0.11	7.6	-18.8	5.9
58	0.90	0.12	7.5	-19.0	5.6
59	0.85	0.11	7.7	-19.0	6.0
60	1.00	0.13	7.7	-19.1	6.3
61	1.00	0.14	7.1	-19.1	6.1
62	1.20	0.15	8.0	-19.1	7.0
63	1.30	0.16	8.1	-19.3	8.0
64	0.97	0.13	7.5	-18.8	7.0
65	0.87	0.11	7.9	-18.6	6.6
66	0.75	0.11	6.8	-18.8	6.8
67	0.87	0.11	7.9	-18.7	7.4
68	1.20	0.14	8.6	-18.8	7.5
69	1.50	0.18	8.3	-19.0	8.5
70	1.10	0.13	8.5	-18.4	7.0
71	1.10	0.14	7.9	-18.3	7.1
72	0.99	0.12	8.3	-18.5	7.2
73	0.60	0.09	6.7	-18.2	6.8
74	0.49	0.08	6.1	-18.3	6.4
75	0.50	0.07	7.1	-18.1	6.3
76	0.55	0.08	6.9	-18.2	6.4
77	0.76	0.10	7.6	-18.6	6.7
78	1.20	0.16	7.5	-19.2	8.5
79	1.10	0.15	7.3	-19.2	8.7
80	1.10	0.15	7.3	-19.4	8.6
81	0.90	0.12	7.5	-19.2	9.4
82	0.92	0.13	7.1	-19.2	8.6
83	0.82	0.11	7.5	-18.8	7.8
84	0.58	0.09	6.4	-18.6	7.6
85	0.43	0.08	5.4	-18.8	6.2
86	0.60	0.09	6.7	-19.4	7.1